

Engineering and Characterization of
Xanthomonas campestris pv. *campestris* Towards an Enhanced
Production of the Exopolysaccharide Xanthan

Dissertation

to obtain the academic title

Dr. rer. nat.

at the Faculty of Biology

Bielefeld University

Tim Steffens

born in Lüdinghausen, Germany

December 2016

Thesis advisors:

Prof. Dr. Karsten Niehaus

Prof. Dr. Alfred Pühler

Dr. Frank-Jörg Vorhölter

Summary

Xanthan is the industrially most important bacterial polysaccharide, with broad fields of application (Hublik 2012). It is produced by the Gram negative phytopathogen *Xanthomonas campestris* pv. *campestris* (Xcc). Presented in this work are three systematical, mutational approaches in order to optimize xanthan production and gain new insights in the Xcc metabolism.

In a first approach three mutant strains, carrying mutations in genes involved in the lipopolysaccharide (LPS) O-antigen biosynthesis, were used. The mutants Xcc H21012 (*wxcB*), Xcc H28110 (*wxcK*) and Xcc H20110 (*wxcN*) were constructed by Barbara Hötte and colleagues (1990) and in this thesis the phenotypic analyses are described. The mutant Xcc H21012 (*wxcB*) was characterized by the inhibition of the entire O-antigen. Moreover, the mutant phenotype was displayed through an increased xanthan production. In Xcc H28110 (*wxcK*) and Xcc H20110 (*wxcN*), no increase in xanthan production was detected. However, a novel LPS phenotype with an extended O-antigen main chain and no O-antigen branches could be detected.

For the second approach, in order to construct a Xcc strain towards enhanced xanthan production, two flagellar genes were mutated to inhibit the motility. First the structural gene *fliC* was mutated, then the basal flagellar gene *fliM*. Mutations were performed in laboratory strain Xcc B100 and in an industrial production strain, Xcc JBL007. Phenotypic analyses revealed the inhibition of motility. Furthermore, both mutational approaches resulted in enhanced xanthan producer strains. Remarkably, even the industrial production strain could be improved. Not only in production, but also in xanthan quality. The xanthan from Xcc JBL007 *fliC*⁻ and Xcc JBL007 *fliM*⁻ showed enhanced rheological properties. Both was shown under distinct industrial cultivation conditions. While the chemical composition did not change between xanthan by the initial or by a mutant strain, notable differences in persistence length could be measured via atomic force microscopy.

During a study with the purpose to identify sucrose related regulators, two novel regulators encoded by *xcc-b100_2791* (*crt1*) and *xcc-b100_2861* (*crt2*) were identified. Since they are putatively involved in Xcc carbohydrate regulation, mutants were constructed by Tobias Loka. As third approach of this thesis the mutant strains Xcc B100 *crt1*⁻ and Xcc B100 *crt2*⁻ were tested towards their cultivation characteristics and production abilities. Both mutants showed

an increased xanthan yield, as compared to the initial strain Xcc B100. During the course of this work, both mutations were transferred into the production strain Xcc JBL007, after the corresponding genes in this strain were identified and sequence homologies were ensured. The xanthan production abilities of the mutant strains were then tested under industrial cultivation conditions. Both mutant strains exceeded the production of the initial strain Xcc JBL007.

Results presented in this study demonstrate the possibility to further improve the xanthan production by Xcc, including the industrial xanthan production, through rational strain design.

Table of Contents

Summary	3
Table of Contents	5
1 Introduction	10
The bacterial genus <i>Xanthomonas</i>	10
The species <i>Xanthomonas campestris</i> pv. <i>campestris</i>	10
The genome as basis for research in <i>Xanthomonas campestris</i> pv. <i>campestris</i>	12
The carbohydrate metabolism in <i>Xanthomonas campestris</i>	16
Structure and biosynthesis of the exopolysaccharide xanthan	18
Industrial relevance of the exopolysaccharide xanthan.....	22
Insights in <i>Xanthomonas</i> exopolysaccharide production.....	23
2 Aims and Approaches	25
3 The Influence of the O-antigen as Target for an Enhanced Xanthan Production in <i>Xanthomonas campestris</i> pv. <i>campestris</i> B100	27
The Gram negative cell envelope	27
General properties of lipopolysaccharides	27
Structure and biosynthesis of lipopolysaccharides	29
Aim	36
Results.....	36
The genetic background of three Xcc B100 strains carrying mutations in the LPS O-antigen biosynthesis	36
Chemical analysis of the O-antigen in three Xcc B100 mutant strains: Xcc H21012 (<i>wxcB</i>), Xcc H20110 (<i>wxcN</i>) and Xcc H28110 (<i>wxcK</i>)	39
Xanthan production of the analyzed Xcc B100 O-antigen mutant strains	44
Discussion	48

Inhibition of the Xcc O-antigen biosynthesis and the possible impact for xanthan production approaches.....	48
Structural analyses of LPS from Xcc H21012 (<i>wxcB</i>), H28110 (<i>wxcK</i>) and H20110 (<i>wxcN</i>) revealed altered O-antigen phenotypes.....	49
Characterization of cultivation phenotypes by Xcc B100 and derived mutant strains Xcc H21012 (<i>wxcB</i>), H28110 (<i>wxcK</i>) and H20110 (<i>wxcN</i>)	52
The influence of a missing or modified LPS O-antigen on the xanthan biosynthesis in Xcc B100	53
4 The Inhibition of Flagellar Structures and the Effects on Xanthan Production and Quality in <i>Xanthomonas campestris</i> pv. <i>campestris</i> B100 and Production Strain JBL007.....	56
General properties of flagella	56
Structure and biosynthesis of the flagellum.....	59
Aim	61
Results.....	62
Construction of the flagellar mutants <i>fliC</i> ⁻ and <i>fliM</i> ⁻ in Xcc	62
Characterization of the Xcc B100 xanthan production after mutagenesis of two flagellar genes.....	63
Construction of Xcc JBL007 mutant strains deficient in flagellar genes <i>fliC</i> and <i>fliM</i> and their phenotypic characterization towards motility.....	65
Xanthan production by production strain Xcc JBL007 and by the derived flagellar mutant strains Xcc JBL007 <i>fliC</i> ⁻ and <i>fliM</i> ⁻ under industrial cultivation conditions	66
Characterization of product quality of xanthan isolated from Xcc JBL007 and flagellar mutant strains.....	72
Chemical properties of the isolated xanthan from Xcc JBL007 and derived mutants Xcc JBL007 <i>fliC</i> ⁻ and Xcc JBL007 <i>fliM</i> ⁻	74
Discussion	77
The potential of flagellar mutants in Xcc for xanthan production	77
Flagellar mutations in <i>fliM</i> and <i>fliC</i> resulted in non-motile strains of Xcc.....	78

Flagellar genes as targets for mutations in Xcc can be beneficial for xanthan production	79
Characterization of rheological properties revealed enhanced viscosities in solutions by xanthan of the flagellar mutants	80
In depth analysis of different xanthan samples indicates an explanation for viscosity changes of flagellar mutant xanthan	81
Conclusions concerning flagellar gene mutations as a targeted mutation approach in Xcc driven by xanthan production	82
5 The Influence of Mutations in Two Regulator Genes of <i>Xanthomonas campestris</i> pv. <i>campestris</i> B100 and Production Strain JBL007 on Xanthan Production	84
Regulation of xanthan production	84
Aim	86
Results.....	86
Two novel regulators are involved in the <i>Xanthomonas campestris</i> pv. <i>campestris</i> carbohydrate metabolism.....	86
Xanthan production of Xcc B100 regulator mutants Xcc B100 <i>crt1</i> ⁻ and Xcc B100 <i>crt2</i> ⁻	87
Xanthan production under industrial conditions by production strain Xcc JBL007 compared to the regulator mutant strains.....	88
Rheological properties of xanthan produced by Xcc JBL007 compared to the rheological properties of xanthan produced by Xcc JBL007 <i>crt1</i> ⁻	92
Discussion	93
Two genes encoding for regulators as mutational targets in Xcc	93
Mutations in two regulator genes are characterized by an increased xanthan production in Xcc	94
Regulator gene mutations as target for an enhanced xanthan production in Xcc	96
6 Concluding Remarks.....	97
The O-antigen biosynthesis as target: Enhanced xanthan productivity and new insights into the Xcc LPS biosynthesis	97

The flagellar biosynthesis as target: Enhanced xanthan quantity and quality.....	100
Regulator genes as targets: A novel approach towards enhanced xanthan production	104
Towards an enhanced xanthan production	106
7 Material and Methods	108
The Influence of the O-antigen as Target for an Enhanced Xanthan Production in <i>Xanthomonas campestris</i> pv. <i>campestris</i> B100.....	108
Strains and cultivation	108
Glucose determination	109
Nitrate determination.....	109
Xanthan and biomass determination	109
LPS isolation	109
Methanolysis and peracetylation of LPS.....	110
Hydrolysis, reduction and peracetylation of LPS	110
Gas Chromatography (GC) (Mass Spectrometry)	111
Sample preparation for MALDI-TOF-MS analysis	111
MALDI-TOF-MS measurements	112
The Inhibition of Flagellar Structures and the Effects on Xanthan Production and Quality in <i>Xanthomonas campestris</i> pv. <i>campestris</i> B100 and Production Strain JBL007	112
Bacterial strains and mutation strategy.....	112
Preparation of chemical competent <i>E. coli</i> cells.....	115
Preparation of electro competent Xcc cells.....	115
Gene comparison between Xcc B100 and Xcc JBL007.....	115
Cultivation conditions	115
Swarming assay.....	116
Xanthan determination.....	116
Rheometrical measurements.....	117
Transmission electron microscopy	117

Atomic Force Microscopy	118
NMR measurements	118
The Influence of Mutations in Two Regulator Genes of <i>Xanthomonas campestris</i> pv. <i>campestris</i> B100 and Production Strain JBL007 on Xanthan Production.....	119
Bacterial strains and mutation strategy.....	119
Preparation of chemical competent <i>E. coli</i> cells.....	121
Preparation of electro competent Xcc cells.....	121
Gene comparison between Xcc B100 and Xcc JBL007.....	121
Cultivation conditions	121
Swarming assay.....	122
Xanthan determination.....	122
Rheometrical measurements.....	123
8 List of Figures and Tables	124
9 References	133
10 Supplement	144
Frequently used abbreviations	144
Supplementary data.....	146
Danksagung.....	152
11 Erklärung	153

1 Introduction

The bacterial genus *Xanthomonas*

Xanthomonads were described in 1921 as *Bacterium vesicatorium*, as tomato pathogen in south Africa (Doige 1921). Afterwards more descriptions of plant pathogenic bacteria followed and they were grouped into one group of *Xanthomonas* by Dowson (Dowson 1939). Species determination was achieved by DNA hybridization, emerged species could be re-classified due to their molecular markers (Vauterin et al. 1995). In 1995 Vauterin et al. grouped 183 strains of *Xanthomonas*. The genus comprises of Gram negative plant pathogens or plant associated bacterial species and is part of the *gamma* subdivision of the *Proteobacteria*. Typical for Xanthomonads is the yellow pigment Xanthomonadin, giving them a more or less yellow appearance and the exopolysaccharide xanthan that is responsible for the colony mucoidy. The cells are rod shaped and 0.4 – 0.6 by 1.0 – 2.9 μm (Vauterin et al. 1995; Rodriguez-R et al. 2012).

Amongst the *Xanthomonas* host plants are many important crops, which makes *Xanthomonas* a severe threat to agriculture. In a study by Mansfield et al. several species of *Xanthomonas* are listed in the top 10 plant pathogens. *Xanthomonas oryzae* infests rice plants, *Xanthomonas campestris* pathovars are a severe threat for all cultivated brassicas, including many crop species and *Xanthomonas axonopodis* is a pathogen for cassava (Mansfield et al. 2012).

The species *Xanthomonas campestris* pv. *campestris*

Xanthomonas campestris pv. *campestris* (Xcc) is the causative agent of the black rot disease in cruciferous crops, including all cultivated brassicas (Figure 1-1) as well as the model plant *Arabidopsis thaliana* (Mansfield et al. 2012; Vicente and Holub 2013). Black rot is considered the most important disease for vegetable brassica crops, including cabbage, cauliflower and others, worldwide. Occurrences are reported from all continents where *Brassicaceae* crops are grown, mostly in warm and humid conditions (Williams 1980; Vicente and Holub 2013). Without host plants Xcc can survive in the soil and they can disperse e. g. through wind, insects or aerosols, but can also be transmitted over seeds, infected soil or plants (Kocks and Zadoks 1996; Vicente and Holub 2013). The cells enter the plants mostly through hydrathodes or

wounds and in general not through stomata. The bacteria move in the vascular system of the plant, leading to darkened veins, other than that chlorotic yellow lesions are typical symptoms of the black rot disease (Williams 1980). Genome wide comparisons led to fundamental insights into the pathogenicity of *Xanthomonas* species, e. g. three secretion systems were detected in Xcc. The type II secretion system (T2SS), the type III secretion system (T3SS) and the type IV secretion system. Through these systems important pathogenicity factors, like cell-wall degrading enzymes or effector proteins, can be secreted (Vicente and Holub 2013). Furthermore, *Xanthomonas campestris* pv. *campestris* produces a biofilm that is important for its phytopathogenic life cycle (Crossman and Dow 2004; Torres et al. 2007). Essential for the Xcc biofilm formation is the exopolysaccharide (EPS) xanthan. Small amounts of xanthan are produced early after the bacteria infect their plant hosts. However, copious amounts of xanthan are produced at later stages of the Xcc infection (Vojnov et al. 2001). At early stages xanthan seems to be necessary for the infection of mesophyll tissue and the vascular system. Nevertheless, too much xanthan production at the early phases of infection might interfere with the adherence of the bacteria to plant cells or inhibit the cells movement through the plant. Conversely, after establishment of the infection, large amounts of xanthan are thought to protect the bacteria against an unfavorable plant environment and stress reactions, like reactive oxygen species (Vojnov et al. 2001).

However, Xcc is not only a model for plant pathology. In large scale industrial processes it is employed as producer of xanthan (Vorhölter et al. 2008; Hublik 2012). Xanthan is used as thickening agent in many fields of application (CPKelco 2008; Hublik 2012) and therefore xanthan is a driving force for biotechnological studies using Xcc.

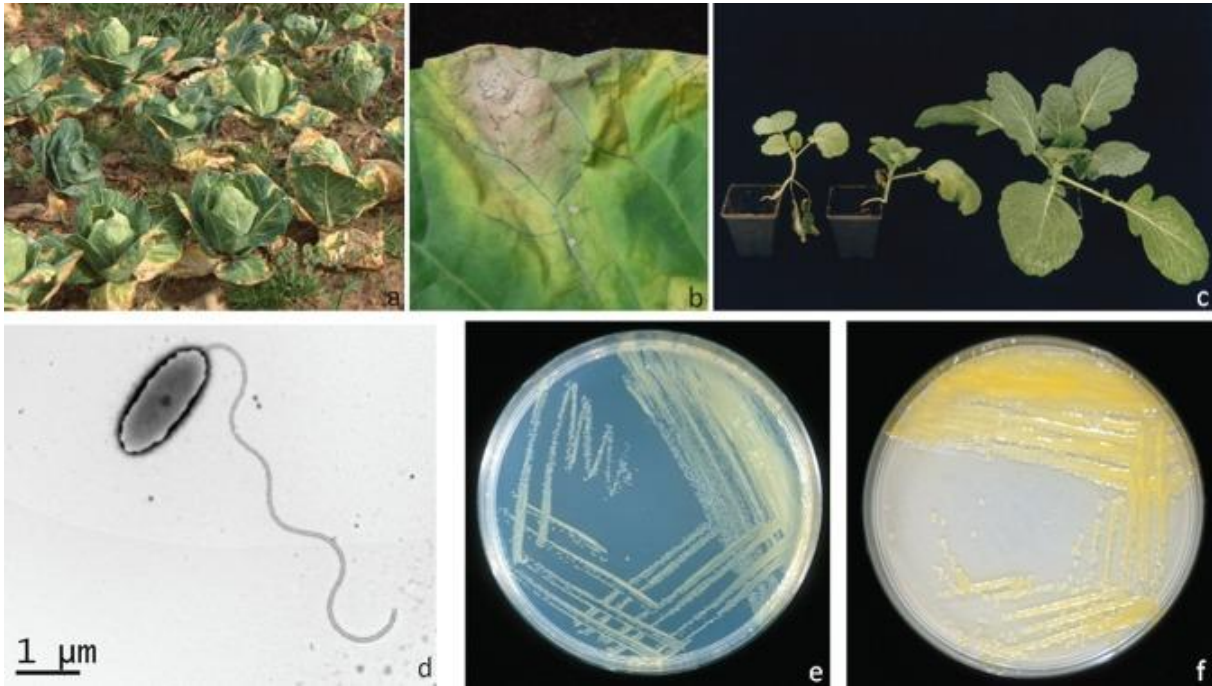


Figure 1-1: The bacterium *Xanthomonas campestris* pv. *campestris*. a: *X. campestris* pv. *campestris* caused black rot on a cabbage field. b: lesion on a cabbage leaf. c: Two infested savoy cabbage plants next to a healthy control. d: Electron microscopy image of a *X. campestris* pv. *campestris* cell, with one polar flagellum. e: *X. campestris* pv. *campestris* growing on Kings medium. f: *X. campestris* pv. *campestris* growing on yeast dextrose calcium carbonate medium. From Vicente and Holub, 2013, License number: 3983650320184.

The genome as basis for research in *Xanthomonas campestris* pv. *campestris*

The foundation for genetic engineering is a good knowledge about genes and their respective genomes. Therefore, the availability of genome sequences is an important asset in research towards strain development. Several genomes of the group *Xanthomonas* are already published (da Silva et al. 2002; Lee et al. 2005; Thieme et al. 2005). Then, in 2008 the genome of *Xanthomonas campestris* pv. *campestris* B100, a strain used in this study, was published (Vorhölter et al. 2008). The genome of Xcc B100 consists of a circular chromosome with 5,079,002 bp (Figure 1-2), with a GC content of 65% and including 4471 predicted protein coding sequences (Vorhölter et al. 2008).

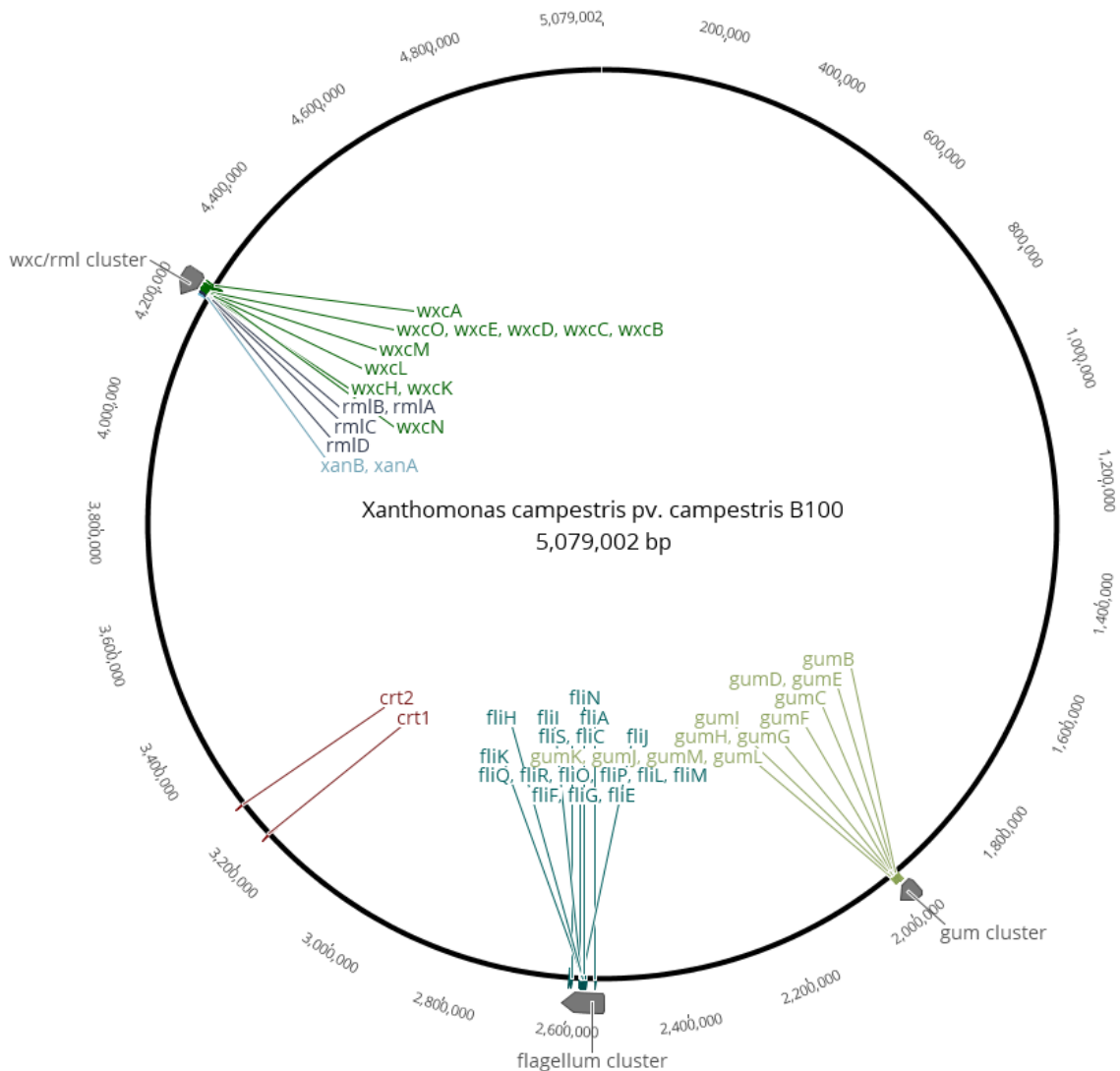


Figure 1-2: Circular genome plot of the *X. campestris* pv. *campestris* B100 genome. Grey arrows highlight gene clusters that were important for this work. Displayed within the plot are the conventional gene names of the specific regions (for the flagellum only the *fli* genes). Xanthan biosynthesis: *gum* cluster; Xanthan and LPS precursors and LPS O-antigen biosynthesis: *wxc/rml* cluster and *xanAB*; flagellar biosynthesis: flagellum cluster. Additionally, regulator genes *crt1* and *crt2* are highlighted. The scale accounts for the genomic positions. Image provided by Dr. Vera Ortseifen.

The genome sequence of Xcc B100 was annotated and used to gain new insights in the Xcc carbohydrate and xanthan metabolism and especially the genetic organization of genes responsible for xanthan production was analyzed. Further, data were used to assign detailed functions to specific genes and to reconstruct the uptake systems of carbon sources. For instance, it was thought that *Xanthomonas campestris* pv. *campestris* was not capable of performing glycolysis or gluconeogenesis, since no phosphofructokinase activity could be

measured in previous studies (Whitfield et al. 1982; Pielken et al. 1988). However, the obtained genome data revealed a gene with high similarities to phosphofructokinase genes, implying that Xcc B100 is capable of performing both, glycolysis and gluconeogenesis (Vorhölter et al. 2008). The Xcc B100 protein in question was isolated and tested for phosphofructokinase activity and indeed, activity could be detected, yet not with ATP, but with pyrophosphate as co-factor (Frese et al. 2014). This represents a striking example for experimental approaches following systemic analyses.

The genes responsible for the xanthan polysaccharide biosynthesis are organized in a gene cluster called *gum*, comprising of 12 genes from *gumB* to *gumM* (Figure 1-2, 1-3) (Vorhölter et al. 2008). A detailed analysis of the *gum* cluster was performed, together with genes responsible for xanthan precursor molecules from the nucleotide sugar metabolism (Figure 1-3). A comprehensive sequence evaluation was executed, because especially these genes are thought to be a characteristic feature throughout the genus *Xanthomonas*. In the study by Vorhölter and colleagues (2008), the sequence of xanthan related genes of Xcc B100 was compared to other *Xanthomonas* species. It became evident that the genes of the *gum* cluster as well as the nucleotide sugar precursor genes, are strongly conserved, but not identical, in different strains of Xcc (Figure 1-3). The differences in the gene sequences increase notably in *X. campestris* pv. *vesicatoria* or in *X. axonopodis* pv. *citri* and *X. oryzae* species (Figure 1-3). Overall, the *gum* gene cluster is mostly controlled by a promotor upstream of *gumB*, however just recently a RNA sequencing approach to elucidate the transcription start sites of Xcc B100 was performed (Alkhateeb et al. 2016). This study revealed additional, yet weaker promoters upstream of *gumD* and upstream of *gumH*. Furthermore, several intergenic and antisense transcription start sites were reported (Alkhateeb et al. 2016).

Other than that the knowledge of the Xcc B100 genome allowed to determine the position of genetic clusters that are essential for the different parts of this work. All approaches have in common that mutations of specific genes in carefully chosen genetic subsets were used to gain knowledge on their influence concerning the production of exopolysaccharide xanthan. First, the *wxc* gene cluster will be of interest. It contains genes responsible for the biosynthesis of the O-antigen polysaccharide of the lipopolysaccharide (LPS). This gene cluster together with genes responsible for the nucleotide sugar biosynthesis that are essential for xanthan production, like *xanAB*, can be found in a direct genetic neighborhood (Figure 1-2). Afterwards, the focus will lay on the inhibition of the flagellar biosynthesis. The biosynthesis

of the flagellum is dependent on around 40 genes of different genetic clusters (Berg 2003). Two genes, from the *fli* gene cluster neighborhood (Figure 1-2) were chosen as mutational targets in order to successfully interfere with the flagellar biosynthesis. Then, in the third part of this work, mutants in genes of two novel regulators were analyzed towards their xanthan production. The carbohydrate related transcriptional regulators Crt1 and Crt2, as well as their respective genes (Figure 1-2) were just recently discovered in Xcc B100 and knowledge about their function, including their role in xanthan production, is still very limited (Leßmeier et al. 2016).

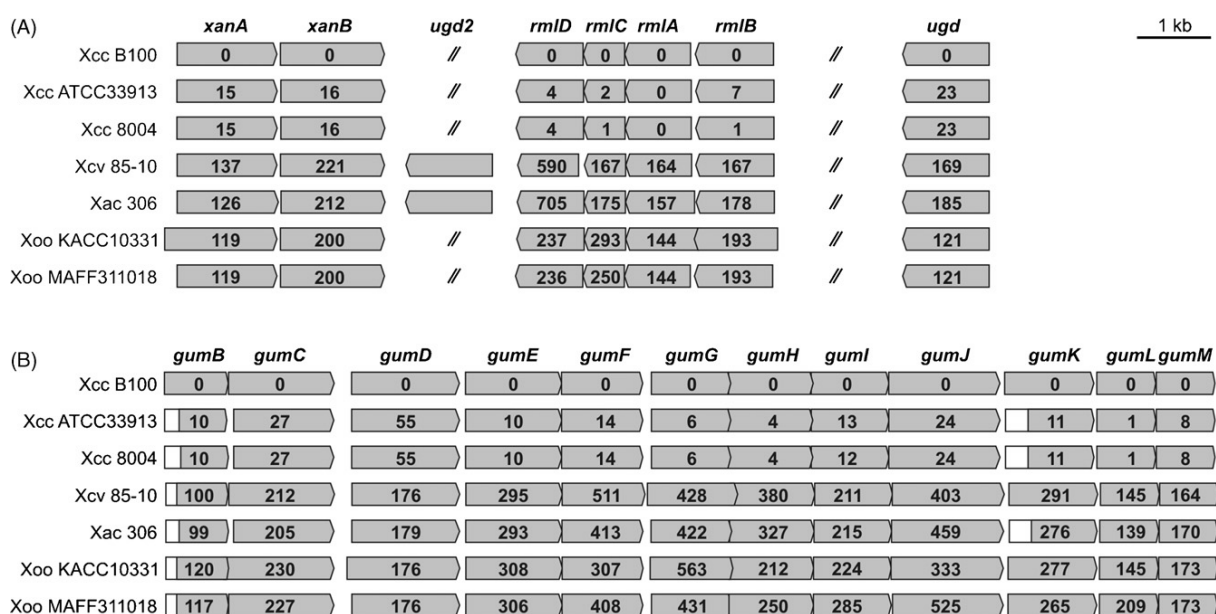


Figure 1-3: Comprehensive sequence analysis of xanthan precursor genes (A) and xanthan biosynthesis *gum* genes (B). Grey arrows show directions and authentic size comparison of the genes. *X. campestris* pv. *campestris* B100 (Xcc B100) is used as basis and compared to *X. campestris* pv. *campestris* ATCC33913 (Xcc ATCC33913), *X. campestris* pv. *campestris* 8004 (Xcc 8004), *X. campestris* pv. *vesicatoria* 85-10 (Xcv 85-10), *X. axonopodis* pv. *citri* 306 (Xac 306), *X. oryzae* pv. *oryzae* KACC 10331 (Xoo KACC10331) and to *X. oryzae* pv. *oryzae* MAFF311018 (Xoo MAFF311018). Conventional gene names are given above the arrows. Numbers within the arrows indicate the deviation of nucleotides. From Vorhölter et al. 2008, License number: 3998990345087.

The carbohydrate metabolism in *Xanthomonas campestris*

The organism *Xanthomonas campestris* is an established model organism for polysaccharide production and several annotated genomes (Vorhölter et al. 2008; Hublik 2012) as well as previous experimental work (Whitfield et al. 1982; Koplín et al. 1992; Koplín et al. 1993; Katzen et al. 1998), made it possible to reconstruct the carbohydrate metabolism. Carbohydrates used by the cell, either for energy production or for building blocks, originate from storage polysaccharides, like glycogen, which can be built by *Xanthomonas*, or from the extracellular space, respectively (Vorhölter et al. 2008). In Xcc B100 15 uptake systems for mono- and disaccharides were identified (Vorhölter et al. 2008). Due to the close structural similarity of different carbohydrates, predictions of transporter specificity are difficult (Blanvillain et al. 2007).

For glucose, the industrially used carbon source (also as sirup, starch or in sucrose (Hublik 2012)), experiments showed that after saccharide uptake by Xcc, there are two possible pathways for additional catabolism, both described by Whitfield and colleagues in 1982 (Whitfield et al. 1982). In an intracellular pathway the glucose is directly imported into the cell and phosphorylated by the glucokinase. The resulting glucose-6 phosphate is then further processed by the oxidization reactions of the pentose phosphate pathway. Through the glucose-6 phosphate dehydrogenase an ester is formed, which is hydrolyzed to 6-phosphogluconate by the 6-phosphogluconolactonase. The other possible pathway is periplasmic and quite similar to the previous. However, the difference is that the phosphorylation occurs later. In the periplasm glucose is processed to gluconate through a glucose dehydrogenase and a gluconolactonase. Then, it is imported into the cytoplasm and the phosphorylation to 6-phosphogluconate is performed by a gluconokinase (Whitfield et al. 1982). It was shown that the latter pathway only plays a minor role in Xcc (Whitfield et al. 1982; Letisse et al. 2002).

The further catalysis of glucose then mainly occurs through the Entner-Doudoroff (ED) pathway and only a minor part is processed via the pentose-phosphate cycle (Whitfield et al. 1982; Pielken et al. 1988; Vorhölter et al. 2008). However, Vorhölter et al. showed that the genetic subset for all necessary enzymes with respect to both pathways is present in Xcc B100. Furthermore, it could be proven that the genetic information for every enzyme involved in the glycolysis and gluconeogenesis are present in the Xcc B100 genome, including the critical phosphofruktokinase (Vorhölter et al. 2008). Additionally, it was shown that the Xcc B100

phosphofructokinase is not ATP but pyrophosphate driven, which explains former inconspicuous test results for both pathways (Frese et al. 2014).

The ED pathway, the pentose phosphate pathway, as well as the glycolysis, all result in a common pathway, starting from glyceraldehyde 3-phosphate and leading to pyruvate. Pyruvate is then metabolized through the tricarboxylate (TCA) cycle in order to produce energy equivalents (Vorhölter et al. 2008).

The synthesis of surface carbohydrates generally depends on nucleotide sugar precursors. Nucleotide sugars represent a donor for monosaccharides as building blocks for polysaccharides. The genes necessary for nucleotide sugar production encode for as much as

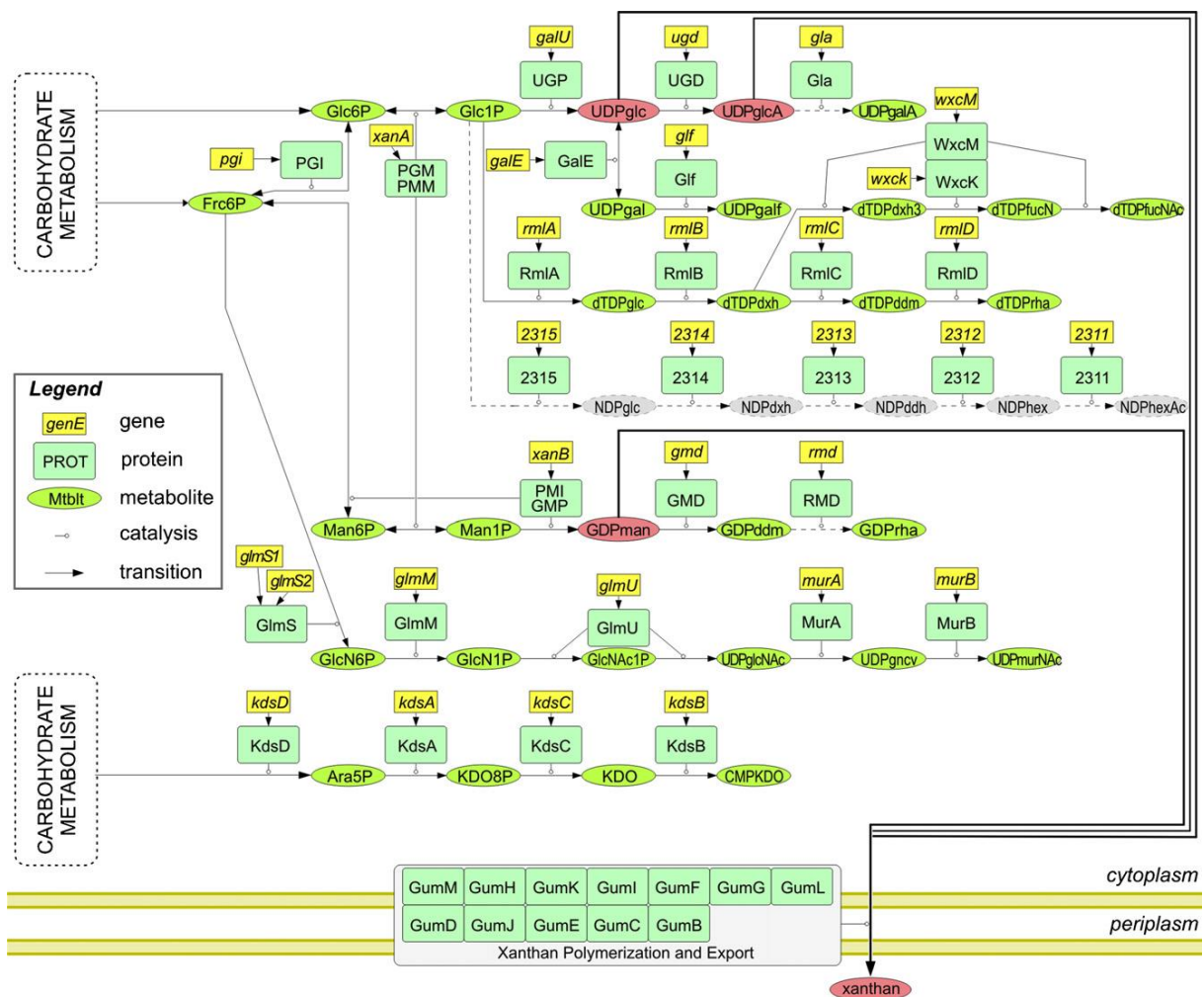


Figure 1-4: Reconstruction of the nucleotide sugar metabolism in *X. campestris* pv. *campestris* B100. Symbols for genes, proteins, metabolites, catalysis and transition are depicted in the legend. Metabolic reconstruction followed the information of the *X. campestris* pv. *campestris* B100 genome annotation. Xanthan, as well as its precursors UDP-glucose, UDP-glucuronic acid and GDP-mannose are highlighted in red. Further, precursor synthesis for LPS and murein are included in the reconstructed network. From Vorhölter et al. 2008, License number: 3983651418225.

29 enzymes that lead to 13 nucleotide sugar building units for surface carbohydrates (Figure 1-4) (Koplin et al. 1992; Koplin et al. 1993; Vorhölter et al. 2001; Vorhölter et al. 2008). The initial molecules for nucleotide sugar synthesis originate from the pentose phosphate pathway, are however not used for energy production. 10 of the 13 nucleotide sugar units, amongst them all the building blocks for xanthan as well as many precursors for LPS, depend on the formation of glucose-6-phosphate and mannose-6-phosphate to glucose-1-phosphate and mannose-1-phosphate, respectively (Figure 1-4). Both conversions are encoded by the gene *xanA* (Vorhölter et al. 2008). The precursors of xanthan and LPS in *Xcc* were described before by Koplin and colleagues (Koplin et al. 1992; Koplin et al. 1993) and as their close relation on a metabolic pathway level suggests, the genes responsible for many xanthan and LPS building blocks, like *xanAB* and *rmIABCD*, are closely arranged in a genomic neighborhood (Figure 1-2) (Vorhölter et al. 2008). This clearly shows the metabolic connection of LPS and xanthan.

Structure and biosynthesis of the exopolysaccharide xanthan

Xanthan is an exopolysaccharide produced by *Xanthomonas* that consists of repeating units formed by D-glucose, D-mannose and D-glucuronic acid (2:2:1) that can be pyruvylated and acetylated (Figure 1-5) (Jeanes et al. 1961; Hublik 2012). The structure was determined in 1975 by Jansson and colleagues (Jansson et al. 1975).

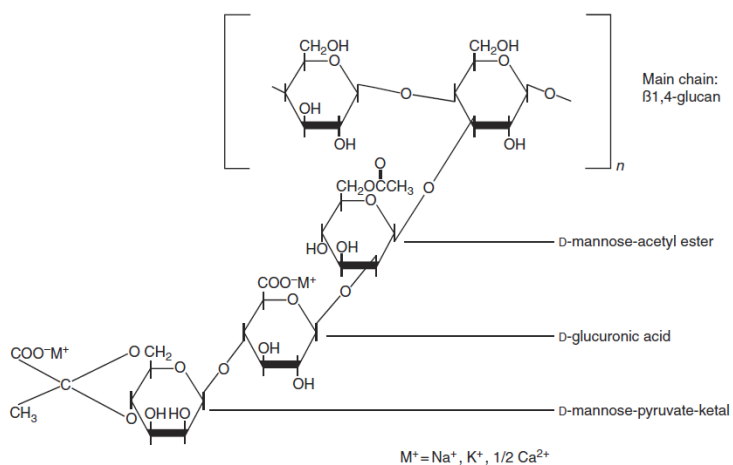


Figure 1-5: Repeating unit of xanthan. Provided with a glucose backbone to which mannose, glucuronic acid and a second mannose are bound. Here the first mannose is shown with an acetate and the second with a pyruvate group. M: Cation binding site. From Hublik 2012.

The 12 genes responsible for xanthan production, with respect to *Xcc*, are clustered in a genomic region called *gum* (Becker et al. 1998; Katzen et al. 1998; Vorhölter et al. 2008). The *gum* cluster encodes for glycosyltransferases, *gumDMHKI*, membrane proteins that form a pore, *gumBC*, *gumLFG* gene products are responsible for the addition of pyruvate and acetate

and *gumE* is thought to be a polymerase. *gumJ* encodes for the protein that translocates the repeating units into the periplasmic space (Becker et al. 1998; Katzen et al. 1998; Vorhölter et al. 2008).

The products of the gum genes are located at the membrane fractions of *Xanthomonas* where polymerization and export occur (Figure 1-6). They need distinct sugar nucleotides and lipid carrier as precursors, just like lipopolysaccharides (LPS) and other surface carbohydrates. More specific, xanthan production depends on the availability of UDP-D-glucose, GDP-D-mannose and UDP-D-glucuronate, as well as undecaprenylphosphate (UndP) lipid carrier (Becker et al. 1998; Vorhölter et al. 2008). GumD, a protein conserved in all sequenced *Xanthomonas* strains, catalyzes the initial reaction by transferring the phospho-glucose of an UDP-D-glucose nucleotide sugar onto the membrane bound UndP lipid carrier, creating undecaprenyl-di-phospho-D-glucose. The second glucose is attached to the growing molecule by GumM, resulting in a β -1,4-glucose disaccharide. The glucose disaccharide represents the backbone of xanthan repeating units. GumH transfers a mannose from GDP-D-mannose as α -1,3 glycosidic bond onto the glucose disaccharide, establishing the first molecule of the xanthan side chain. Next, a glucuronic acid moiety is β -1,4 linked to the glucose-glucose-mannose trisaccharide by GumK, using UDP-D-glucuronic acid. A second mannose, originating from GDP-D-mannose, characterizes the last monosaccharide residue in the xanthan pentasaccharide repeating unit. The mannose is β -1,2 linked to the gluconate by the glycosyltransferase GumI (Vorhölter et al. 2008). Other than through the sugar residues, xanthan is characterized by its non-sugar constituents acetate and pyruvate, which can be added to both mannose residues at a varying degree (Katzen et al. 1998; Vorhölter et al. 2008). GumL adds a pyruvyl group to the outer and GumF adds an acetyl group to the inner mannose. Furthermore, GumG can add acetyl groups to a non-pyruvylated outer mannose, representing the last step of repeating unit synthesis. The function of the described proteins was established on experimental level by Katzen and colleagues and later supported by genomic data (Katzen et al. 1998; Vorhölter et al. 2008), however experimental data as evidence for the function of the gene products of *gumE* and *gumJ* are yet missing. Still, with the help of obtained genomic data, bioinformatical tools and comparison to model proteins of enteric bacteria, xanthan biosynthesis reactions were proposed due to homologies to the *Enterobacteriaceae* Wzy-dependent polymerization and export machinery (Figure 1-6) (Whitfield 2006; Vorhölter et al. 2008). GumJ mutations showed to be lethal in *Xanthomonas*,

while on a cell-free basis it did not affect xanthan production. Moreover, through similarities with the *E. coli* Wzx protein, GumJ is thought to be responsible for the transport of the UndP-bound xanthan repeating unit across the membrane (Vorhölter et al. 2008). GumB showed similarities to the protein Wza. Wza is an exporter, organized in four domains and located in the outer membrane of *E. coli* (Vorhölter et al. 2008). GumC shows similarities to Wzz-family proteins that were thought to be responsible for chain length determination. However, mutation of *gumC* did not lead to low-molecular weight xanthan (Katzen et al. 1998). Yet, Galvan and colleagues showed that co-overexpression of *gumB* and *gumC* led to an increase in polymer chain length, implying that these proteins together are somehow involved in chain length modulation (Galván et al. 2013).

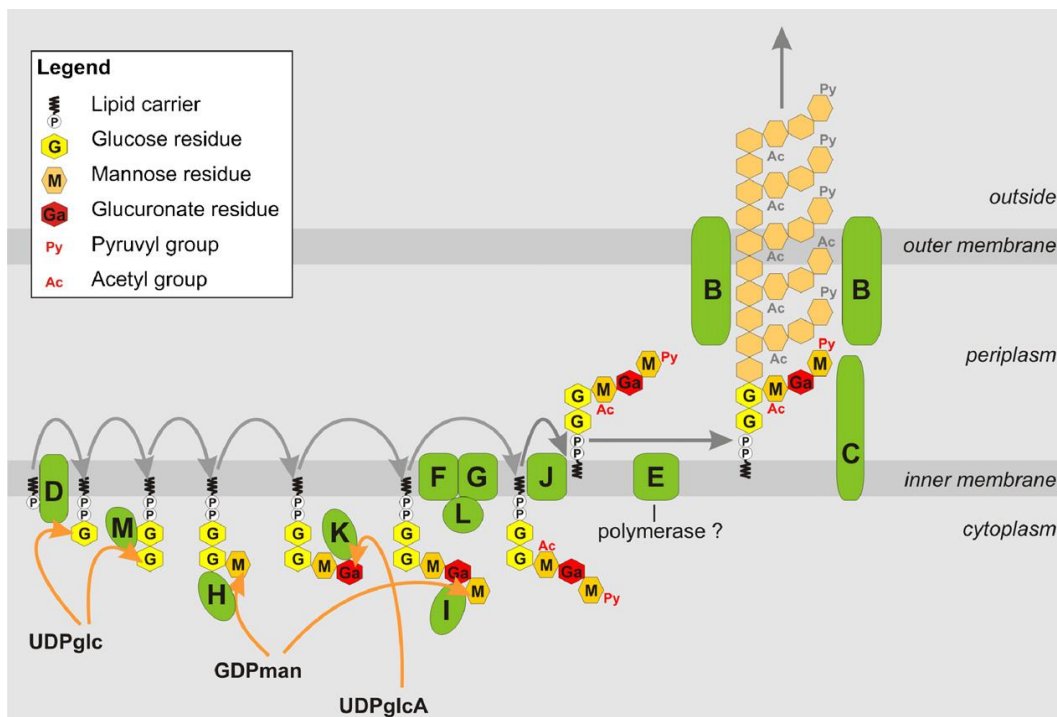


Figure 1-6: Model of the *X. campestris* xanthan biosynthesis. Proteins encoded by the *gum* genes are depicted in green. Initially UDP-glucose (UDPglc) is added onto an UndP lipid carrier by GumD at the inner phase of the inner membrane. Subsequently GumMHI add a second glucose, as backbone, two mannoses, as well as a glucuronic acid. The mannose originates from GDP-mannose (GDPman) and the glucuronic acid from UDP-glucuronic acid (UDPglcA). The outer mannose can be pyruvylated by GumL or both mannoses can be acetylated by GumFG. The repeating units are translocated into the periplasm by GumJ, polymerized, putatively by GumE and exported by GumBC. From Vorhölter et al. 2008, License number: 3983651418225.

GumC also showed sequence similarities to the *E. coli* Wzc protein, which forms a protein complex with Wza (Collins et al. 2007). Therefore GumC might link the production at the inner membrane to the export carried out by GumB (Vorhölter et al. 2008). No clear function could be assigned to the protein GumE, although it is highly conserved in *Xanthomonas* (Katzen et al. 1998). However, it was predicted to be an integral membrane protein, which resembles the polymerase Wzy (Vorhölter et al. 2008). Therefore, GumE is the most likely candidate for the polymerase functions, although experimental validation is still needed (Whitfield 2006; Vorhölter et al. 2008). In the light of the genome data, coupled with *in silico* predictions and former experimental data, a xanthan biosynthesis model was constructed by Vorhölter and colleagues (Figure 1-6) (Vorhölter et al. 2008). The gum genes seem to be conserved to a varying degree, yet only in the *Xanthomonas* group, implying that xanthan synthesis is restricted to this genus (Vorhölter et al. 2008).

The structural composition of xanthan is subject of a long lasting discussion (Norton et al. 1984) and there are no validated molecular masses available, yet they most likely are in the range of millions of Daltons. Hublik tested different samples and results showed masses of 7 – 7.74 million Da (Hublik 2012). It was revealed that xanthan can build helical structures, however this seems to be dependent on external factors, like temperature, salts and pH (Gulrez et al. 2012). Also if native xanthan occurs as single or double strand was under debate. In recent years Atomic Force Microscopy was applied to reveal the structural composition of xanthan. Just recently it was shown that xanthan fibers of around 2 nm height exist, which is close, but not exactly fitting the prediction of double stranded helical xanthan that is 1.8 nm (Moffat et al. 2016). In this case xanthan was imaged in an ordered conformation, due to xanthan preparation. Xanthan in a disordered or random coil conformation was shown to have a significantly lower height of around 0.178 nm (Gulrez et al. 2012). Furthermore, Moffat and colleagues could show that xanthan not only exists in one stage, but that the helical structure is often unraveled at their respective ends. The height of the helix prepared with a specific method was 1.6 nm, while the height of the unraveled strands was only 0.6 nm, less than half of the helical structure (Moffat et al. 2016). This indicates that the xanthan structure is more complex than expected for a helical structure of two dimerized strands (Moffat et al. 2016). Also, no clear length distribution for xanthan strands, neither for their persistence length, is measurable (Teckentrup et al. 2016, accepted).

Industrial relevance of the exopolysaccharide xanthan

Xanthan was initially described in 1961, after a research group of the US Department of Agriculture was screening for microbial polymers with potential biotechnological impact (Jeanes et al. 1961). The screened bacterium *Xanthomonas campestris* was selected, since it produced a vast amount of the exopolysaccharide xanthan (Figure 1-7). Xanthan was cleared as safe food additive in 1969 by the US Food and Drug Administration and in 1980 the



Figure 1-7: Culture broth of *X. campestris* pv. *campestris* JBL007. Sample was cultivated in production medium and harvested in the stationary phase. Depicted is the culture directly after harvest from a fermenter.

European Commission followed (Hublik 2012).

Xanthan was assigned to the number E415. The high industrial relevance of xanthan can be explained by its extraordinary qualities as rheological control agent in aqueous systems and by its stabilizing properties in suspensions and emulsions (Hublik 2012). Xanthan

provides a unique combination of commercially interesting features. It provides high viscosity even at low concentrations, it shows thermal stability and retains its features up to 70 – 80°C. In addition, xanthan maintains its characteristic viscosity properties at a pH range from 2 – 12, unless the temperature is above 40°C in strong acidic or alkaline conditions. It provides pseudoplastic characteristics with a decrease of viscosity at increasing shear rates. Furthermore, xanthan is stable in salt solutions and resistant to degradation by most enzymes (CPKelco 2008; Hublik 2012).

Today, xanthan is the commercially most important biological polysaccharide and companies in Europe, Asia and America produced around 160,000 t in 2014, applying fermenters with capacities of up to 350,000 l (Dr. G. Hublik personal communication). The polymer is used for many applications from food production to oil drilling. The deviation of xanthan consumption strongly correlates with the oil price (Hublik 2012). In the food and feed sector xanthan is used e. g. as stabilizer for example in salad dressings, soups and sauces. In personal care products, like toothpaste, xanthan provides uniformity and stability, so that it can be pumped or squeezed easily and in pharmaceutical products, like tablets, xanthan can be used to create a retarded drug release (Hublik 2012). Also in technical and industrial applications xanthan is used for a wide range of tasks. Amongst others it is used in cleaners for good pH stability and

in agricultural chemicals in order to suspend the active ingredients. Additionally, it is used in oil drilling to help cool and lubricate the drill bit (Hublik 2012).

Due to increasing production capacities and fields of application, research with industrially relevant outcome is promoted. Obviously, the construction of potent or better xanthan producer strains is one center of attention in xanthan research. However, since several years a lot of effort was put in the determination of xanthan characteristics and the molecular connections to e. g. viscosity (CPKelco 2008; Gulrez et al. 2012; Galván et al. 2013; Moffat et al. 2016). The insights arising through studies, such as in depth Atomic Force Microscopy, opened up another field of interest for xanthan research. Determination of xanthan quality, e. g. of different strains or different measured characteristics and the construction of strains with an increased quality product, became an unneglectable target.

Insights in *Xanthomonas* exopolysaccharide production

This work is based on the extraordinary potential of carbohydrate analyses in *Xanthomonas*. Bacteria of the *Xanthomonas* genus are model organisms for a wide range of scientific questions, from phytopathogenicity to industrial biotechnology (Dow et al. 1995; Katzen et al. 1998; Molinaro et al. 2003; Newman et al. 2007; Torres et al. 2007; Silipo et al. 2008; Vorhölter et al. 2008; Hublik 2012; Schatschneider et al. 2013). Both in common is *Xanthomonas*' ability to build a biofilm employing the exopolysaccharide xanthan as matrix. In this work a focus on biotechnology and on the characteristics of the exopolysaccharide xanthan was laid. The aim of the study was to get new insights into the carbohydrate metabolism of *Xanthomonas* and to enhance xanthan production. In order to achieve that, competing metabolic pathways and xanthan regulation were used as targets for rational strain design.

The scientific outcome of this work is dependent on the bacterial background, therefore different *Xanthomonas campestris* pv. *campestris* strains were used to widen the knowledge in *Xanthomonas* carbohydrate research. For initial approaches regarding xanthan production and for an approach targeting the LPS biosynthesis, the strain *Xanthomonas campestris* pv. *campestris* B100 (Xcc B100) was used, since the wild type lipopolysaccharide (LPS) structure is known (Molinaro et al. 2003; Silipo et al. 2005), the genome was published in 2008 (Vorhölter et al. 2008) and systems biology, as well as metabolic engineering and a metabolic model of this bacterium are established (Schatschneider et al. 2011; Schatschneider et al. 2013).

Additionally, for a promising outcome regarding xanthan production, the strain *Xanthomonas campestris* pv. *campestris* JBL007 (Xcc JBL007), a xanthan high producer strain provided by Jungbunzlauer Austria AG, was used to establish significant knowledge for industrial xanthan production.

2 Aims and Approaches

The purpose of this work was to gain insights into the carbohydrate metabolism of the EPS producing bacterial species *Xanthomonas campestris* pv. *campestris*, by characterizing the impact of different mutations. The project was carried out in close cooperation with an industrial partner: Jungbunzlauer Austria AG. Three distinct approaches targeting the LPS biosynthesis, the flagellar biosynthesis and carbohydrate related regulation, were applied in order to optimize and characterize the Xcc xanthan production (Figure 2-1).

In the first approach three Xcc strains, carrying mutations in the genes *wxcB*, *wxcK* and *wxcN*, respectively, were analyzed. The *wxc* gene cluster is responsible for the biosynthesis of the Xcc LPS O-antigen and the required precursors are nucleotide sugars. Xanthan also depends on nucleotide sugar precursors and therefore mutations in *wxc* genes might be beneficial for xanthan production, since a competing metabolic pathway was inhibited. To test this hypothesis, LPS and xanthan phenotype analyses were performed.

The second part focusses on the potential to enhance the Xcc xanthan production after inhibiting the flagellar biosynthesis. Resources otherwise used for the flagellar biosynthesis or protons that are not required as driving force for the flagellar rotation, might be beneficial for xanthan production. Furthermore, an altered flagellar related signaling towards biofilm and EPS production could lead to enhanced xanthan production. In order to test these assumptions the flagellar genes *fliM* and *fliC* were mutated and the mutant strains could be tested towards their phenotypes.

During a regulator fishing approach, two novel carbohydrate related transcriptional regulators, Crt1 and Crt2, were detected in Xcc B100. Through their involvement in the Xcc carbohydrate metabolism, the regulators might have an impact on the Xcc xanthan production. Therefore, the xanthan production of mutant strains deficient in *crt1* and *crt2* should be analyzed.

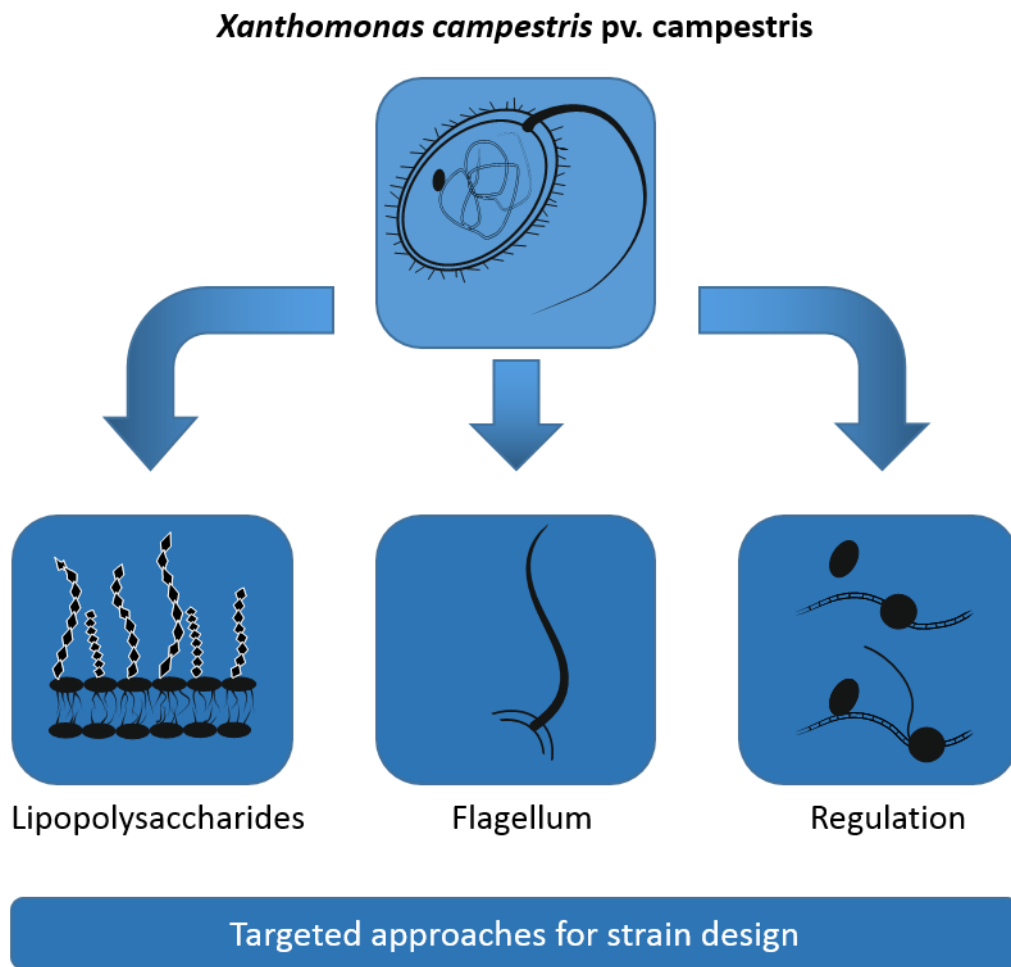


Figure 2-1: Schematic overview of the presented thesis. Three distinct approaches were chosen to obtain improved xanthan production strains and to reveal new insights into the Xcc metabolism. Mutations in genes of the Xcc LPS biosynthesis, the flagellar biosynthesis or in different regulator genes, build up the fundamental design of this work.

3 The Influence of the O-antigen as Target for an Enhanced Xanthan Production in *Xanthomonas campestris* pv. *campestris* B100

The Gram negative cell envelope

Xanthomonas, amongst many other bacteria, like the model organism *E. coli*, belongs to the Gram negative bacteria (Vorhölter et al. 2001). Next to them another group of bacteria exists, the Gram positive bacteria, comprised of members like *Bacillus* or *Corynebacterium* (Kunst et al. 1997; Kalinowski et al. 2003). Gram negative or positive is the description for the two groups of eubacteria and the separation is named after a staining method by Hans Christian Gram (Gram 1884). Gram positive bacteria possess a cell membrane, surrounded by thick layers of peptidoglycans, forming a cell wall that is responsible for retaining the staining. Also in Gram negative bacteria peptidoglycan can be found, but the peptidoglycan cell wall is way thinner than in Gram positive bacteria and, moreover, it lays between two membranes (Raetz and Whitfield 2002). Furthermore, the peptidoglycan in Gram negative bacteria is DAP-type peptidoglycan, while in most gram positives the peptidoglycan is lysine-type (Neyen and Lemaitre 2016). Like Gram positive bacteria, Gram negative bacteria possess a phospholipid bilayer membrane surrounding the cytoplasm, yet they additionally show a second membrane that builds up the border to the surrounding medium. This membrane is called outer membrane and is assembled by a layer of phospholipids at the inner phase and glycolipids, mostly lipopolysaccharides, at the outer phase (Raetz 1990; Rietschel et al. 1994; Raetz and Whitfield 2002).

General properties of lipopolysaccharides

Lipopolysaccharides (LPS) are a feature unique to Gram negative bacteria, in fact only very few Gram negative species, like the genus *Sphingomonas* or *Sorangium cellulosum*, without conserved LPS structures are known (Alexander and Rietschel 2001; Keck et al. 2011). Moreover, LPS are essential to the bacteria, since they provide structural stability. Additionally, the LPS layer is comprised of many anionic groups and therefore associated with cations. These properties build up an effective barrier for external stress factors (Alexander and Rietschel 2001). The total exterior part of the bacterial outer membrane are covered with

proteins and mostly LPS, while the inner part of the membrane consists of phospholipids and proteins (Alexander and Rietschel 2001). One cell contains approximately 3.5 million LPS molecules, covering $4.9 \mu\text{m}^2$, for *E. coli* that means, three quarters of the cell are covered by LPS (Rietschel et al. 1994). LPS were described more than 100 years ago, when guinea pigs were treated with heat inactivated cells of *Vibrio cholerae*, which led to toxic shock reactions in the animals (Rietschel and Cavaillon 2003). Richard Pfeiffer concluded that a heat stable toxin has to be present in the bacteria and in order to distinguish these toxins from known exotoxins he termed them endotoxins (Alexander and Rietschel 2001). Today it is known that the severe reactions are due to the presence of LPS and because of the life threatening shock reactions by LPS, these molecules are of significant scientific importance (Rietschel et al. 1994; Medzhitov and Janeway 2000; Alexander and Rietschel 2001; Raetz and Whitfield 2002).

The threshold for immune reactions can vary, but in humans picomolar concentrations of LPS trigger immune responses (Alexander and Rietschel 2001). The innate immune system in mammals reacts towards a strictly conserved structure inside the LPS, termed lipid A. The lipid A is conserved throughout the Gram negative kingdom and so is the innate immune response through the ancient toll-like receptor 4 (TLR-4) that is present on macrophages and endothelial cells.

Although numerous studies elucidated LPS interactions and responses in animals, reactions of LPS in plants and plant pathogens are not fully understood. In 2005 a study by Silipo et al. not only clarified the Xcc LPS structure, but also showed parallels in PAMP (pathogen associated molecular pattern) recognition of the mammalian innate immune system and plant stress responses (Silipo et al. 2005). Additionally, several other publications describe a stress reaction of plants towards LPS and parts of a signal transduction cascades were shown (Steffens, Duda, et al. 2016). Only recently a plant receptor that triggers responses towards LPS was discovered (Ranf et al. 2015). This receptor is one of only few known plant stress receptors.

Structure and biosynthesis of lipopolysaccharides

The general structure and biosynthesis of LPS are conserved throughout Gram negative bacteria (Figure 3-1). LPS consist of three distinct structural parts. The first part is the lipid A. It consists of two glucosamine (GlcN) molecules to which different fatty acids are bound. Further, position 1 of the first and position 4 of the second GlcN can be decorated, for example with phosphate or phospho-ethanolamine groups (Raetz and Whitfield 2002). The acylation pattern can vary, e. g. tetra-, penta- or hexa-acylated lipid A species are commonly found. Nevertheless, not only the number of fatty acids vary, to date also a vast amount of different fatty acids are reported as parts of the lipid A (Alexander and Rietschel 2001). Four fatty acids can directly bind to the GlcN molecules via ester- or amide-bonds, called primary acyl chains. Further, secondary acyl chains may be bound to hydroxylated primary fatty acids (Raetz and Whitfield 2002). The classical model, comprised from enteric bacteria, contains saturated (R)-3-hydroxylated primary and non-hydroxylated secondary fatty acids built by 12 to 14 carbons (Alexander and Rietschel 2001). Additionally different other acyl chain length are reported as

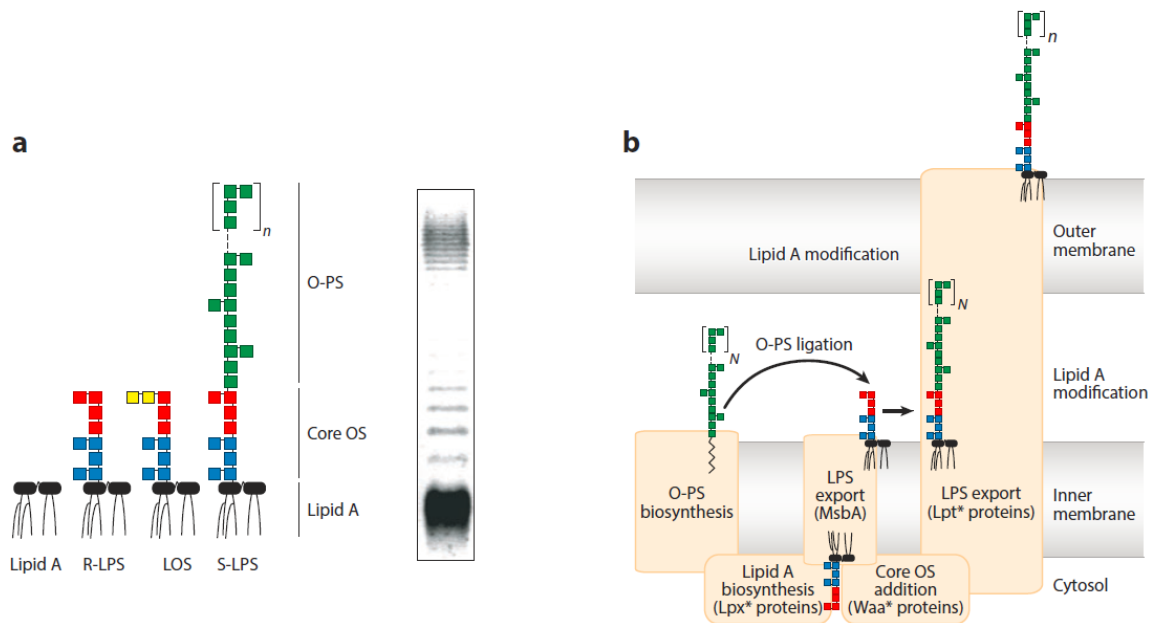


Figure 3-1: General overview of LPS structure and biosynthesis. a: Depicted are the different forms and states of LPS molecules, next to that a SDS-PAGE of LPS is shown. The lowest, heavily stained band represents lipid A-core LPS, then each band represents LPS with growing repeating units in the O-antigen (from *E. coli*). b: Overview of the principal steps for LPS transport. Abbreviations: R-LPS: rough LPS, LOS: lipooligosaccharide, S-LPS: smooth LPS, OS: oligosaccharide, PS: polysaccharide. From Whitfield and Trent, 2014.

part of the lipid A. For example, in *Xcc* hydroxylated and non-hydroxylated fatty acids containing eleven carbon atoms are reported (Silipo et al. 2005; Silipo et al. 2008). The lipid A is the membrane anchor of the LPS and is the most conserved and essential part of the molecule, although the amount and length of the fatty acids, as well as the decorations at the GlcN molecules, may vary (Raetz 1990; Alexander and Rietschel 2001; Raetz and Whitfield 2002).

The second part is called core region. The core region itself is comprised of two fragments, the inner and outer core. The first molecule of the inner core that is connected to the lipid A, is as conserved. It is always a molecule of kdo (2-keto-3-deoxyoctulosonic acid and it was shown that bacteria without lipid A-kdo are in general not viable (Whitfield and Trent 2014). Interestingly, this structure is usually sufficient to trigger the full immune response towards LPS. Apart from kdo, the inner core can vary in different species of LPS from different bacteria (Alexander and Rietschel 2001; Raetz and Whitfield 2002). In *Xcc*, however, the inner core contains not more than one kdo (Silipo et al. 2005). The outer core is comprised by mostly hexoses forming an oligosaccharide. The hexoses may vary in different species and also their length might vary, even in different LPS molecules on one bacterial cell. As example, in *Xcc* the core oligosaccharide is build up by a kdo, followed by a mannose and a glucose residue, to which two terminal mannoses may or may not be bound (Silipo et al. 2005). Furthermore, the core region often carries phosphate containing substituents (Alexander and Rietschel 2001). For *Xcc* it is reported that to the kdo and inner most mannose, galacturonic acid residues can be bound via phospho-di-ester groups or a phospho-amide group can be substituted (Silipo et al. 2005).

The longest and most exposed part of the LPS is also the most variable part, called O-antigen, O-chain, O-polysaccharide or short OA and it is bound to the core region. As the name suggests, it is a polysaccharide comprising repeating units of two to eight monosaccharide residues which may repeat up to 50 times (Alexander and Rietschel 2001). The composition of the O-antigen is highly species- and strain-specific and only very few bacterial strains have been shown to contain homopolymeric O-antigens (Alexander and Rietschel 2001). The O-antigen is not essential to the bacteria, without it the LPS is called R-LPS for rough-LPS and when the O-antigen is present, the LPS is called S-LPS or smooth-LPS (Figure 3-1, a). The names were given due to the bacterial colony morphology (Raetz and Whitfield 2002). However, for enterobacterial pathogens it is important to maintain the O-polysaccharide, since it protects

them from phagocytes, it protects the bacteria against the invasion of antimicrobial agents and can even mimic mammalian glycostructures (Alexander and Rietschel 2001).

The biosynthesis of LPS molecules originates, like for other saccharides, from the nucleotide sugar pools of the bacteria (Raetz and Whitfield 2002). The synthesis follows the general structure of LPS and therefore, the different enzymes responsible for LPS biosynthesis are encoded by different gene clusters (Raetz and Whitfield 2002). Best described is the lipid A biosynthesis in *E. coli*, but it is very similar in many other Gram negative bacteria. The responsible gene cluster for lipid A biosynthesis is called *lpx* and reactions start with the nucleotide sugar UDP-GlcNAc (UDP-N-acetyl-glucosamine) that is acylated with β -hydroxymyristate (3-OH C:14:0) by the acyl-transferase LpxA. The fatty acid is provided by an acyl-carrier-protein (ACP). In the next step the product is de-acetylated by an enzyme called LpxC followed by an acylation reaction and incorporation of a second β -hydroxymyristate, carried out by LpxD. The product is UDP-2,3-diacyl-glucosamine and again the fatty acid substrate is donated by an ACP-thioester. In the next reaction the UDP pyrophosphate bond is cleaved by the pyrophosphatase LpxH to form 2,3-diacyl-glucosamine-1-phosphate, termed lipid X. LpxB, is a disaccharide synthase that condensates lipid X with a UDP-2,3-diacyl-glucosamine and forms a β -1,6 bound lipid A disaccharide precursor. This molecule is phosphorylated at the 4' position by the kinase LpxK, using an ATP and creating a molecule called lipid IV_A. After the lipid IV_A is built, a specific reaction happens that explains why the inner core part kdo is essential and used as marker for LPS. Before the lipid A is completely synthesized, the core cluster enzyme WaaA transfers kdo onto the lipid IV_A, in *E. coli* two, in Xcc one (Raetz and Whitfield 2002; Silipo et al. 2005). Kdo donor is the sugar nucleotide CMP-kdo. Only after that the last steps of lipid A synthesis occur, since the acyl-transferases LpxL and LpxM require a kdo carrying substrate. In *E. coli* they add lauroyl and myristoyl, from acyl-ACP donors as secondary fatty acids to the distal glucosamine to form the completed lipid A. Different fatty acids can be incorporated at different temperatures, for example in *E. coli* *lpxL* has a homologue that is expressed at low temperatures and uses palmitoleate instead of lauroyl as substrate (Raetz and Whitfield 2002; Raetz et al. 2007). Additionally, the lipid A can be further modified, following growth condition changes, including temperature and pH. Different bacteria may react in specific manners (Raetz and Whitfield 2002; Whitfield and Trent 2014).

The core region is synthesized as elongation of the kdo containing lipid A. Mostly peripheral membrane enzymes with glycosyltransferase activity are needed (Whitfield and Trent 2014) and essential precursors for core biosynthesis are nucleotide sugars. The enzymes necessary for LPS core biosynthesis are encoded by operons in the *waa* gene cluster. Since the core region is not as conserved as the lipid A, the assembly might differ in distinct bacterial strains. As well as for the lipid A, model organisms for core biosynthesis are *E. coli* and *S. typhimorium*. Different bacteria may show a different set of enzymes, but sequencing of genomes from other bacteria, showed homologues to enzymes present in the model organisms (Raetz and Whitfield 2002). The first molecule in the *waa* gene cluster is called *waaA*. Still, the protein WaaA occurs already during lipid A biosynthesis to introduce kdo, like described above. Not many enzymes responsible for glycol-decorations of the inner core region are known and based on structure analysis, also in *Xanthomonas* enzymes for the addition of phosphate and galacturonic acid onto the kdo have to be present are, however, not yet described.

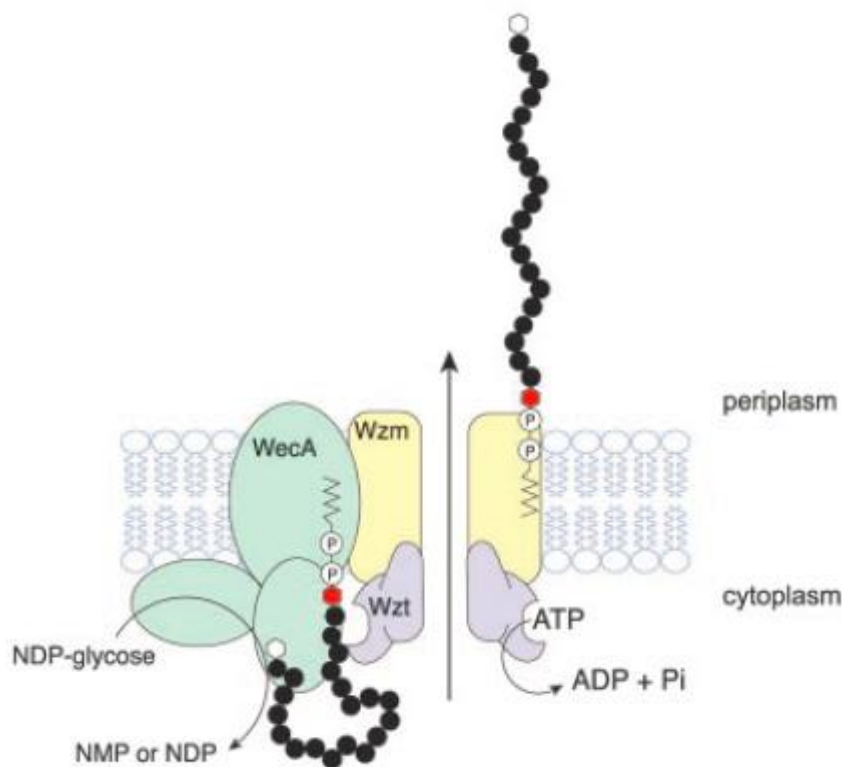


Figure 3-2: ABC-transporter dependent O-antigen synthesis and transport. Glycosyltransferases (green) use nucleotide sugars for the chain polymerization, while the ABC-transporter formed by Wzt (purple) and Wzm (yellow) hydrolyses ATP and translocates the lipid carrier-bound O-Antigen through the membrane. Adapted from Raetz and Whitfield 2002.

The outer core itself is an oligosaccharide, mostly compiled of hexoses, and shows a high variability between bacterial species. In Xcc, the precursor nucleotide sugar metabolism was described by Vorhölter and colleagues (2008) and the LPS structure was elucidated in 2005 by Silipo and others. Therefore, it is known that the first molecule after the kdo of the inner core in *Xanthomonas campestris* pv. *campestris* is a mannose. Then, a glucose follows as second hexose of the outer core region and a terminal mannose disaccharide can be non-stoichiometrically bound to the glucose. Since the LPS of Xcc contains either both terminal mannoses or none of them, it is likely that the disaccharide is built and then transferred to the glucose (Silipo et al. 2005).

The biosynthesis of the O-antigen varies in many ways between bacterial species, which might also explain its vast variability. However, the initiation of the synthesis happens when a sugar-1-P residue is transferred onto an UndP lipid carrier, forming an UndPP (undecaprenylpyrophosphate) intermediate. The pyrophosphate group later serves as energy donor for the ligation onto the Lipid A-core molecule (Raetz and Whitfield 2002). There are three different mechanisms described on how O-antigens can be polymerized, the Wzy-dependent, the synthase dependent and the ABC-transporter dependent pathway (Raetz and Whitfield 2002). Here the ABC-transporter dependent pathway should serve as example for the polymerization procedure (Figure 3-2), since Xcc uses this pathway and it is studied in *E. coli*. A homologue of the gene *wecA*, a GlcNAc-1-phosphate transferase, transfers GlcNAc-1-phosphate onto the UndP lipid carrier. This molecule serves as primer, before the O-antigen can be polymerized. First, an adapter molecule is bound between primer and polymer, in *E. coli* this is a single mannose added by WbdC (Raetz and Whitfield 2002). In contrast to the repeating unit moieties, the primer- and adapter-sugars occur only once per O-antigen. The polymerization is carried out by the successive addition of repeating unit sugar residues onto the non-reducing terminus of the UndPP lipid carrier acceptor. The responsible transferases can be monofunctional or can add multiple residues of a given linkage type (Raetz and Whitfield 2002). The O-antigen of *Xanthomonas campestris* pv. *campestris* was described by Molinaro et al. in 2003 for the strain 8004. It comprises repeating units of an α - and β -rhamnose backbone, to which N-acetyl-fucosamine (FucNAc) is bound as branch at every second rhamnose (Figure 3-3) (Molinaro et al. 2003). The precursor molecules originate from the nucleotide sugar pool. Data to reveal information about the identity of the precursors were mostly obtained through computational genome annotation of the strain Xcc B100

membranes and are driven by ATP hydrolysis. LptBFG form an ABC protein complex. The transport out of the inner membrane is initiated through LptFG and LPS molecules are transferred through the periplasmic components LptCAD_N. The C-terminus of LptD forms a large pore through the outer membrane with LptE sitting inside and occluding the channel (Whitfield and Trent 2014). Although *E. coli* and *Xcc* share many details regarding their LPS biosynthesis, it is known that the reported export machinery is not conserved throughout all bacteria (Whitfield and Trent 2014) and whether or not it is similar in *Xcc* is unclear.

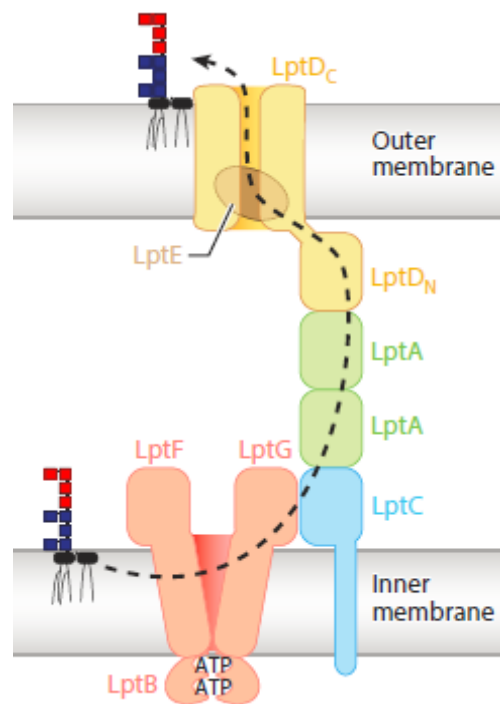


Figure 3-4: The LPS export machinery. Lpt proteins span the periplasm and the outer membrane. ATP hydrolysis is the driving force behind the transport. The LPS is extracted from the inner membrane and transported through a pore onto the outer membrane. Adapted from Whitfield and Trent, 2014.

Aim

The hypotheses to be tested was a putative competition between the LPS biosynthesis and xanthan production. The building blocks, meaning different nucleotide sugars and Undp lipid carrier, are common to both pathways, therefore a direct competition could be expected. To test this hypothesis, three distinct O-antigen mutant strains were chosen and should be analyzed towards their respective xanthan production and towards their LPS phenotypes.

Results

The genetic background of three Xcc B100 strains carrying mutations in the LPS O-antigen biosynthesis

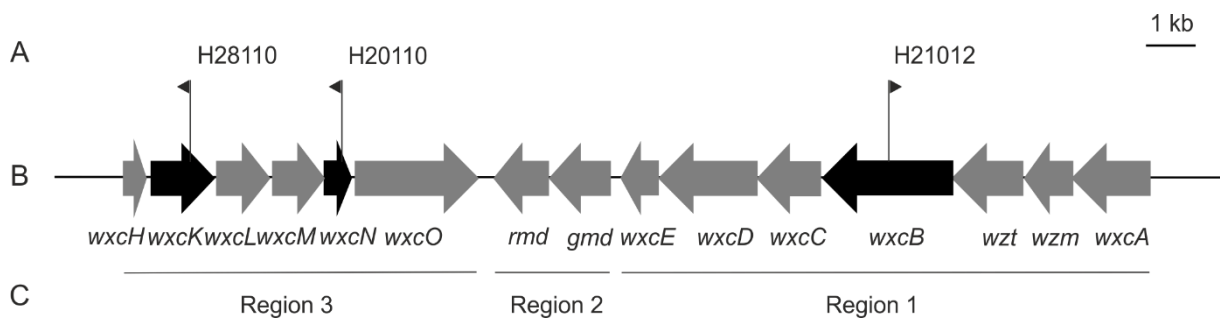


Figure 3-5: Genetic background of the LPS O-antigen biosynthesis in *Xanthomonas campestris* pv. *campestris* B100. A: Mutant names Xcc H21012 (*wxcB*), Xcc H28110 (*wxcK*) and Xcc H20110 (*wxcN*) and positions of Tn5 insertions in the Xcc B100 genome (Hötte et al. 1990; Vorhölter et al. 2001). The flag shows the orientation of the *lacZ* reading frame. B: Map of the *wxc* gene cluster including the conventional gene names. Mutated genes are shown in black. C: Functional organization of the gene cluster following the analyses of Vorhölter and colleagues (Vorhölter et al. 2001): Region 1 is putatively involved in the biosynthesis of the poly-rhamnan backbone, region 2 is crucial for the nucleotide sugars biosynthesis leading to GDP-rhamnose. Region 3 is putatively responsible for the N-acetyl-fucosamine branches of the Xcc O-antigen. Adapted from Steffens et al. 2016.

The *wxc* gene cluster in Xcc is responsible for the biosynthesis of its O-antigen (Figure 3-5). Initially, the gene cluster was identified by sequence analysis of the cosmid pXCB1002 (Hötte et al. 1990). Then, the genes were mutated by Tn5-*lacZ* transposon or intersposon insertions, allowing a first description of mutant phenotypes (Hötte et al. 1990; Vorhölter et al. 2001). The whole cluster was divided in three distinct regions (Figure 3-5). Region 1 comprises seven genes all of which seem to be essential for the O-antigen biosynthesis in Xcc (Vorhölter et al. 2001). Region 2 consists of two genes and both gene products are part of the nucleotide sugar

metabolism in Xcc (Figure 3-6). Functions for the gene products of Region 3 genes could not yet be attributed on the basis of experimental data, since no mutant phenotype could be detected. Annotation through sequence analysis however, revealed a putative function of region 3 gene products in the biosynthesis and transfer of a N-acetyl-3-amino hexose (Vorhölter et al. 2001). N-acetyl-fucosamine (FucNAc) was subsequently identified as part of the Xcc O-antigen (Molinaro et al. 2003), therefore the proteins from region 3 genes are most likely involved in the assembly of the OA branches.

Figure 3-6 shows a reconstructed metabolic pathway of the nucleotide sugar metabolism, under consideration of xanthan and the O-antigen of Xcc. Both, LPS and xanthan have a long history in *Xanthomonas* research, still it has never been tested if mutations in the LPS might affect xanthan production, although they even depend on the same precursor pool of nucleotide sugars (Vorhölter et al. 2008). For the approach to analyze the potential of O-antigen mutants for xanthan production, three mutant strains were chosen, Xcc H21012 (*wxcB*), H28110 (*wxcK*) and H20110 (*wxcN*), which were constructed by Hötte et al. (1990) as Tn5-*lacZ* insertions (Simon et al. 1989). The mutant in *wxcB*, H21012, is a *wxc* region 1 mutant and was previously described as OA lacking bacterial strain of Xcc (Vorhölter et al. 2001). The genes *wxcK* and *wxcN* of *wxc* region 3 do not share the same transcriptional unit with region 1 (Figure 3-5). Furthermore, in the initial phenotype characterization of those mutants no missing or altered O-antigen, as compared to the wild type, could be detected (Vorhölter et al. 2001). Still, both genes were assigned to putative functions in branching of the Xcc O-antigen (Figure 3-6) and therefore structural analyses should help to elucidate a specific phenotype. While for *wxcK* an annotation implies a function in the nucleotide sugar generation of the OA branch precursor dTDP-FucNAc, as thought for region 3 genes, no clear annotation was achieved for *wxcN* (Vorhölter et al. 2001). The executed approaches followed these considerations, with the aim to determine the LPS, especially, the OA phenotypes and to elucidate the impact of O-antigen mutations on xanthan production.

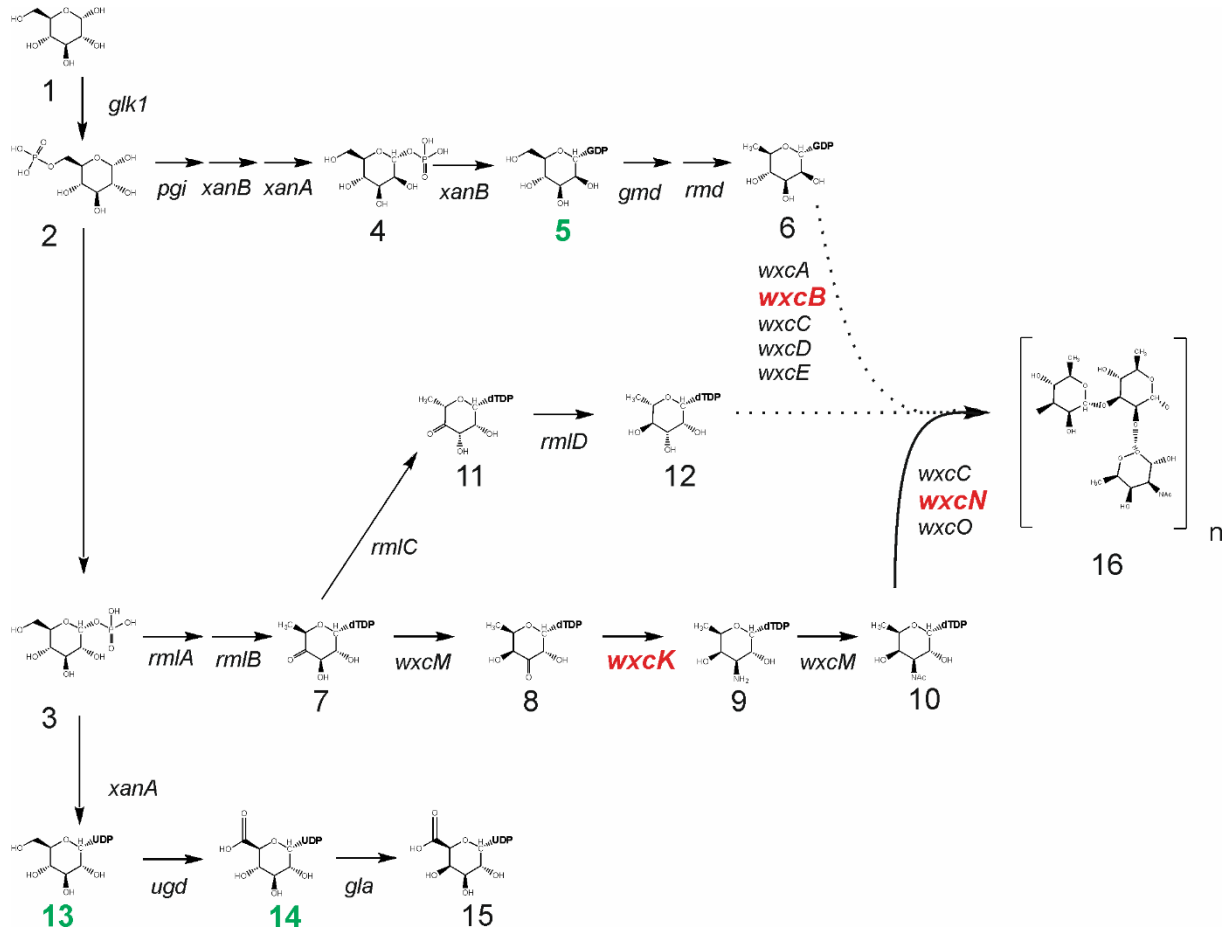


Figure 3-6: Relevant details of the *Xanthomonas campestris* pv. *campestris* nucleotide sugar metabolism producing precursors for the LPS O-antigen and the exopolysaccharide xanthan. Enzymatic reactions are indicated by arrows and names of the involved genes. Mutated genes of the strains Xcc H21012 (*wxcB*), Xcc H20110 (*wxcN*) and Xcc H28110 (*wxcK*) are shown in bold red letters at their respective position within the metabolic pathway. Molecules are numbered as follows: 1: D-glucose; 2: D-glucose 6-phosphate; 3: D-glucose 1-phosphate; 4: D-mannose 1-phosphate; 5: GDP-D-mannose; 6: GDP-D-rhamnose; 7: dTDP-4-keto-6-deoxy-D-glucose; 8: dTDP-3-keto-6-deoxy-D-galactose; 9: dTDP-3-amino-3,6-dideoxy-D-galactose (dTDP-D-fucosamine); 10: dTDP-N-acetyl-fucosamine; 11: dTDP-4-keto-6-deoxy-L-mannose; 12: dTDP-L-rhamnose; 13: UDP-D-glucose; 14: UDP-D-glucuronic acid; 15: UDP-D-galacturonic acid; 16: OA repetitive subunit, dashed lines indicate uncertainties regarding the OA biosynthesis from rhamnose precursors. Xanthan precursors (5, 13, 14) are marked in green. From Steffens et al. 2016.

Chemical analysis of the O-antigen in three Xcc B100 mutant strains: Xcc H21012 (*wxcB*), Xcc H20110 (*wxcN*) and Xcc H28110 (*wxcK*)

In order to analyze the O-antigen phenotypes, LPS were isolated applying the hot phenol / water method by Westphal and Jann (1965) from liquid Xcc cultures. Since xanthan production in minimal medium hinders LPS isolation, complex medium was used for cultivation. LPS constituents were first analyzed by GC after methanolysis and peracetylation of the LPS (Figure 3-7). Additionally, MALDI-TOF-MS with isolated LPS was performed (Figure 3-8). The

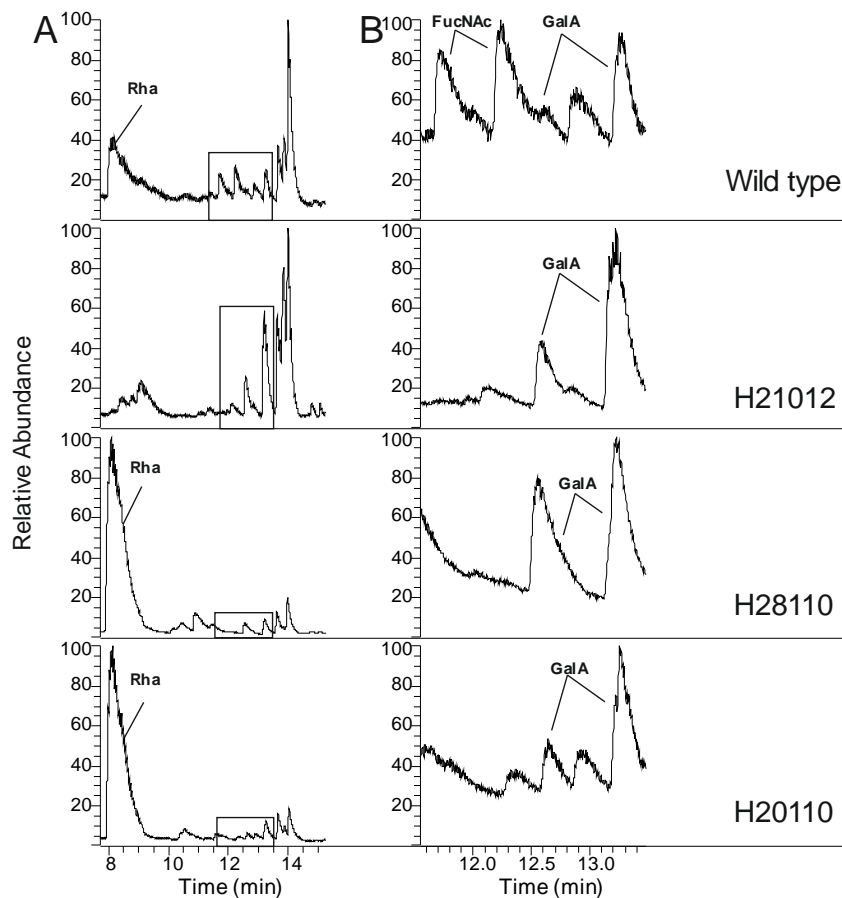


Figure 3-7: Analysis of the LPS O-antigen constituents of *Xanthomonas campestris* pv. *campestris* B100 wild type and derived mutant strains by gas chromatography following methanolysis. Wild type data are compared to H21012 (*wxcB*), H28110 (*wxcK*) and H20110 (*wxcN*). A: Complete chromatogram with the O-antigen main constituent rhamnose (Rha) followed by a box indicating signals related to the second O-antigen constituent N-acetyl fucosamine (FucNAc) and LPS core moieties. B: Zoom-in of the boxed area of the chromatogram with peaks identified as O-antigen constituent FucNAc and the LPS core constituent galacturonic acid (GalA). Both are represented by two peaks. Measurements were carried out after LPS isolation applying the hot phenol/water method followed by methanolysis with 0.5 M HCl in methanol and the respective peracetylation of 100 µg LPS. From Steffens et al. 2016.

previous study on the O-antigen of Xcc B100 by Vorhölter et al. used SDS-PAGE analysis to characterize the LPS (Vorhölter et al. 2001). Here the LPS should be studied by in depth structural analyses, especially to determine a phenotype for the region 3 mutants Xcc H20110 (*wxcN*) and Xcc H28110 (*wxcK*).

In Figure 3-7 the obtained GC-MS results are depicted, with peaks representing the LPS constituent derivatives. For the Xcc B100 wild type, a peak for rhamnose followed by a double peak of FucNAc were detected. Together these analytes represent the Xcc O-antigen (Molinaro et al. 2003). Following the OA constituents core saccharides eluted from the GC column, consisting of a galacturonic acid double peak, mannose and glucose (Figure 3-7), all have been described by Silipo and colleagues (Silipo et al. 2005). In addition to the GC-MS analysis, MALDI-TOF-MS was carried out. For the Xcc B100 wild type, mass deviation revealed the presence of repeating units by rhamnose and FucNAc (Figure 3-8).

The mutant strain Xcc H21012 (*wxcB*) showed different results during structural investigations. Here no peaks for rhamnose, nor for FucNAc could be detected via GC-MS (Figure 3-7). Thus indicating that no O-antigen is present in the mutant strain. These results were validated by the MALDI-TOF-MS measurement, as no OA repeating units could be observed (Figure 3-8). However, the spectra of Xcc H21012 (*wxcB*) were used to assign masses to lipid A and rough-type LPS moieties, since no O-antigen signals were overlapping. The masses were calculated in agreement to the initial compositional determination by Silipo and colleagues for Xcc LPS (Silipo et al. 2005). Two forms of lipid A moieties were detected, a tetra- and a penta-acylated form. Furthermore, typical heterogeneity in fatty acid composition could be shown for both lipid A residues (Figure 3-8).

In a study prior to this work, no phenotype could be detected for *wxc* region 3 mutants (Vorhölter et al. 2001), yet here the GC analysis of Xcc H28110 (*wxcK*) showed unexpected peak deviations. No FucNAc signals could be observed, unlike in the Xcc B100 wild type LPS, which indicated the inhibition of the FucNAc side branches. Moreover, a vast increase in rhamnose was detected, indicated by the peak intensity compared to the wild type (Figure 3-7), while of both LPS species 100 µg were used. These results needed to be verified by MALDI-TOF-MS and indeed the mass spectra and their respective patterns appeared to be strikingly different from the wild type (Figure 3-8). The MS peaks showed a regular deviated pattern,

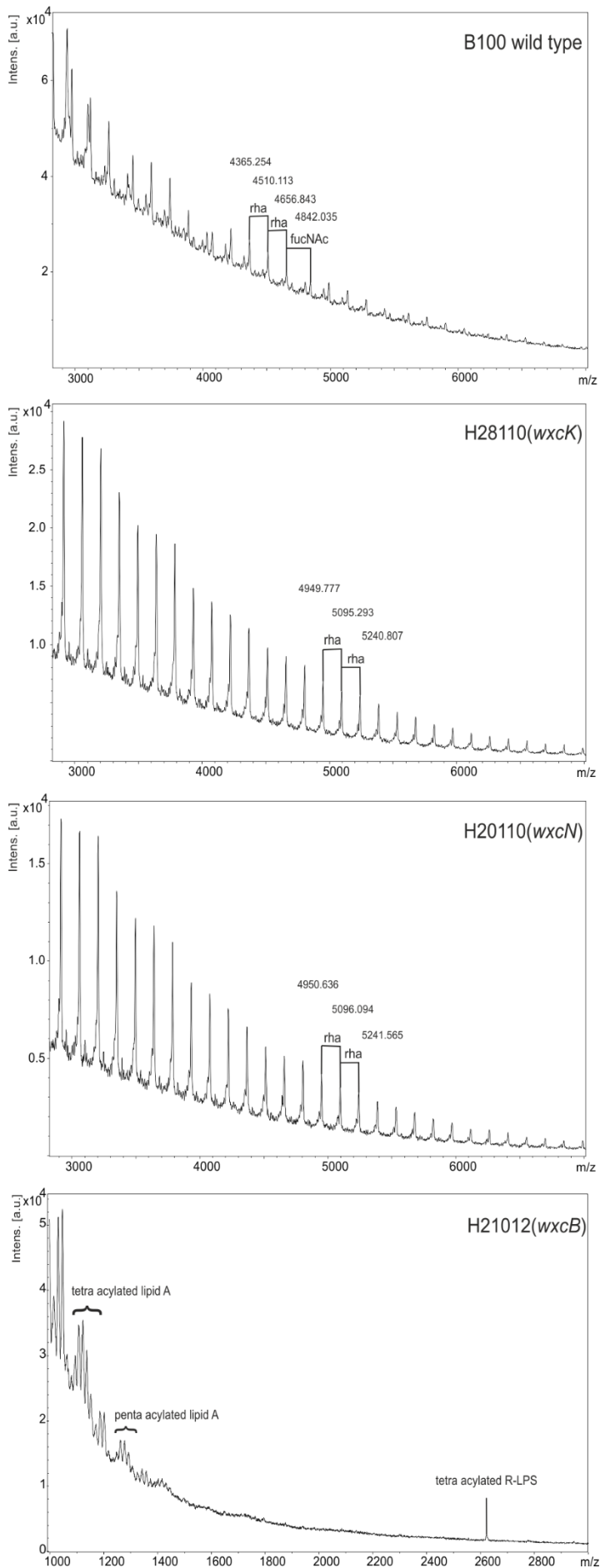


Figure 3-8: MALDI-TOF-MS analysis of the LPS O-antigen of *Xanthomonas campestris* pv. *campestris* B100 wild type, the O-antigen branch mutants Xcc H28110 (*wxcK*) and Xcc H20110 (*wxcN*) and O-antigen deficient mutant Xcc H21012 (*wxcB*). Spectra related to the mutants Xcc H28110 (*wxcK*), Xcc H20110 (*wxcN*) and to the wild type O-antigen were compared in order to verify the inhibition of the OA side branches and the increase in rhamnose moieties. Displayed are ranges of the spectra with a focus on the O-antigen constituents, rhamnose (rha) and N-acetyl fucosamine (FucNAc). Examples of repeating peaks are highlighted. No OA residues were detected in the LPS of H21012 (*wxcB*), but different lipid A moieties and a peak representing the rough-type LPS could be measured. Measurements were carried out with 5 μ g LPS of each strain. From Steffens et al. 2016.

with peaks occurring after 145 – 146 Da, representing OA backbone constituent rhamnose. The increased peak heights and areas, as compared to the same amount of wild type LPS, confirmed the increased amount of rhamnose moieties.

Results obtained by analyses of Xcc H20110 (*wxcN*) LPS showed similarities to the results of H28110 (*wxcK*). Also prior to this work no phenotype could be assigned to the mutant strains. Both GC profiles looked quite similar, no FucNAc could be detected, while an enlarged peak of rhamnose was observed (Figure 3-7). MALDI-TOF-MS data also showed highly regular spectra with peaks that differed in 145 – 146 Da, again representing rhamnose. Moreover, the peaks showed an increased area (Figure 3-8), thus supporting the GC results.

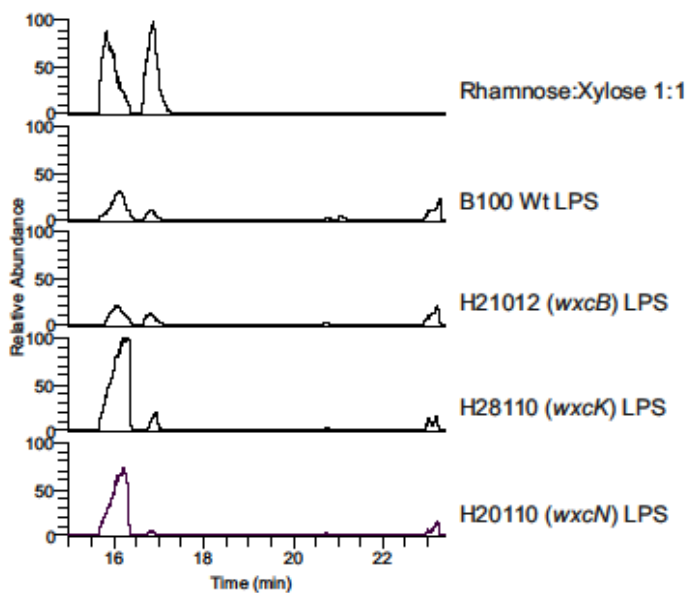


Figure 3-9: GC chromatograms of a rhamnose:xylose 1:1 (20 µg) standard, Xcc B100 wild type and OA mutant strains. Due to the standard peaks a response factor for rhamnose towards xylose could be calculated. B100 Wild type data were compared to the *wxcB* mutant H21012, *wxcK* mutant H28110 and *wxcN* mutant H20110 towards their rhamnose amounts, after hydrolysis and reduction of 500 µg LPS. Standard chromatogram is depicted as zoom to optimize the view. From Steffens et al. 2016.

Table 3-1: Analysis of the O-antigen constituent rhamnose of *Xanthomonas campestris* pv. *campestris* B100 wild type and three mutant strains. Results were obtained by gas chromatography following hydrolysis and reduction of 500 µg LPS each. The depicted amounts are the mean values of two peracetylated replicates. For the *wxcB* mutant H21012 only one measurement could be used. From Steffens et al. 2016.

Strain	Rhamnose (µg)	Standard Deviation (µg)	Percentage of rhamnose in the total LPS (%)	Rate of Rhamnose as compared to Xcc B100
Xcc B100	80.6	10.5	16	1
Xcc H21012 (<i>wxcB</i>)	45.5	--	9	0.56
Xcc H28110 (<i>wxcK</i>)	255.8	2.2	51.5	3.17
Xcc H20110 (<i>wxcN</i>)	403.6	8.5	80.5	5.01

In order to get deeper insights into the obtained results, especially with regard to the amounts of OA constituent rhamnose, quantitative sugar analysis was performed. Therefore, LPS was hydrolyzed followed by reduction of the sugar residues and peracetylation. As internal standard, 15 µg of xylose was used. To calculate the amounts of rhamnose out of the standard, a response factor of rhamnose as compared to xylose had to be determined. The obtained GC chromatograms are shown in Figure 3-9 (validation measurement: Supplementary figure 1) and the calculated values are depicted in Table 3-1 (calculation: Supplementary table 1). The calculated rhamnose amounts of 255.8 µg and 403.6 µg for Xcc H28110 (*wxcK*) LPS and H20110 (*wxcN*) LPS, respectively, strikingly confirmed the previously described results, since the Xcc B100 wild type LPS showed a total rhamnose content of 80.6 µg. These amounts equaled for more than three times as much rhamnose as in the B100 wild type LPS for the *wxcK* mutant and even five times more in the *wxcN* mutant (Table 3-1). Further, the percentage of rhamnose in the total LPS was calculated. 16% of the Xcc wild type LPS were rhamnose, while 51.5% in H28110 (*wxcK*) and 80.5% in H20110 (*wxcN*) showed to be rhamnose (Table 3-1). Surprisingly, also in the *wxcB* mutant H21012 rhamnose signals were detected. A total amount of 9% or 45.5 µg was observed, which accounted for approximately half of what was detected in the wild type. Still, both the GC after methanolysis and especially the MALDI-TOF-MS (Figure 3-7, Figure 3-8) showed no signals of an OA in the *wxcB* mutant. Based on the obtained results a model for the LPS phenotypes of the three mutant strains, as compared to the B100 wild type was constructed (Figure 3-10). For Xcc B100 the established LPS structure was analyzed, while for every mutant a LPS phenotype was detected. Data from LPS analysis after methanolysis and essentially the MALDI-TOF-MS measurements supported the assumption that Xcc H21012 (*wxcB*) comprises no O-antigen, but a rough-type LPS (Figure 3-10). Additionally, following the results depicted in Figure 3-7, Figure 3-8 and in Table 3-1, for the first time a LPS phenotype for Xcc *wxc* cluster region 3 mutants could be assigned. In both mutants, Xcc H28110 (*wxcK*) and H20110 (*wxcN*), no side branch residue FucNAc could be detected. However, in either of the mutants a vast increase in rhamnose moieties was analyzed, supporting a LPS phenotype without side branches, but with prolonged rhamnose backbone, as shown in Figure 3-10.

Next to the LPS phenotypes, the xanthan phenotypes should be determined to distinguish the impact of the mutations.

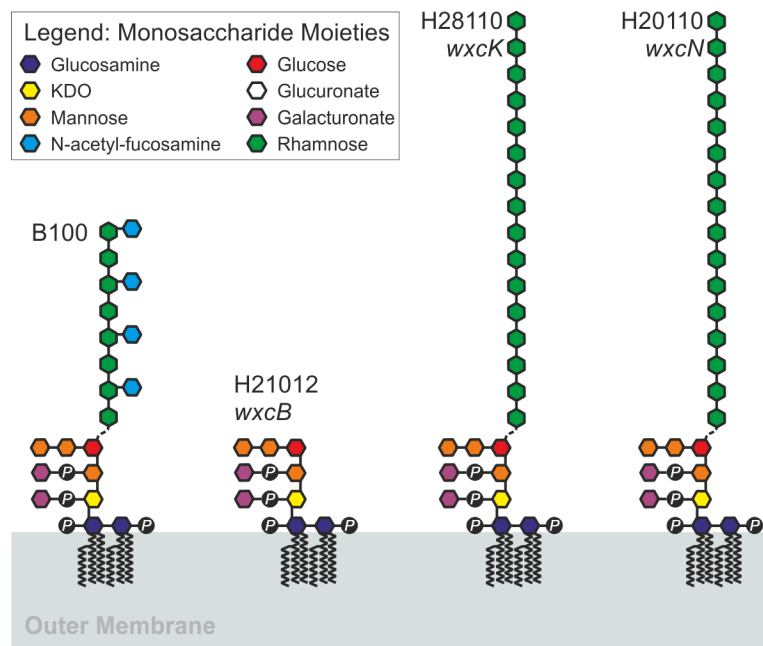


Figure 3-10: Model of putative LPS structures of the *Xanthomonas campestris* pv. *campestris* B100 wild type and the mutants Xcc H21012 (*wxcB*), Xcc H28110 (*wxcK*) and (*wxcN*) following obtained results. Data indicated an elongation of the O-antigen rhamnose main chain in both of the branchless mutants, implying that the FucNAc branches play a role in O-antigen chain length determination. The linkage type between the rough-type LPS to the O-antigen is unknown and thus shown as a dashed line. The legend indicates the monosaccharide moieties. From Steffens et al. 2016.

Xanthan production of the analyzed Xcc B100 O-antigen mutant strains

All Xcc strains were grown in shaking flasks, simultaneously and under the same conditions of 30°C and 180 rpm. As medium, XMD minimal medium (Schatschneider et al. 2013) containing 0.6 g nitrate per liter as nitrogen source and 30 g per liter glucose was applied. To test the effects of O-antigen mutations on xanthan production, xanthan harvest occurred after 96 h. Example cultivations are shown in Figure 3-11, depicted values however, also include two further cultivation approaches, which can be found in the Supplement (Supplementary figure 2).

The Xcc B100 wild type stopped growing and entered the stationary culture phase after approximately 50 h at OD600 values of around 1.5 – 1.7 (Figure 3-11), with a mean growth rate of 0.053 h⁻¹. During the course of the whole cultivation 15 – 19 g l⁻¹ glucose were consumed by the B100 wild type, implying that glucose was not a limiting factor, since substantial amounts remained as resource for xanthan production in the stationary phase

(Figure 3-11). Nitrate concentration was inversely correlated to the growth, meaning that the culture stopped growing when nitrate exhaustion was reached. In the wild type cultivation nitrate was consumed after around 48 h (Figure 3-11).

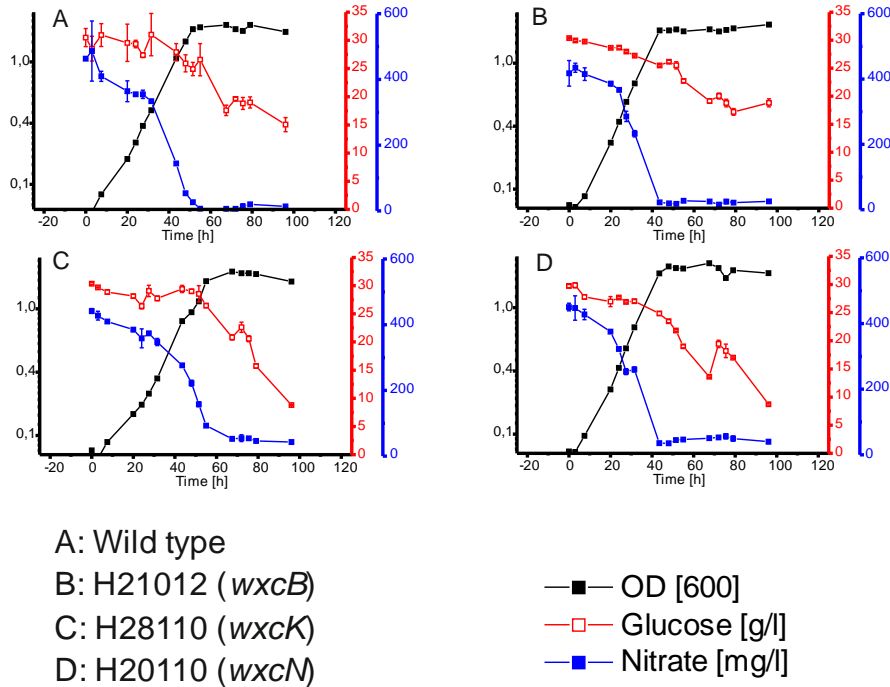


Figure 3-11: Cultivation of the *Xanthomonas campestris* pv. *campestris* B100 wild type (A), mutants Xcc H21012 (*wxcB*) (B), Xcc H28110 (*wxcK*) (C) and Xcc H20110 (*wxcN*) (D). All strains were grown in XMD minimal media with $0.6 \text{ g l}^{-1} \text{ KNO}_3$ as nitrogen source and supplemented with 30 g l^{-1} glucose as carbon source, at 30°C and 180 rpm. The cultivation occurred simultaneously under the same conditions for 96 h. Displayed are the culture titer (OD), glucose and nitrogen concentration over time. From Steffens et al. 2016.

Cultures of the O-antigen mutant Xcc H21012 (*wxcB*) started to enter the stationary phase after around 44 h at OD600 values of approximately 1.6 to 1.8, representing an enhanced mean growth rate of 0.062 h^{-1} as compared to the wild type (Figure 3-11). With $10 - 13 \text{ g l}^{-1}$ Xcc H21012 (*wxcB*) consumed less glucose than the wild type. Still, the nitrate showed to be the limiting growth factor with an exhaustion after 44 h. The faster nitrate consumption of the *wxcB* mutant was in agreement with the accelerated culture growth (Figure 3-11).

The slowest growth, as compared to the other strains, was measured in the Xcc H28110 (*wxcK*) strain. After approximately 67 h and optical densities of OD600 1.7 – 1.9 the strain entered the stationary phase, representing a mean growth rate of 0.043 h^{-1} (Figure 3-11). Although the cultures of the *wxcK* mutant grew slower, their maximum OD values were not affected. Furthermore, it was detected that the glucose consumption was increased in contrast to the wild type as well as the *wxcB* mutant. Cultures of H28110 (*wxcK*) consumed more than 20 g l^{-1}

of glucose (Figure 3-11), one of three cultures used even all of the 30 g l⁻¹. Yet, the nitrate concentration inversely followed the culture growth like in the other strains and reached a limiting level after around 67 h (Figure 3-11).

Unlike in the LPS phenotypes, the growth phenotypes of H28110 (*wxcK*) and Xcc H20110 (*wxcN*) were different. The stationary phase was entered after around 50 h with a mean growth rate of 0.059 h⁻¹ and OD600 values reached up to 2, which even exceeded the Xcc B100 wild type strain (Figure 3-11). Remarkably, the glucose consumption of the *wxcN* mutant was quite similar to the *wxcK* mutant, as more than 20 g l⁻¹ of glucose was used in every culture (Figure 3-11). Most of the given nitrate was consumed after 44 h, again correlating with a growth arrest (Figure 3-11).

In order to reveal significant insights into *Xanthomonas campestris* glycobiology, xanthan analyses are an essential asset. Here the production was measured as dry weight [g] xanthan per [g] biomass of ten replicates (Supplementary tables 2 and 3). This way the impact of hindering effects during sample handling with viscous xanthan solutions should be minimized. Samples were harvested after 96 h late in the stationary phase, to ensure a maximized production for all strains.

The xanthan production of OA mutant Xcc H21012 (*wxcB*) showed a significant increase as compared to the B100 wild type. With approximately 6.3 g g⁻¹, the production represented an increase of more than 1 g xanthan per g biomass (Figure 3-12). On the contrary neither of the side branch mutants H28110 (*wxcK*) and H20110 (*wxcN*) showed a relevant increase in productivity (Figure 3-12). The B100 wild type produced about 5 g g⁻¹, while the mutants Xcc H20110 (*wxcN*) and H28110 (*wxcK*) produced 5.5 and 5.3 g xanthan per g biomass, respectively.

Significance was tested with the help of a t-test and the calculated p-values are 0.03 for the *wxcB* mutant, 0.94 for the *wxcK* mutant and 0.42 for the *wxcN* mutant.

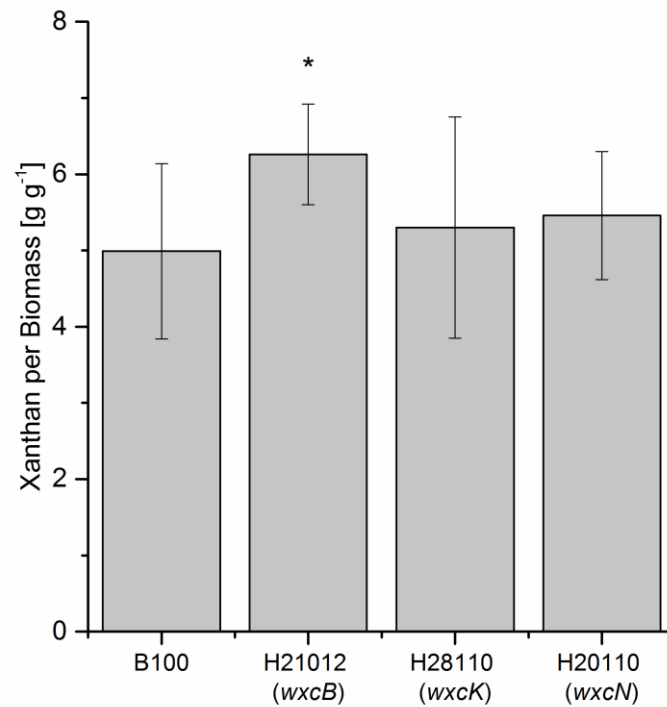


Figure 3-12: Xanthan production of *Xanthomonas campestris* pv. *campestris* B100 wild type and derived mutants H21012 (*wxcB*), H28110 (*wxcK*) and H20110 (*wxcN*). Production was measured as dry weight [g] xanthan per [g] biomass. Samples from 10 replicates each (Supplementary tables 2 and 3). Harvest was after 96 h in the late stationary phase. Bars give the normalized mean xanthan yields, with error bars indicating the standard deviations. Xanthan production was compared in regard to Xcc B100 production. * indicates a *p*-value of < 0.05. From Steffens et al. 2016.

Discussion

Inhibition of the Xcc O-antigen biosynthesis and the possible impact for xanthan production approaches

The genes for mutational analyses were carefully chosen, after studying the metabolic network of the nucleotide sugars as well as LPS biosynthesis. Naturally, it was important that the xanthan production is not negatively affected and furthermore, it was important to inhibit only unessential parts of the LPS biosynthesis. In general, it has never been possible to obtain LPS free mutants, at least the lipid A is needed to maintain an outer membrane barrier (Raetz and Whitfield 2002). Therefore the O-antigen was used as target, since the genes encoding are not essential and the LPS structure should provide stable cells that are able to survive industrial cultivations. On the other hand, the building blocks used for the O-antigen are still considerable. In *E. coli* 75% of the cellular surface are covered by LPS, whereby the OA, as a polysaccharide, requires most of the nucleotide sugars during LPS biosynthesis (Raetz and Whitfield 2002). Next to the savings in sugar precursors, the availability of lipid carriers, which are shared by LPS and xanthan production (Raetz and Whitfield 2002; Vorhölter et al. 2008), might be favorable for xanthan production.

Initially, the gene *wxcB* was chosen for analysis, since in a previously performed LPS analysis on Xcc H21012 (*wxcB*), no signs of an OA could be detected (Vorhölter et al. 2001). The gene is located in region 1 of the O-antigen biosynthesis cluster *wxc*. Genes located in this cluster are thought to be essential parts of the Xcc OA biosynthesis, since their products are responsible for the poly-rhamnan backbone construction (Vorhölter et al. 2001). Although the gene is described with a putative kinase function essential for the Xcc O-antigen (Vorhölter et al. 2001), the precise function remains obscure. Nevertheless, a recent study in *Xanthomonas euvesicatoria* (Jones et al. 2004), formally *X. campestris* pv. *vesicatoria*, predicted *WxcB* to be an important factor in cellular motility as well as in cell wall and membrane synthesis (Park et al. 2014). Additionally, Park and colleagues reported increased biofilm production for a *wxcB* mutant. Since xanthan builds up the matrix of the Xcc biofilm, the reported increase could be connected to xanthan production (Crossman and Dow 2004; Torres et al. 2007). However, although the LPS was analyzed, no effects were detected in the *Xanthomonas euvesicatoria wxcB* mutant (Park et al. 2014).

An additional target was the gene *wxcK*, which is located within the *wxc* cluster region 3. Genes of this cluster are putatively involved in O-antigen branching, which in Xcc means, they are involved in biosynthesis or transfer of FucNAc residues. The gene *wxcK* is reported to encode for an enzyme that is involved in the synthesis of dTDP-FucNAc, the precursor nucleotide sugar for the Xcc OA (Vorhölter et al. 2001). As a third target, the gene *wxcN* was used. Like *wxcK*, *wxcN* is part of region 3 within the *wxc* gene cluster. It encodes for a small membrane protein that is putatively involved in O-antigen branching (Vorhölter et al. 2001), possibly by the transfer of FucNAc residues. Although the branches of the O-antigen do not account for as many resources, compared to the whole O-antigen, it was thought that this approach might be sensible, since still considerable amounts of resources might be saved. Around one third of the Xcc O-antigen should consist of FucNAc (Molinaro et al. 2003) and for each branch an UndP lipid carrier might be saved, because each sugar residue is bound to one lipid carrier (Vorhölter et al. 2001). Moreover, the approach to inhibit only the branches of the O-antigen represents the smallest intrusion, considering the cellular stability and taken into account that the strains should be feasible for industrial cultivations.

The LPS of applied mutant strains Xcc H28110 (*wxcK*) and Xcc H20110 (*wxcN*) was previously analyzed, yet no alterations in the O-antigen could be detected (Vorhölter et al. 2001). However, analyses were carried out applying SDS-PAGE, therefore in depth analyses to reveal the exact chemical composition should help to elucidate a phenotype for *wxc* region 3 mutants and validate their putative functions as essential for OA branching.

Polar effects of the Tn5 insertions cannot be excluded. Still, for this study it was not essential to describe distinct gene functions. In order to analyze if mutants of genes necessary for the O-antigen biosynthesis are feasible targets for an enhanced xanthan production, only an inhibiting effect on the OA was crucial. Furthermore polar effects affecting both, region 1 and region 3, can be excluded, as they do not belong to the same transcriptional unit.

Structural analyses of LPS from Xcc H21012 (*wxcB*), H28110 (*wxcK*) and H20110 (*wxcN*) revealed altered O-antigen phenotypes

For a structural analysis of the LPS from H21012 (*wxcB*), H28110 (*wxcK*) and H20110 (*wxcN*), compared to the Xcc B100 wild type LPS, GC analysis was performed after methanolysis and peracetylation of purified LPS samples. Additionally MALDI-TOF-MS was performed. In a

previous study in 2001 these LPS species have been briefly characterized by gel electrophoresis (Vorhölter et al. 2001), however, GC and MALDI-TOF-MS analyses are able to reveal structural details that cannot be resolved on a gel. Therefore especially the previous inconspicuous results of Xcc H20110 (*wxcN*) and Xcc H28110 (*wxcK*) LPS characterization could be re-evaluated.

First, Xcc wild type B100 was used for GC and MALDI-TOF-MS measurements and in both approaches the molecular residues of rhamnose and FucNAc could be detected, which is in accordance to the described structure (Molinaro et al. 2003). The MALDI-TOF-MS experiment even revealed nicely how the repeating units were distributed.

In contrast to that the data obtained by GC and especially by the MALDI-TOF-MS experiment showed that the O-antigen was not present in the *wxcB* mutant. No signs of a distribution of repeating units, like in Xcc B100, could be detected. Therefore, data previously obtained by Vorhölter and colleagues (Vorhölter et al. 2001), can be confirmed on a deeper molecular level. Moreover, the revealed MALDI-TOF-MS data of mutant Xcc H21012 (*wxcB*) could be used to identify LPS core and lipid A residues, which is difficult when the O-antigen is present, since they are overlaid by OA peaks. Different species of core-lipid A residues, which are often composed by various or different amounts of fatty acids, could be calculated. All detected molecules were in accordance to the structural Xcc LPS determination by Silipo and colleagues (Silipo et al. 2005). Yet, in depth quantitative sugar analysis surprisingly revealed around half of the amount of rhamnose that was found in Xcc B100 LPS, was found in Xcc B100 H21012 (*wxcB*). Still, it is arguable that no OA was part of the LPS of the *wxcB* mutant H21012. This was confirmed by the MALDI-TOF-MS. The spectra clearly showed that no O-antigen was present, otherwise OA signals would have been measured, just like in the Xcc B100 spectra. Therefore, the rhamnose in the Xcc H21012 (*wxcB*) sample might not have originated from the LPS itself, but e. g. from intermediate precursors which were isolated along the LPS. Since only some structural similarities of the *wxcB* gene product to the N-terminal and central methyltransferase as well as kinase domains of *E. coli* O9 WbdD were detected (Hagelueken et al. 2012), the function of WxcB is still obscure. Therefore it could be possible that the O-antigen is indeed synthesized, but the transfer might be inhibited. Different results were published for a *wxcB* mutant in *X. euvesicatoria* by Park and colleagues. In their mutant, they did not detect a LPS phenotype that differed from the wild type in a gel-electrophoresis based analysis (Park et al. 2014). It could already be shown that in depth chemical analyses can reveal

phenotypes that are not resolvable on a gel, however also polar effects of the Tn5 insertion in the used strain Xcc H21012 (*wxcB*) cannot be excluded. Furthermore, fundamental differences in the repertoire of LPS biosynthetic genes between *X. campestris* pv. *campestris* and *X. euvesicatoria* are known (Thieme et al. 2005), hence it is unclear whether the specific role of *wxcB* is similar in both bacterial species. Overall, the obtained results support the findings of Vorhölter and colleagues that no O-antigen is present in the LPS of Xcc H21012 (*wxcB*) and that *wxc* region 1 is essential for Xcc LPS O-antigen biosynthesis (Vorhölter et al. 2001), as depicted in the LPS model of this work (Figure 3-10).

A *wxcK* mutant should be inhibited in the generation of dTDP-FucNAc, the putative precursor of the Xcc O-antigen branches (Vorhölter et al. 2001). Nevertheless, since no phenotype that might hint towards LPS alteration was detected in a first study of Xcc H28110 (*wxcK*) (Vorhölter et al. 2001), the obtained GC results for its LPS were unexpected. The FucNAc signal that was clearly identified in the Xcc B100 wild type LPS chromatogram, could not be observed in the *wxcK* mutant strain. This indicates that Xcc B100 H28110 (*wxcK*) is indeed a mutant not capable of synthesizing the O-antigen side branches. Moreover, the striking increase in rhamnose was a second, unexpected change in the LPS structure, as compared to the wild type molecule. Both results that were separating the LPS of H28110 (*wxcK*) from Xcc B100 LPS could be confirmed by MALDI-TOF-MS. The observed, regular pattern of mass peaks indicated a homopolymer and the mass deviations in between the peaks pointed towards rhamnose as component of that polymer. Furthermore, the peak heights also indicated a notable increase in rhamnose moieties. All obtained results support the presence of a novel, yet undescribed, LPS phenotype with an elongation of the O-antigen backbone, while no branches are present. The exact same phenotype was observed in the mutant Xcc B100 H20110 (*wxcN*) that was also tested before and without resolving of a phenotype (Vorhölter et al. 2001). Thus, the novel findings of the *wxcK* mutant LPS got verified. Further, these results indicated the essential role of *wxc* cluster region 3 for the O-antigen branches.

After purifying of the sugar components from the LPS and addition of an internal standard, the exact amounts of sugars in the different LPS species could be determined with the help of a reference factor. This way it was possible to state if the changes in rhamnose moieties were really considerable. With three and five times as much rhamnose as the wild type for H28110 (*wxcK*) and H20110 (*wxcN*), respectively, the previous GC and MALDI-TOF-MS results were strikingly confirmed, showing a significant increase of rhamnose in the O-antigen backbone.

Taken together, obtained results strongly support a novel Xcc LPS phenotype, where the absence of the OA branches leads to an elongation of rhamnose based O-antigen main chain. This indicated that the O-antigen backbone in Xcc is synthesized independently of the branching FucNAc molecules, as was already described for *X. campestris* pv. *vitians* (Molinari et al. 1999). Chain length regulation in LPS is still under debate and in 2014 King and colleagues described a variable geometry model (King et al. 2014). In their study a model based on the abundance of two proteins, WbdA and WbdD, was proposed. The obtained results fit nicely for the tested *E. coli* O9a OA length distribution, however, for Xcc B100 the FucNAc branches seem to be important in the determination of the OA chain length, as was shown in this study. In contrast to the Xcc B100 LPS, the *E. coli* O9a O-antigen is not branched, therefore the model of King and colleagues might simply not be applicable or has to be extended for the Xcc or branched O-antigens in general.

Characterization of cultivation phenotypes by Xcc B100 and derived mutant strains Xcc H21012 (*wxcB*), H28110 (*wxcK*) and H20110 (*wxcN*)

Other than determining the LPS phenotypes, a major goal was to determine the xanthan production of the three mutant strains Xcc H21012 (*wxcB*), H28110 (*wxcK*) and H20110 (*wxcN*) as compared to the B100 wild type.

During cultivation a differential behavior concerning glucose consumption could be detected, as both branchless mutants, Xcc H28110 (*wxcK*) and Xcc H20110 (*wxcN*), consumed more glucose than the wild type. Yet, the xanthan production was rather unaffected. In contrast, the Xcc H21012 (*wxcB*) mutant took up less glucose than Xcc B100, while the xanthan production was significantly increased. These findings hint towards a differential usage of glucose in the mutants as compared to the wild type. Xanthan is mainly produced during the stationary phase, after nitrogen supply becomes the limiting growth factor and there is still a carbon source available in the medium (Kreyenschulte et al. 2014). This was in accordance to the growth and nitrate consumption of the best xanthan producer Xcc H21012 (*wxcB*) which was 3 – 8 h faster than in the wild type, although less glucose was used in total. However, similar nitrate consumption was detected in Xcc H20110 (*wxcN*), which showed no increase in xanthan production.

Overall, it can be summarized that the nitrate consumption was indeed the limiting growth factor for all tested strains, but the remaining glucose was not entirely used for xanthan production. This indicated a differential usage of glucose in the mutant strains and in the B100 wild type. For instance, the O-antigen phenotype of the tested mutant strains indicated another usage of nucleotide sugar precursors. In Xcc B100 other and different amounts of nucleotide sugars had to be used as compared to Xcc H28110 (*wxcK*) and Xcc H20110 (*wxcN*), in which no dTDP-FucNAc could be consumed, but more of rhamnose containing nucleotide sugars were needed. Furthermore, in Xcc H21012 (*wxcB*) putatively less nucleotide sugars were used for the O-antigen expression. How exactly the differential glucose consumptions are connected to the nucleotide sugar metabolism remains unclear and more research effort has to be put into resolving this question. However, a maintenance coefficient of 0.33 mmol glucose per g and h was established for modeling the Xcc metabolism (Letisse et al. 2002; Schatschneider et al. 2013). This might serve as a start for modelling the O-antigen mutants in a large scale metabolic model and eventually determine the glucose flux. In any case, the results, especially in Xcc H21012 (*wxcB*), indicated that it is possible to alter the glucose usage by inhibiting competing pathways, like the O-antigen biosynthesis.

The influence of a missing or modified LPS O-antigen on the xanthan biosynthesis in Xcc B100

In general the results obtained for Xcc H21012 (*wxcB*) are in agreement with results from *X. euvesicatoria*, since Park and colleagues reported an increase in biofilm production for a *wxcB* mutant and considering that xanthan builds the matrix of the *Xanthomonas* biofilm (Crossman and Dow 2004; Park et al. 2014). Furthermore, the results indicate a connection between LPS and xanthan biosynthesis, as the inhibition of the O-antigen led to an enhanced xanthan production. This connection might well occur on the level of nucleotide sugar precursors, because the building block nucleotide sugars for both, xanthan and LPS, are closely connected (Vorhölter et al. 2001; Vorhölter et al. 2008). It could be possible that the unrequired precursors for LPS or OA biosynthesis were redirected towards xanthan production. However, an additional factor could be the availability of not only building blocks, but for O-antigen biosynthesis unused undecaprenyl lipid carrier, which are important molecules in xanthan as well as LPS biosynthesis (Raetz and Whitfield 2002; Vorhölter et al.

2008; Hublik 2012). Still, the increased production of biofilm and xanthan could as well be explained by the change of the bacterial surface characteristics, due to a lack of O-antigen polysaccharides. Additionally, a decreased motility was measured in Xcc H21012 (*wxcB*) (data not shown) that was also reported for *X. euvesicatoria* (Park et al. 2014). This might further support the increase in xanthan production, since a general connection between down regulation of cell motility and start of biofilm production was observed for *Escherichia coli* and *Pseudomonas aeruginosa* (Lavery et al. 2014).

The detected LPS or O-antigen phenotypes for the mutants Xcc H20110 (*wxcN*) and Xcc H28110 (*wxcK*), could explain their unremarkable xanthan production. Putative reasons for an enhanced xanthan production while the O-antigen is inhibited are e. g. the increased availability of xanthan precursor nucleotide sugars or a compromised bacterial surface. However, both reasons are not applicable for the mutants in *wxcK* and *wxcN*. Both mutants showed a longer than normal O-antigen main chain, while the branches were missing. This indicated that no sugar nucleotides were saved during O-antigen production. Also, due to the long O-antigen backbone, no significant alterations in the bacterial surface as compared to the wild type strain condition should have occurred. It is difficult to point out explanations for an increased biosynthesis towards the O-antigen rhamnose backbone, while the FucNAc branches are inhibited, since the LPS biosynthesis in xanthomonads is not fully understood. It seems that branching of the O-antigen is a limiting step in its biosynthesis. Enzymes with a higher turnover towards the rhamnose main chain could therefore be a result of a blocked branching. Also, it could be possible that specifically the precursor biosynthesis leading towards rhamnose is fed, especially if one considers dTDP-rhamnose to be the O-antigen precursor, as has been previously published (Koplin et al. 1993), and its close connection to dTDP-FucNAc biosynthesis.

An in depth analysis on the connection of intermediate molecules and their products, like xanthan and LPS, in Xcc could provide data to verify or falsify the different hypotheses and would clearly be a substantial step towards understanding the often complicated carbohydrate metabolism.

The analysis of the three O-antigen mutant strains Xcc H21012 (*wxcB*), H28110 (*wxcK*) and H20110 (*wxcN*) revealed new insights in the field of carbohydrate research in *Xanthomonas campestris* pv. *campestris*. The mutant in *wxcB* was not affected in terms of viability and completely lost its O-antigen. The mutants in *wxcK* and *wxcN* were inhibited in the FucNAc

branches of the OA, displaying the first experimental evidence showing that *wxc* cluster region 3 is responsible for the branching of the Xcc O-antigen. Previously, this was postulated on the basis of genomic data analysis (Vorhölter et al. 2001). Noticeably, enhanced amounts of rhamnose constituents were detected in both, H28110 and H20110, as compared to the Xcc B100 wild type, indicating an impact on the OA branches of the still obscure O-antigen chain length regulation in *Xanthomonas*.

Additionally, it was possible to reveal an enhanced xanthan production in the mutant Xcc H21012 (*wxcB*), compared to the wild type, which shows the possibilities of inhibiting competing metabolic pathways for bacterial strain design.

4 The Inhibition of Flagellar Structures and the Effects on Xanthan Production and Quality in *Xanthomonas campestris* pv. *campestris* B100 and Production Strain JBL007

General properties of flagella

For bacteria motility can be an essential asset in order to find the most favorable environmental conditions. The flagellum enables bacterial cells to move within their environment and to reach the best available surroundings. The flagellum consists of a basal body, including a rod that spans the membrane parts and is associated with the flagellar motor and a switch. Outside of the membrane, the flagellar hook, bound to that the filament as well as a cap structure, are located (Berg 2003; Schuhmacher et al. 2015). The flagellum is a complex and, in terms of resources, expensive structure, even for monotrichous bacteria. In *E. coli*, a bacterium with an average of four flagella, the assembly and operation can consume 2% and 0.1%, respectively, of the cellular energy (Macnab 2003; Zhao et al. 2014). Furthermore, the filament protein FliC is, with approximately 20,000 copies per filament, one of the most abundant proteins in the bacterial cell (Berg 2003; Macnab 2003).

Overall, the flagellar structure is conserved, however, number and location of the flagella are specific to bacterial species and can reach from one, e. g. in *Xanthomonas campestris*, to a maximum of 25 in *Bacillus subtilis* or up to several hundred in *Vibrio parahaemolyticus* (Yang et al. 2009; Schuhmacher et al. 2015). Number and location of flagella are a result of the bacterial environment, for instance a polar flagellum is often a sign for fast swimmers in liquid environments (Schuhmacher et al. 2015). The most common flagellation patterns are monotrichous, amphitrichous, lophotrichous and peritrichous (Figure 4-1) (Schuhmacher et al. 2015). Monotrichous means only one (polar) flagellum is expressed. A bacterium is amphitrichous flagellated when it expresses two flagella, each at one pole and lophotrichous, when numerous flagella occur at one pole. Peritrichous means that several flagella are expressed at numerous locations. The exact mechanism how bacteria regulate number and

location of their respective flagella still has to be assessed, however, it was shown that in several species the conserved proteins FlhF and FlhG play a crucial role (Schuhmacher et al.

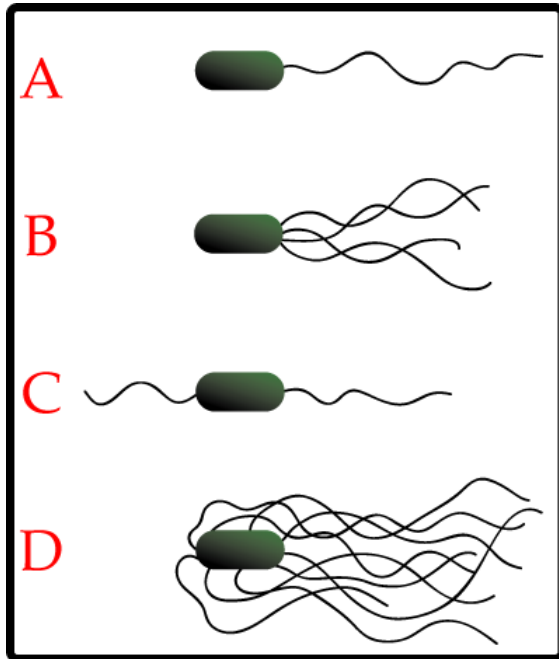


Figure 4-1: General schematic arrangement of bacterial flagella. A: Monotrichous; B: Lophotrichous; C: Amphitrichous; D: Peritrichous. <https://commons.wikimedia.org/wiki/File:Flagella.png>; CC BY 3.0.

2015). For example in monotrichous bacteria, like *Xanthomonas*, it was shown that deletion of *flhF* led to absence or mislocalization of the flagellum, while overexpression led to hyperflagellation (Schuhmacher et al. 2015). On the other hand, deletion of *flhG* led to hyperflagellation of the cells, indicating an opposing physiological role. Furthermore, it seems that the flagellar C-ring, including FliM, might play a role in the bacterial flagellation pattern, since FlhG can interact with FliM, however the purpose still has to be evaluated (Schuhmacher et al. 2015).

The movement occurs through rotation of the thin helical filament (Berg 2003) that is exposed into the surrounding medium. The necessary force for the rotational movement is generated by motor proteins, mostly driven by the proton motive force (Berg 2003) and therefore, the flagellar movement is powered by the same force that is essential for ATP production (Steigmiller et al. 2008). Nevertheless, in a few cases the rotary movement is not driven by the proton gradient, but by the gradient of sodium ions, as has been shown for *Vibrio* spp. (Berg 2003).

For peritrichously flagellated cells, such as *E. coli*, a swim speed of around 30 diameters per second was measured (Berg 2003). The motor proteins MotA and MotB are stationary, as they are bound to the bacterial peptidoglycan (Macnab 2003). Together these proteins generate the torque for rotation through proton flux. The energy is transferred to the basal flagellar body through a rotor, consisting of the protein FliG. The basal flagellar body consists of the MS-ring, to which the rotor is attached, a rod that spans the periplasmic space, a periplasmic P-ring and an outer membrane L-ring and together with the motor, the basal body transfers the torque to the flagellar hook and filament (Macnab 2003). Bacteria are able to rotate their flagella in counterclockwise (CCW) and clockwise (CW) direction. This change of rotational

direction enables the bacteria to actively swim towards favorable environments, while chemotaxis receptors help to control the rotational direction (Berg 2003; Macnab 2003). However, in order to change between CCW and CW, a switch, consisting of the proteins FliM, FliN and the FliG rotor, is necessary, for instance shown in *Salmonella* (Macnab 2003). FliG is involved in torque generation as well as switching, while FliM is the endpoint of the sensory output. The role of FliN has yet to be elucidated, but is thought to also be involved in transferring the sensory output (Macnab 2003; Zhao et al. 2014). Through chemotactic receptors environmental signals are transmitted and when the sensory protein CheY is phosphorylated, it binds to the flagellar switch and biases the flagellum to a CW rotation and tumbling (Macnab 2003).

The measurements of proton fluxes needed for the flagellar rotations are not trivial, since the general proton influx is higher than just the flux needed for flagellar rotations. Still, a measurement in *Streptococcus* sp. strain V4051, revealed that 1,200 protons are needed per rotation and the bacteria in that particular experiment showed a rotational top speed of 65 Hz, which means the proton flux per motor per second equals to 78,000 protons (Berg 2003). However, also rotations of around 300 Hz might be possible (Oster and Wang 2003). Furthermore, it was shown that the bacterial flagellar motor generates around 200 pN of force, making it the most powerful molecular motor (Oster and Wang 2003).

Quite recently it was described that the flagellum can be glycosylated. Until now it was not shown that peritrichous bacteria like *E. coli* carry glycan structures at their flagellum, nevertheless for polar flagellated bacteria flagellar glycosylation seems to be rather common (Merino and Tomas 2014) and the nucleotide sugar precursors might be shared with e. g. EPS and LPS precursors. Number, location and length of glycosylations vary between species and also conserved motifs, as well as heterogeneity could be observed. *Pseudomonas aeruginosa*, a close relative to *Xanthomonas*, is a monotrichous polar flagellated bacterium that shows heterogenic glycan structures at its flagellin that can consist of up to eleven monosaccharides. While the number of reported flagellin glycans increases, knowledge about their biological functions remains limited. However, flagellar glycosylations are thought to be important for host cell recognition and bacterial virulence (Merino and Tomas 2014).

Structure and biosynthesis of the flagellum

The flagellum, as large and complex structure, also has a complex biosynthesis (Figure 4-2). Different gene clusters with about 40 genes and thousands of proteins are needed to complete the assembly (Macnab 2003; Yang et al. 2009). Additionally, it was shown that the gene expression for the flagellar assembly is organized in a hierarchical manner, from early class I to late class III genes (Berg 2003; Macnab 2003; Yang et al. 2009). In *Xanthomonas campestris*, the σ^{70} factor RpoD is responsible for the expression of class I genes, which encode for the master regulators for the flagellar biosynthesis. Class I proteins RpoN2 (σ^{54}) and FleQ activate the class II genes. These genes include the flagellar-type III secretion system (F-T3SS) and the genes responsible for the basal body biosynthesis. FliA (σ^{28}) another class II protein, is responsible for the expression of late or class III flagellar genes, and it is the regulator for several motility/chemotaxis related genes (Yang et al. 2009). However, FliA is inhibited by FlgM, a class I protein, until the early flagellar structures are assembled. Only then FliA can activate the class III genes, like the filament encoding *fliC* or cap proteins (Berg 2003; Yang et al. 2009). This way it is ensured that genes are only expressed at their respective time and no energy is wasted (Berg 2003).

The structural assembly starts with the integral membrane parts and the MS-ring is synthesized first (Macnab 2003). The simplest structure ever found during mutational studies was the MS basal ring (FliF) to which FliG and the C-ring, consisting of FliM and FliN, are bound (Berg 2003). The MS-ring has a passive role, however it is essential, since it builds the foundation for flagellar structure and synthesis through the export apparatus, the flagellar type III secretion system (F-T3SS). The export machinery is built after the basal body is completed and the proteins FlhAB and FliHIOPQR are required. The F-T3SS is used to pass the other structural components through the center of the MS-ring (Berg 2003). With the help of cytoplasmic chaperones further proteins are led to the transport system and the flagellar rod is assembled from proximal to distal. This includes the proteins FlgBCFG, further FliE is essential for the rod biosynthesis. It is not needed for the rod structure, but supposed to form a junction zone between the MS-ring and the proximal part of the rod (Berg 2003; Macnab 2003). For further structural growth the L- and P-rings are necessary. Their components are secreted into the periplasm by the signal-peptide-dependent secretory machinery (Sec), with the help of chaperones like FlgA (Berg 2003). The P-ring assembly is associated with FlgI and the L-ring consists of the lipoprotein FlgH (Berg 2003; Macnab 2003). The following flagellar

substructure that is assembled, is the hook. FlgE is the initial protein and as soon as L- and P-ring are completed, the proteins FlgK, FlgL and FljD are added in that order (Berg 2003).

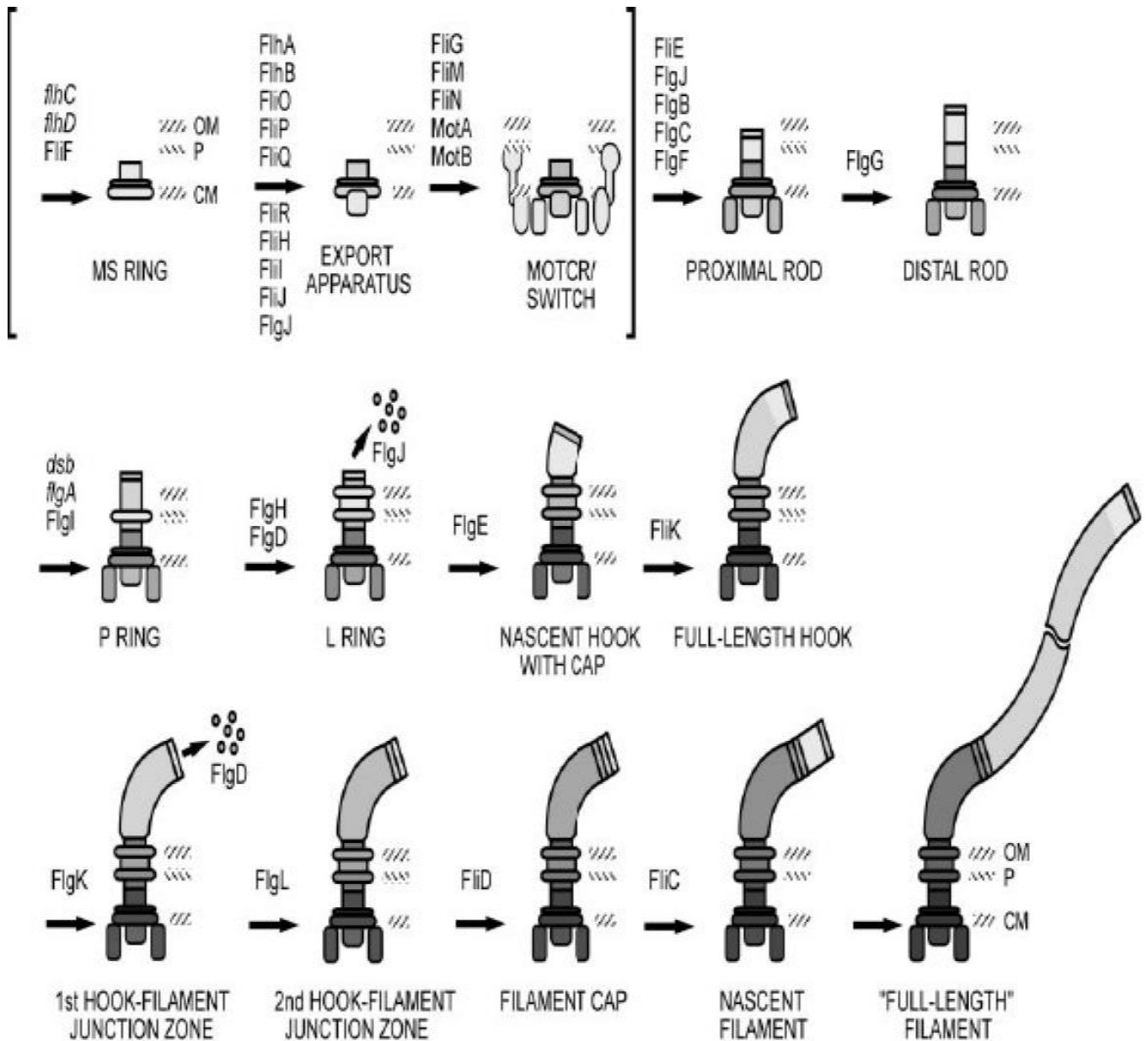


Figure 4-2: Schematic overview of the conserved flagellar assembly and genes involved in this process.

Depicted is the pathway from *Salmonella*. The name of the respective substructures is given under the images. Names of the genes involved in the biosynthesis of given substructures are depicted at the arrows. Brackets indicate substructures that are assembled prior to the flagellar type III system. Biosynthesis starts with a basal body, followed by the export apparatus. Only then structural parts, including hook and filament can be assembled. From Macnab, 2003.

Interestingly, the hook always shows a quite constant length of about 55 nm that is determined by the distal hook cap FlgD. The mechanism behind this is not fully understood, however, it was shown that the protein FliK seems to play a role in length determination of the hook structure (Berg 2003; Macnab 2003). Onto the hook the by far biggest structure of the flagellum is built, the filament. One flagellar filament can consist of up to 20,000 proteins of filament protein FliC (flagellin) (Macnab 2003). Apparently there is no length control mechanism involved in filament construction and if it breaks, it can regrow. In the end the filament is capped by FliD (Berg 2003; Macnab 2003). Mutants without this cap protein dump flagellin in the surrounding medium (Berg 2003). The rotation driving motor proteins MotAB can presumably be incorporated into the flagellar structure at any time. MotB binds to the periplasmic peptidoglycan, thus opening proton channels in the MotAB complex (Berg 2003). This ensures the driving force for the completed flagellum.

Aim

The basic hypothesis was that inhibition of the flagellar biosynthesis and related proton driven motility might be beneficial for the Xcc xanthan production. The flagellum is a cost intensive structure, in terms of energy and building block consumption, and additionally it is involved in signaling processes. Two flagellar genes, *fliC* and *fliM*, were mutated and the resulting strains should be analyzed towards their xanthan characteristics, to validate the hypothesis.

strain Xcc JBL007 of the Jungbunzlauer Austria AG. The genome of the production strain was sequenced at the CeBiTec (Bielefeld University) and could be worked with as draft genome. Knock-out mutants, resulting in kanamycin resistant strains Xcc *fliC*⁻ and Xcc *fliM*⁻, were constructed using a vector based integration (Figure 4-3). Briefly, the kanamycin resistance gene carrying vector pk18mob (Schäfer et al. 1994) was used as backbone and central parts of the genes Xcc *fliC* and *fliM*, respectively, were cloned into the multiple cloning site. The constructs were then transformed into *E. coli* DH5 α and cells were plated on kanamycin containing agar plates. Additionally blue-white selection was performed. Vectors were checked for integration of the specific gene insert. Positive constructs were then electroporated into Xcc.

Characterization of the Xcc B100 xanthan production after mutagenesis of two flagellar genes

First a positive mutant for the *fliC* gene could be constructed and xanthan analysis was started immediately. Five cultivations in XMD minimal medium, supplemented with 0.6 g per l nitrate and 30 g per l glucose were carried out. Xanthan harvest was after 96 h of cultivation and depicted values are of dried xanthan. Strains that are compared were grown simultaneously. The Xcc B100 wild type produced approximately 6.1 g xanthan per g biomass, while the mutant strain Xcc B100 *fliC*⁻ showed a mean production of 7.8 g g⁻¹ (Figure 4-4). This equaled for a mean productivity increase of 1.6 g xanthan per g biomass.

When the Xcc B100 *fliM*⁻ mutant was constructed, xanthan analyses were performed instantaneously. However, in the background of the laboratory strain B100 only two measurements could be executed. Nevertheless, promising results were gained for the mutant inhibited in *fliM*. While the Xcc B100 wild type produced a mean of 5.5 g xanthan per g biomass, the mutant produced 6.6 g g⁻¹, also showing an enhanced production, with a xanthan gain of more than 1 g per g biomass (Figure 4-5).

Due to the shown potential and the possibility to work with a production strain in order to generate data with high industrial impact, both mutations should be transferred into the background of Jungbunzlauer Austria AG strain Xcc JBL007. This strain was also used for deeper phenotypical analyses.

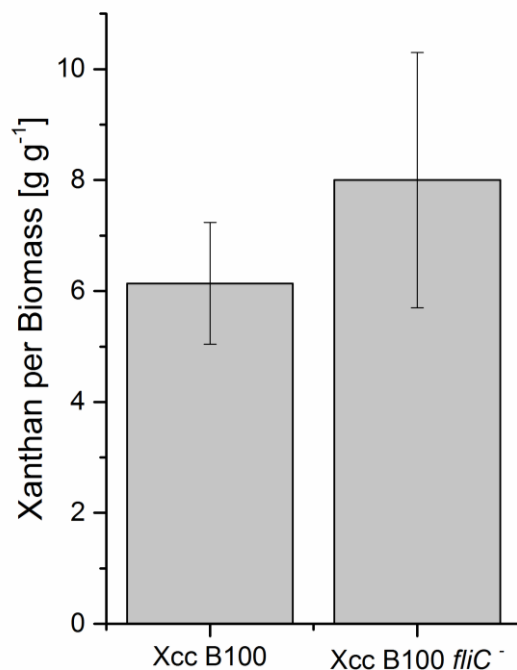


Figure 4-4: Xanthan production of *Xanthomonas campestris* pv. *campestris* B100 wild type and derived mutant *fliC*⁻. Production was measured as dry weight [g] xanthan per [g] biomass. Samples from five replicates each. Harvest was after 96 h in the late stationary phase. Bars give the normalized mean xanthan yields, with error bars indicating the standard deviations. Values are depicted in Supplementary table 5.

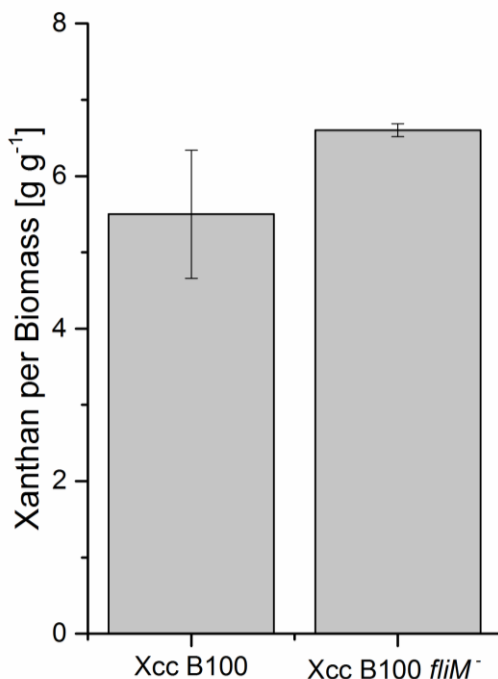


Figure 4-5: Xanthan production of *Xanthomonas campestris* pv. *campestris* B100 wild type and derived mutant *fliM*⁻. Production was measured as dry weight [g] xanthan per [g] biomass. Samples from two replicates each. Harvest was after 96 h in the late stationary phase. Bars give the normalized mean xanthan yields, with error bars indicating the standard deviations. Values are depicted in Supplementary table 5.

Construction of Xcc JBL007 mutant strains deficient in flagellar genes *fliC* and *fliM* and their phenotypic characterization towards motility

The genetic background and gene sequence of the flagellar genes is strongly conserved between the laboratory strain Xcc B100 and production strain Xcc JBL007. Hence, the same approach for mutant construction was used and plasmid integration mutants Xcc JBL007 *fliC*⁻ and Xcc JBL *fliM*⁻ were constructed according to the description above.

After the mutations of *fliC* and *fliM* were transferred into the production strain Xcc JBL007, phenotypical analyses were performed. This way the impact of the mutations should be determined. Transmission electron microscopy (TEM) was applied in order to see if the bacteria possess a flagellum, only a substructure or if they are non-flagellated. The cells were taken from liquid culture, gently washed and transferred to Formvar-coated grids for electron microscopy. Strain Xcc JBL007, the initial and production strain, expressed flagella that could be observed after negative staining with uranyl acetate and TEM (Figure 4-6). In both mutant strains no flagellum could be observed (Figure 4-6). However, in order to validate the microscopy results a swarming assay was carried out. Bacteria were applied in the middle of a 90 mm petri dish, filled with 0.3% agar containing complex medium. Incubation occurred for 48 h at 30°C. If there is a working flagellum, a round halo around the inoculation point, indicating swarming, can be expected. Indeed this halo was detected when the initial strain Xcc JBL007 was tested (Figure 4-6). This clearly showed the swarming ability of that strain. For both equally treated mutant strains no swarming was detected. The bacteria were viable and grew, but only at their respective inoculation spot and no swarming halo was developed (Figure 4-6).

In summary, successful inhibition of the flagellum and derived motility was obtained in two mutant strains, deficient in the flagellar genes *fliC* and *fliM*, respectively, which were then used to test xanthan production in comparison to the initial strain Xcc JBL007.

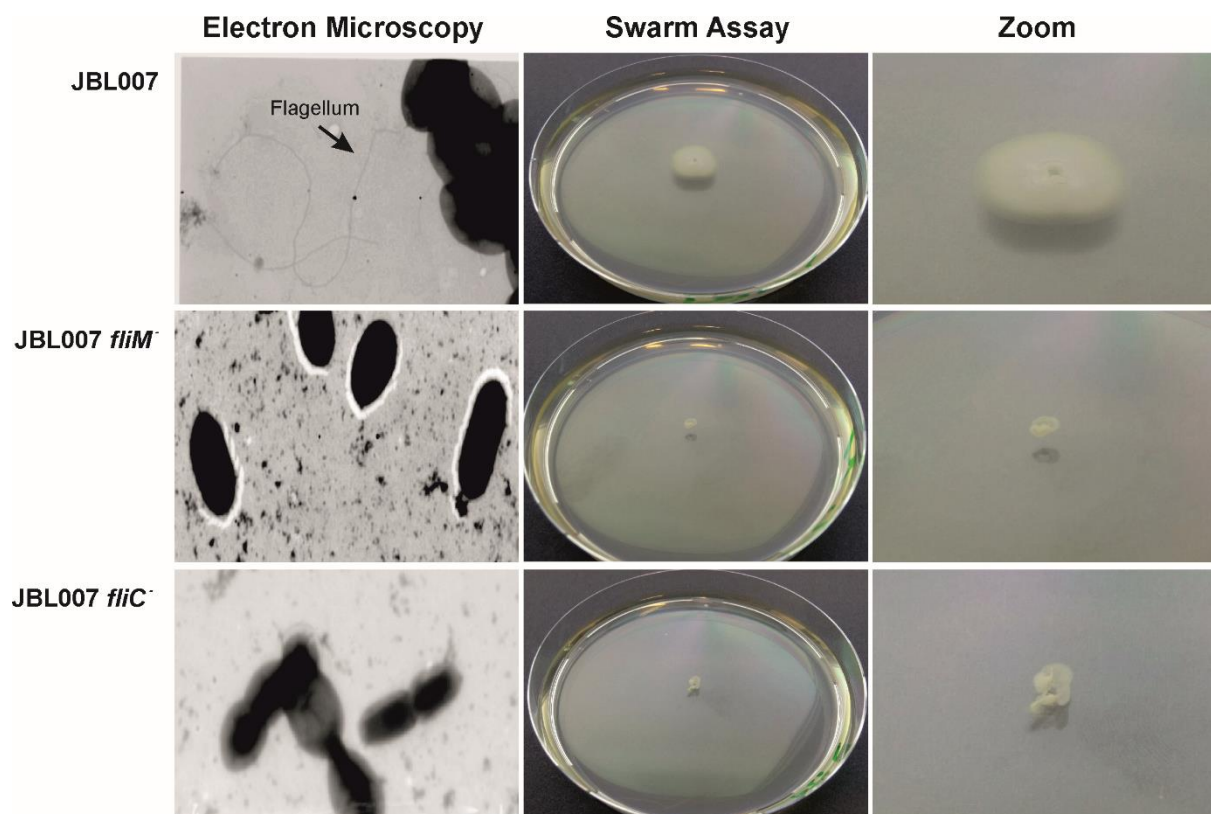


Figure 4-6: Transmission electron microscopy and swarm assay of the strain Xcc JBL007 and derived mutants *fliM*⁻ and *fliC*⁻. Cells for microscopy were harvested at mid-growth-phase. Swarming was tested on 90 mm 0.3% agar plates. Plates were incubated for 48 h. Bacteria are motile when a halo appears on the plates (JBL007), otherwise they are non-motile (mutant strains).

Xanthan production by production strain Xcc JBL007 and by the derived flagellar mutant strains Xcc JBL007 *fliC*⁻ and *fliM*⁻ under industrial cultivation conditions

Depicted results were obtained at Jungbunzlauer Austria AG in Pernhofen, Austria. The strains were taken for cultivation, applying the industrial cultivation and analyses methods, under xanthan production conditions and production quantity and quality were compared to the initial strain Xcc JBL007.

Fermentations were carried out in 10 l scale with a xanthan production medium at pH 7. Oxygen was monitored and stirring as well as gas flow was adjusted in order to ensure that the oxygen supply was increased with growth and viscosity. Nitrogen and glucose consumption were only checked to ensure regular culture development. Inoculation occurred with 400 ml overnight culture of the respective strains. Fermentations were carried out as triplicates, while in each fermentation round all three strains were cultivated in parallel. Depicted xanthan values are of dried samples.

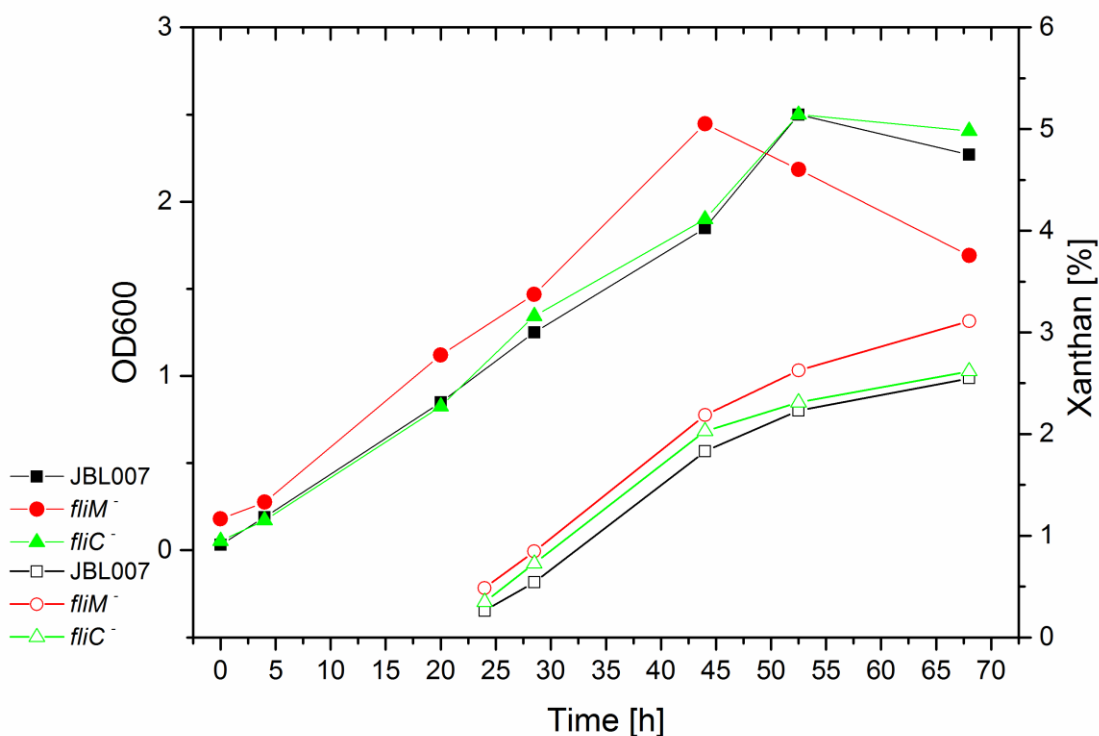


Figure 4-7: Fermentation of *Xanthomonas campestris* pv. *campestris* JBL007 and derived mutants JBL007 *fliC*⁻ and JBL007 *fliM*⁻. Depicted is the growth behavior (OD600) with filled symbols and xanthan production [% (w/v) of the culture] with open symbols. Fermentation was carried out in minimal medium with 0.2 g l⁻¹ corn-extract, 0.6 g l⁻¹ of a nitrogen source and 45 g l⁻¹ glucose from glucosesirup.

Table 4-1: Xanthan production of *Xanthomonas campestris* pv. *campestris* JBL007 and derived mutants JBL007 *fliC*⁻ and JBL007 *fliM*⁻ after fermentation. Depicted are the individual values of three measurements and their respective mean with according standard deviation. Harvest occurred after 68 h.

Fermentation	Xanthan yield (g l ⁻¹)			Mean
	1	2	3	
JBL007	25.5	30.6	29.75	28.47 +/- 2,4
JBL007 <i>fliM</i> ⁻	31.1	34.7	29.8	31.87 +/- 2,1
JBL007 <i>fliC</i> ⁻	26.2	33.5	28.6	29.43 +/- 3

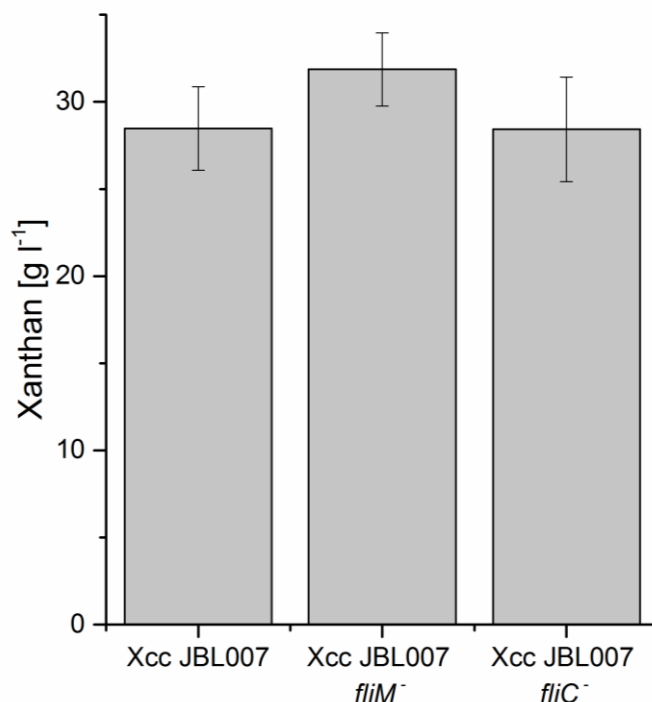


Figure 4-8: Xanthan production of *Xanthomonas campestris* pv. *campestris* JBL007 wild type and derived mutants *fliC*⁻ and *fliM*⁻. Production was measured as dry weight [g] xanthan per [l] culture. Samples from 3 fermenter replicates each. Bars give the mean xanthan yields, with error bars indicating the standard deviations.

The growth of Xcc JBL007 and Xcc JBL007 *fliC*⁻ was very similar (Figure 4-7), with growth until optical densities at 600 nm of 2.5 after 52.5 h, indicating nitrogen starvation. For Xcc it is known that nitrogen limitation marks the start of the stationary phase and xanthan production increases (Kreyenschulte et al. 2014). In the stationary phase a slight decrease in the OD occurred. Xcc JBL007 *fliM*⁻ showed slightly different behavior. It grew faster than the other two strains and reached its maximum OD₆₀₀ of 2.45 after 44 h, also representing a faster use of nitrogen. Then the OD decreased (Figure 4-7). Fermentation was stopped after 68 hours. Next to the growth, xanthan production was monitored as g l⁻¹ [% (w/v)], as this method was suggested by Jungbunzlauer Austria AG since biomass is no relevant factor in the industrial production. Figure 4-7 shows timelines for xanthan production. The first measurement occurred after 24 hours. Xcc JBL007 had produced 2.64 g l⁻¹, Xcc JBL007 *fliC*⁻ 3.5 g l⁻¹ and Xcc JBL007 *fliM*⁻ had already produced 4.86 g l⁻¹. The xanthan amount increased with the growth of the cultures and at the end of the fermentation run Xcc JBL007 produced a total of 25.5 g l⁻¹ xanthan, while the *fliC* mutant showed a production of 26.2 g l⁻¹. Compared to each other Xcc

JBL007 *fliC*⁻ produced 3% more than the initial strain (Table 4-1, fermentation 1). However the best producer strain was Xcc JBL007 *fliM*⁻ with a total production of 31.1 g l⁻¹, indicating an increase of 22% as compared to Xcc JBL007. The *fliM* mutant strain reached the endpoint amount of 26 g l⁻¹ xanthan of the other two strains around 14 h before they did (Figure 4-7). Since xanthan production can differ between fermentations the cultivations were repeated to validate the production values (Table 4-1, fermentations 2 and 3). During the second fermentation run Xcc JBL007 produced 30.6 g l⁻¹ xanthan, while Xcc JBL007 *fliC*⁻ and Xcc JBL007 *fliM*⁻ produced 33.5 g l⁻¹ and 34.7 g l⁻¹, respectively. This accounted for an increase of 10% and 13% compared to the strain JBL007. The third fermentation was different, here only a very slight increase in xanthan production for Xcc JBL007 *fliM*⁻ was detected, while JBL007 *fliC*⁻ even produced a little less xanthan than the initial strain Xcc JBL007 (Table 4-1). However, it could be concluded that both flagellar mutant strains are useful xanthan producers with a better outcome than the initial strain Xcc JBL007, with Xcc JBL007 *fliM*⁻ being the best producer (Figure 4-8). A mean endpoint xanthan production of 28.47 g l⁻¹ was measured for the Xcc JBL007 strain, while 31.87 g l⁻¹ and 29.43 g l⁻¹ were measured for the derived mutants *fliM*⁻ and *fliC*⁻, respectively. This accounted for an improved production of around 3% for the *fliC* mutant and an improved production of around 12% for the *fliM*⁻ strain, while all three strains were treated identical. These results are in accordance with Erlenmeyer flask cultivation test triplicates, obtained at Jungbunzlauer Austria AG, with production medium (Table 4-2).

Table 4-2: Xanthan production of *Xanthomonas campestris* pv. *campestris* JBL007 and derived mutants JBL007 *fliC*⁻ and JBL007 *fliM*⁻ after shaking flask cultivations. Depicted are the individual values of three measurements and their respective mean with according standard deviation.

Cultivation	Xanthan yield (g l ⁻¹)			Mean
	1	2	3	
JBL007	15.7	18.7	23.8	19.4 +/- 3.3
JBL007 <i>fliM</i> ⁻	20.3	21.7	23.6	21.9 +/- 1.4
JBL007 <i>fliC</i> ⁻	18.5	25.4	25.3	23.1 +/- 3.2

The best producing strain Xcc JBL007 *fliM*⁻ was tested in comparison to Xcc JBL007 in a fed batch fermentation. The medium was like the previously described medium, except that 0.7 g l⁻¹ nitrogen was used. Furthermore after 29 h 700 ml of 34% glucosesirup was added to increase the carbon source in the medium. In Figure 4-9 this time point is marked with an arrow and a kink to a steeper growth is visible after glucose addition. After 52 h the transition into the stationary phase was reached at OD values of 2.8 and 2.7 for Xcc JBL007 and Xcc JBL007 *fliM*⁻, respectively. The slight increase in optical densities at the transition phase, as compared to the previous fermentations, could be explained with the nitrogen supply of 0.7 g l⁻¹ in contrast to 0.6 g l⁻¹ in the previous described fermentations. The culture density stayed at this level in the Xcc JBL007 *fliM*⁻ strain, while the Xcc JBL007 strain started to grow again after some hours in the stationary phase to an OD of more than 3. Due to the additional glucose the fed batch fermentations went on for 72 h. Again, the *fliM* mutant strain produced more xanthan than the control strain Xcc JBL007 (Figure 4-9). The total xanthan production was 31.45 g l⁻¹ for the strain Xcc JBL007 and 33.1 g l⁻¹ for the strain Xcc JBL007 *fliM*⁻ in a first fermentation. In the following fermentation yields of 31.6 g l⁻¹ and 35.8 g l⁻¹ for Xcc JBL007 and Xcc JBL007 *fliM*⁻, respectively, were achieved (Table 4-3). Taken together this again showed a substantially increased xanthan production of the *fliM* mutant. These results underline the production potential of the *fliM* mutant strain. Furthermore, to sum up the results of the fed batch cultivation, the xanthan yields could be increased in both strains, Xcc JBL007 and in the derived *fliM* mutant, as compared to the previous, non-fed batch approach, yet the flagellar mutant still showed to be a better production strain than Xcc JBL007.

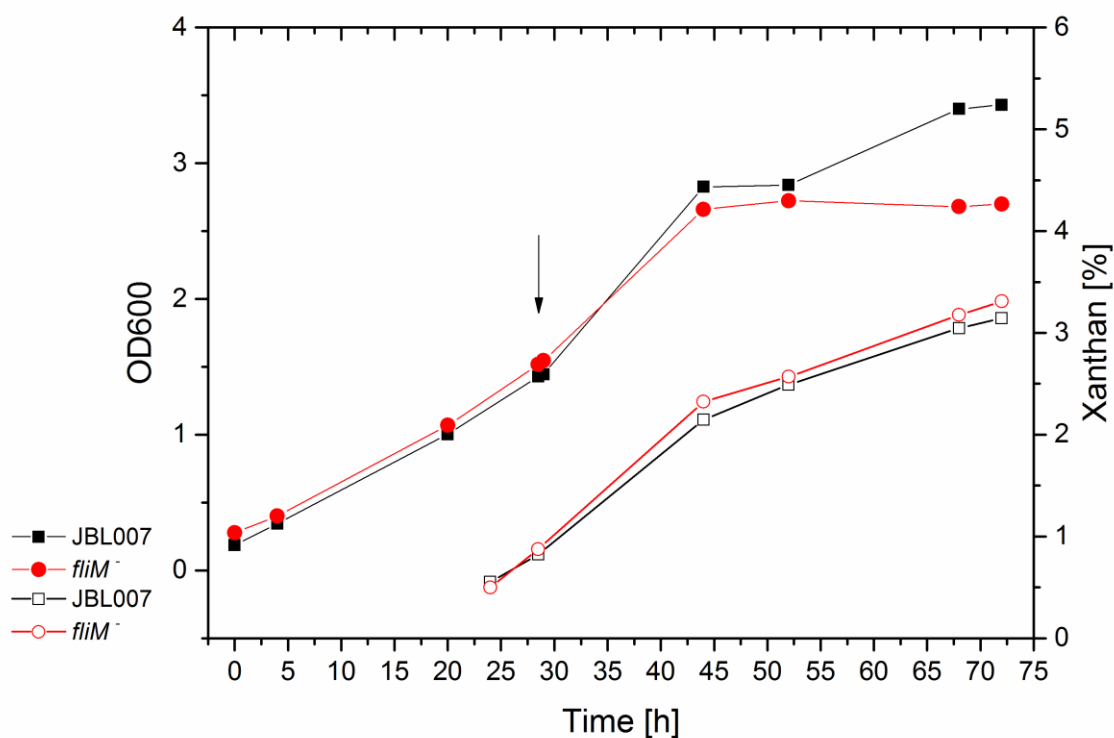


Figure 4-9: Fed batch Fermentation of *Xanthomonas campestris* pv. *campestris* JBL007 and derived mutant JBL007 *fliM*⁻. Depicted is the growth behavior (OD600) with filled symbols and xanthan production [% (w/v) of the culture] with open symbols. Fermentation was carried out in minimal medium with 0.2 g l⁻¹ corn-extract, 0.7 g l⁻¹ nitrogen source and 45 g l⁻¹ glucose from glucosesirup. The arrow indicates the addition of 700 ml 34% glucosesirup after 29 h.

Table 4-3: Xanthan production of *Xanthomonas campestris* pv. *campestris* JBL007 and derived mutant JBL007 *fliM*⁻ after fed batch fermentations. Depicted are the individual values of two measurements. Harvest occurred after 72 h.

Fermentation	Xanthan Yield (g l ⁻¹)	
	1	2
Xcc JBL007	31.45	31.6
Xcc JBL007 <i>fliM</i> ⁻	33.1	35.8

Characterization of product quality of xanthan isolated from Xcc JBL007 and flagellar mutant strains

Characteristics of xanthan and its properties were tested extensively (Casas et al. 2000; CPKelco 2008; Hublik 2012) and an important factor for the industrial relevance of xanthan are the rheological properties, since it is used as thickening agent.

Already during the cultivations the culture broth of the flagellar mutants seemed thicker than the broth of Xcc JBL007. Thus, the viscosities of the xanthan from the strain Xcc JBL007 compared to the mutants in *fliC* and *fliM* were tested, to gain information about the xanthan characteristics. Results from rheological measurements of 1% (w/v) xanthan solutions in distilled water at room temperature are depicted in Figure 4-10 and the according values are shown in Table 4-4. For all of the three tested strains high viscosities and a gel-like liquid at low shear rates were observed. Moreover, a decrease in viscosity over growing shear rates could be measured (Figure 4-10). Interestingly, enhanced viscosities for both of the flagellar mutants could be measured over the whole range of tested viscosities, as compared to the strain Xcc JBL007. Differences were especially vast during low shear rates and decreased towards high shear rates (Table 4-4). Still, while the difference at low shear rates was in the range of 90%, even at the highest measured rate, the difference in viscosity was as much as 18% when compared Xcc JBL007 *fliM*⁻ to Xcc JBL007. For Xcc JBL007 *fliC*⁻ the difference was still around 5%. In order to verify these results viscosity measurements with a different xanthan sample from each strain were performed (Supplementary table 6). Although the depicted values differ from those shown in Table 4-4, the general conclusion was validated, since both of the mutant strains produced xanthan with enhanced viscosities. The overall differences in viscosities were due to the different xanthan samples. The first set of measurements was performed with xanthan harvested at Jungbunzlauer Austria AG and the validation measurement was performed with xanthan harvested in Bielefeld at the CeBiTec, from flask cultivations and with different medium.

In order to test if the xanthan samples of the different strains had the same chemical composition and conformation Nuclear Magnetic Resonance (NMR) measurements and Atomic Force Microscopy (AFM) were performed.

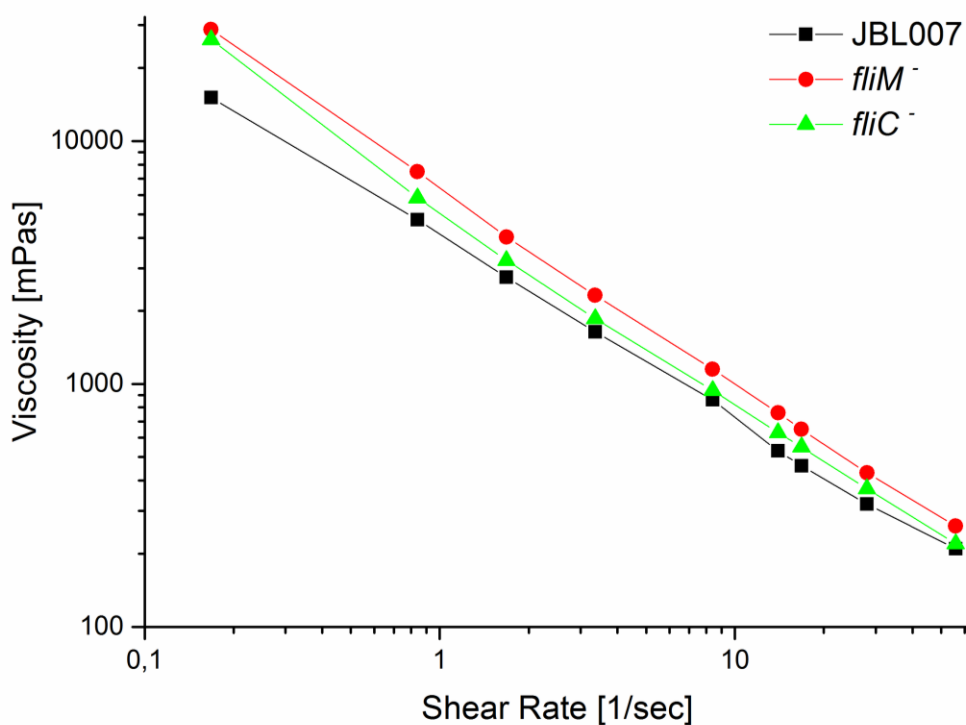


Figure 4-10: Viscosity of the *Xanthomonas campestris* pv. *campestris* strains JBL007 and derived mutants JBL007 *fliC*⁻ and JBL007 *fliM*⁻ in a logarithmic scale. Xanthan was harvested from fermenter cultivations, dried and milled. Measurements were carried out with 1% (w/v) xanthan in water at room temperature.

Table 4-4: Measured viscosity values of *Xanthomonas campestris* pv. *campestris* strains JBL007 and derived mutants JBL007 *fliC*⁻ and JBL007 *fliM*⁻. Measurements were carried out with 1% (w/v) of dried and milled xanthan in water at room temperature.

Shear rate (1*sec ⁻¹)	JBL007 (mPas)	JBL007 <i>fliM</i> ⁻ (mPas)	JBL007 <i>fliC</i> ⁻ (mPas)
0,168	15090	28760	26170
0,84	4750	7490	5840
1,68	2750	4030	3230
3,36	1640	2320	1860
8,4	860	1150	940
14	530	760	630
16,8	460	650	550
28	320	430	370
56	210	260	220

Chemical properties of the isolated xanthan from Xcc JBL007 and derived mutants Xcc JBL007 *fliC*⁻ and Xcc JBL007 *fliM*⁻

With the help of NMR it is possible to determine the exact molecular composition of the xanthan molecule. Equally treated xanthan from Xcc JBL007 and both derived mutants was analyzed by ¹H-NMR at 90°C (Figure 4-11). The results clearly revealed that the chemical properties of xanthan molecules from the initial strain Xcc JBL007 and derived *fliC* and *fliM* mutants were identical (Figure 4-11). All signals of the three tested xanthan samples behaved alike. This was not only true for the sugar ring protons in the region from roughly 4 – 6 ppm, but also for the pyruvate and acetate decorations (Figure 4-11). The lower y-axis scale for the spectrum of Xcc *fliC*⁻ was due to technical, not biological reasons. Still, higher viscosities for the mutant strains were measured. Viscosity and rheological properties of xanthan in solution depend on its molecular weight, conformation and stiffness (Rinaudo et al. 1983). Therefore, a suitable method to check for differences in xanthan conformation and length of the molecule is Atomic Force Microscopy (AFM), which was already used to describe xanthan molecules (Gulrez et al. 2012; Galván et al. 2013). Xanthan from the initial strain Xcc JBL007 was compared to xanthan derived from the best producing strain Xcc JBL007 *fliM*⁻. Values and example images are provided in Table 4-5 and Figure 4-12. Overall 16 samples of xanthan strands from JBL007 and 21 strands from the *fliM* mutant were analyzed. The average length was 2,453 nm for Xcc JBL007 and 2,764 nm for the mutant strain. However, since the xanthan fibers were divers in length, a large standard deviation was observed. More striking was the persistence length, as indication for the fibers stiffness. A substantial increase in Xcc JBL007 *fliM*⁻ xanthan could be observed. A persistence length of 54 nm for the mutant strain was observed, while the initial strain showed an average persistence length of 33 nm.

Whereas the NMR measurements did not show chemical differences in the xanthan molecules, changes in the xanthan conformation could be revealed by AFM.

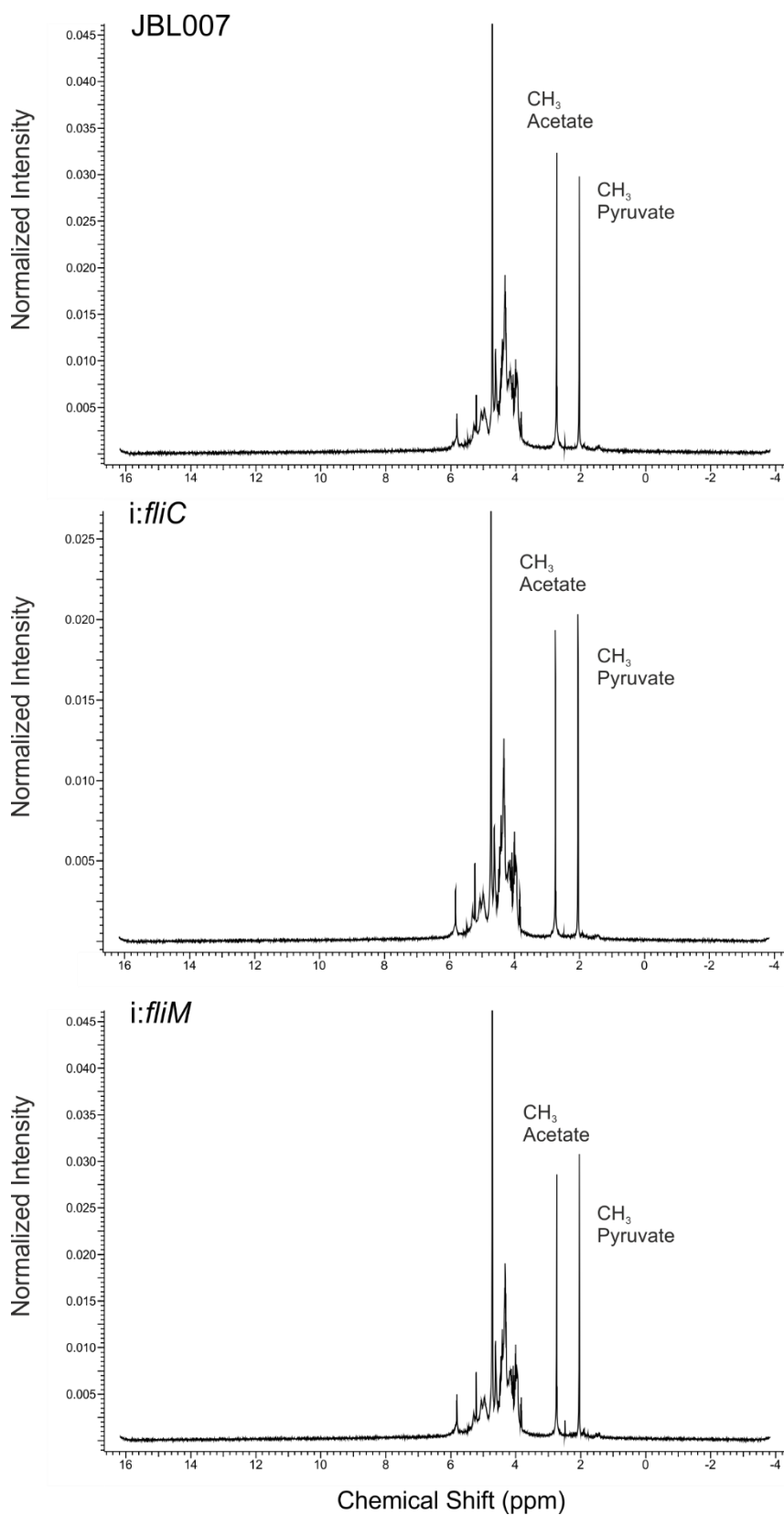
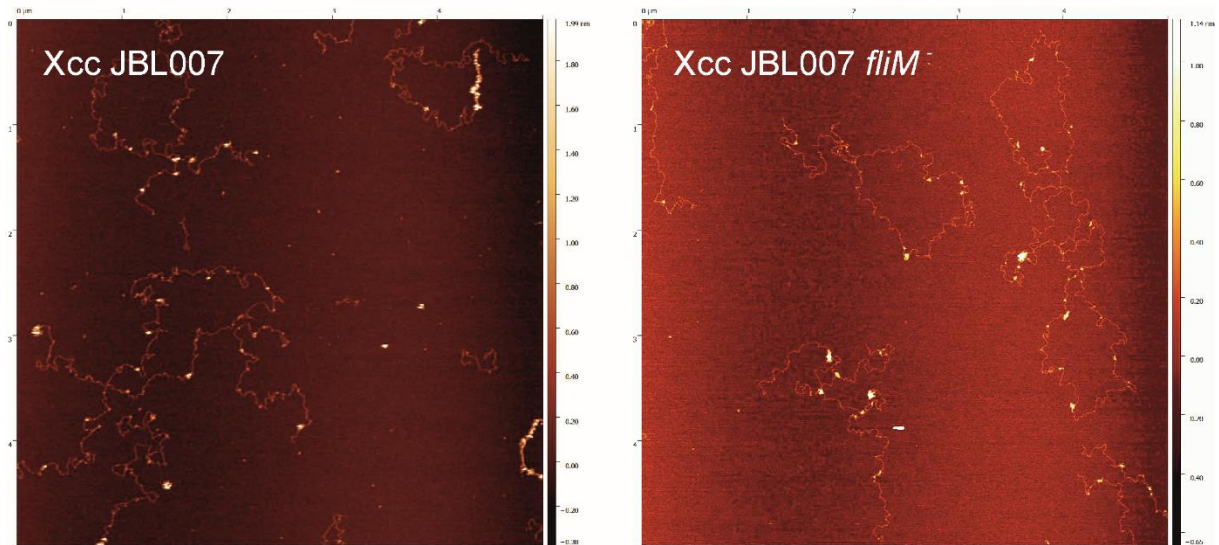


Figure 4-11: ¹H-NMR of Xanthan isolated from Xcc JBL007 and derived mutants JBL007 *fljM*⁻ and JBL007 *fljC*⁻. Samples were solved in D₂O. The differences in scaling of the y-axis are due to slightly different amounts of xanthan used for the measurements. Highlighted are the methyl groups of the xanthan acetate and pyruvate groups. Sugar ring proton signals occur at around 4 – 6 ppm.

A:



B:

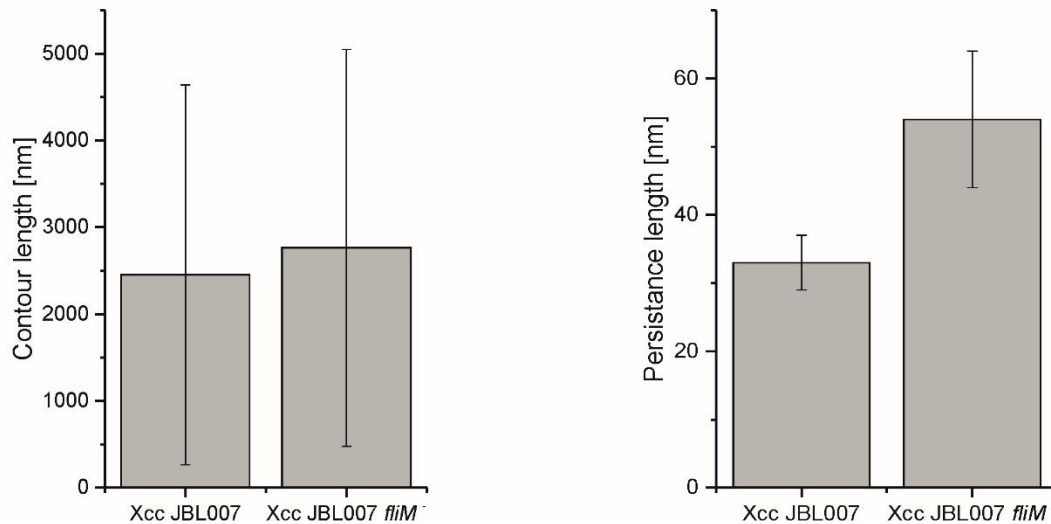


Figure 4-12: Atomic force microscopy analysis of xanthan by Xcc JBL007 and derived mutant Xcc JBL007 *fliM*⁻.

A: Topography of single xanthan fibers in example AFM images of equally prepared xanthan samples. Samples were harvested after 68 h of fermentation. B: Measured xanthan characteristics (contour length and persistence length) shown as bar diagrams of the mean values with standard deviation. Measured were 16 strands for Xcc JBL007 and 21 strands for Xcc JBL007 *fliM*⁻.

Table 4-5: Comparison of xanthan fibers from Xcc JBL007 and Xcc JBL007 *fliM*⁻ xanthan. Data were derived by atomic force microscopy. Shown are the mean values with standard deviation of 16 samples for Xcc JBL007 and 21 for Xcc JBL007 *fliM*⁻.

Strain	Contour length (nm)	Persistence length (nm)
Xcc JBL007	2453 ± 2189	33 ± 4
Xcc JBL007 <i>fliM</i> ⁻	2764 ± 2287	54 ± 10

Discussion

The potential of flagellar mutants in Xcc for xanthan production

Overall the construction of flagellar mutants followed considerations implying that an inhibition in the flagellar biosynthesis might be beneficial to EPS. For instance, flagellin encoded by *fliC* alone has approximately 20,000 copies per flagellum (Macnab 2003). Furthermore, in *E. coli* the flagellar assembly makes up to 2% and the operation makes around 0.1% of the cellular energy costs (Zhao et al. 2007). Although *E. coli* produces more than one flagellum, on average four (Berg 2003), even one flagellum costs a substantial amount of resources. Also the, for rotation essential, proton flux (Berg 2003) might be decreased in flagellar mutants. The result of this could be a more efficient ATP production that may be beneficial for xanthan production. Other than that yet unknown signaling effects may influence the xanthan production, since it is known that the flagellum is involved in signaling towards biofilm production, with xanthan as essential part of the Xcc biofilm (Crossman and Dow 2004). Such signaling effects were already shown, e. g. in *Bacillus subtilis* (Belas 2013). Strains that were inhibited in the flagellar rotation showed an increased biofilm production, including increased production of extracellular matrix. In this case it became apparent that the flagellum also has mechanosensory functions (Belas 2013). Further, it was described that both, xanthan and the flagellum are influenced by the DSF regulation. DSF is, among other functions, involved in regulation of genes for EPS biosynthesis and secretion, as well as in regulation of the flagellar biosynthesis and motility (He and Zhang 2008). Furthermore, in *P. aeruginosa* the flagellum and biofilm including EPS formation are inversely regulated, especially under high-viscosity conditions (Caiazza et al. 2007). A malfunction on this level might enhance production of the primary structural component of the biofilm, which in *Xanthomonas* is xanthan.

Additionally in *P. aeruginosa* it was shown that the flagellar gene expressions are decreased while a biofilm matures and that to an unknown extend cyclic di-GMP is involved (Guttenplan and Kearns 2013). Other than that it is notable that for *Pseudomonas aeruginosa* the decrease in motility promotes a more structured and stable three-dimensional architecture within the biofilm (Guttenplan and Kearns 2013).

In order to perform the mutations in two different strains, the genomic organization had to be checked in Xcc B100 and Xcc JBL007. Fortunately, the genomic neighborhood is annotated

fairly similar, and the genes even showed an identical sequence, for both *fliC* and *fliM*. This clearly facilitated the transfer of mutations into both strains.

Flagellin (FliC) is one of the most abundant proteins of bacterial cells and it might be involved in signaling leading to biofilm formation (Berg 2003; Zhao et al. 2007). *fliC* represents a class III flagellar gene, meaning that this gene is expressed late in the flagellar biosynthesis (Yang et al. 2009). Moreover, a mutation in the flagellin gene was thought to be sensible in order to construct viable and structural stable cells that are able to survive industrial cultivation conditions.

The *fliM* gene is a class II flagellar gene that is expressed quite early during the flagellar biosynthesis (Yang et al. 2009). It interacts with the clutch protein CheY and is responsible for the clockwise or counterclockwise movement of the bacterial flagellum (Toker et al. 1996; Guttenplan and Kearns 2013; Zhao et al. 2014). The prediction of a phenotype for the mutant was not easy, since several phenotypes are reported in *Salmonella typhimorium* (Toker et al. 1996). However, FliM is important for signaling events that might lead to biofilm formation and also the inhibition of the entire flagellum might be favorable for xanthan production.

The results of the production studies as well as the enhanced xanthan viscosity were remarkable, yet, polar effects of the mutations cannot be excluded due to the integration of the vector. Still, for the outcome of the study it was not essential to specifically avoid polar effects.

Flagellar mutations in *fliM* and *fliC* resulted in non-motile strains of Xcc

As described in literature (Yang et al. 2009) one polar flagellum was observed in Xcc JBL007, after electron microscopy was performed. In contrast to that no flagellar structures were detected in either of the mutant strains. For the *fliC* mutant this represented the expected phenotype, since the biosynthesis of the protein flagellin, which is the protein that builds up the flagellar filament, was inhibited. However, it is not possible to say whether the membrane based flagellar parts, like the rotary motor, were synthesized or not, since these structures cannot be resolved by the applied electron microscopy. Still, the results of the swarming analysis showed that Xcc JBL007 *fliC*⁻ is indeed a non-motile strain. For mutations in the *fliM* gene several phenotypes were reported in *Salmonella typhimorium*. Depending on the location of the mutation, a flagellum with a bias towards the counterclockwise switch, poorly

motile or non-flagellated bacteria were detected (Toker et al. 1996). Yet, the constructed strains in this study carried a plasmid integration in *fliM*, implying a vast interruption of the gene that should lead to non-flagellated strains. Fortunately, it was possible to observe the phenotype by EM and by a swarming test. No flagellum was observed in any of the recorded cells during microscopy and further no swarming could be detected. Thus, results strongly indicate that the strain Xcc *fliM*⁻ is a non-flagellated, non-motile strain.

Flagellar genes as targets for mutations in Xcc can be beneficial for xanthan production

Mutation analysis was started in laboratory strain Xcc B100 and for both flagellar approaches, a mutation in *fliC* and in *fliM*, respectively, promising xanthan production results could be obtained. Then, in order to test the industrial potential of the approaches, it was possible to transfer both mutations to the xanthan high producer strain Xcc JBL007 and to test the new constructed strains Xcc JBL007 *fliC*⁻ and Xcc JBL007 *fliM*⁻ at the production facility of Jungbunzlauer Austria AG in Austria under industrial conditions. Working so close to the industrial process, by using e. g. industrial strains and medium, added a deeper value to the obtained results. Applied to the tested mutant strains it appeared that Xcc JBL007 *fliC*⁻ produced more xanthan than the flagellin carrying initial strain Xcc JBL007. However, in the *fliC*⁻ mutant the production was still less than the production in the mutant Xcc JBL007 *fliM*⁻. Xcc JBL007 *fliM*⁻ showed a mean production increase of more than 10% in the flask cultivations, as well as in the fermenter approaches, whereas both were performed at the Jungbunzlauer Austria AG campus with industrial production medium. Even in the fed batch approach a remarkable mean increase of almost 10% was measured for Xcc JBL007 *fliM*⁻. Why the mutant Xcc JBL007 *fliM*⁻ produced more xanthan than the *fliC*⁻ mutant is not yet clear, but *fliM* represents a class II and *fliC* a class III, late, gene in the flagellar assembly (Yang et al. 2009). Thus, one possible explanation could be that in the *fliC* mutant the basal flagellar body was built, while this was not the case in a mutant for *fliM*, as shown by Toker and colleagues (Toker et al. 1996). Additionally, the proton influx or signaling events could differ in both mutations and this might play a role in the differential xanthan production of both strains. For instance, it might be possible that the flagellum still rotates to some extent in Xcc JBL007 *fliC*⁻, which might influence the mechanosensory signaling towards biofilm and EPS production. It was already shown that rotation is an important factor in *B. subtilis* biofilm and EPS regulation

(Belas 2013). Moreover, since the production of Xcc JBL007 *fliM*⁻ showed a vast increase as compared to the initial strain, at least for this mutant it is unlikely that only structural components and building blocks were the source of the enhanced xanthan biosynthesis. Therefore, the influence of regulation could be important for the measured effects, since it is known that e. g. the important regulator molecule DSF is involved in both, xanthan and flagellar regulation (He and Zhang 2008).

For the fed batch approach, the increase in xanthan production of Xcc JBL007 *fliM*⁻ as compared to JBL007, could be explained similarly. Yet, compared to the unfed fermentations both, the *fliM* mutant strain and the initial Xcc JBL007 strain showed a gain in xanthan yields. Therefore, it is likely that an additional increase in cell density, due to a higher amount of nitrogen, 0.7 g l⁻¹ compared to 0.6 g l⁻¹, and feeding of carbon, were the source of the increased yields. Still, it has to be taken into account that the production increase is limited. Naturally, more cells produce more xanthan, if the optimal amounts of resources are available. However, in the executed cultivation approaches a high demand of oxygen was detected, although stirring and air inflow were at their maximum capacities. Therefore, further increase in feeding and production is only possible if oxygen supply can be enhanced, while energy consumption for cooling can be dealt with. Since industrial xanthan production is an energy intensive process (Hublik 2012), the latter might actually be the biggest problem for industrial scale cultivations.

Characterization of rheological properties revealed enhanced viscosities in solutions by xanthan of the flagellar mutants

Differences in viscosities over a range of applied shear ranges, is a typical behavior for non-Newtonian liquids and is known to decrease while the applied shear rates increase. This was also reported to appear in xanthan solutions (Casas et al. 2000; CPKelco 2008). Therefore, the obtained distribution of viscosity values was perfectly normal. Further, the differences in xanthan viscosity by xanthan of the same strains but under different cultivation conditions was not surprising. It is well known that viscosity values are linked to and influenced by different conditions (CPKelco 2008; Gulrez et al. 2012). Therefore the change of media and from fermenter to Erlenmeyer flasks was expected to generate some kind of different values. However, important to note is that although all viscosity values changed, the general outcome

of the experiment was comparable. In both approaches the xanthan by the flagellar mutants Xcc JBL007 *fliC*⁻ and Xcc JBL007 *fliM*⁻ showed increased viscosity values, as compared to the respective xanthan by Xcc JBL007.

The general increase in viscosity values or thickening characteristics of the xanthan harvested from both of the flagellar mutant strains that were detected in both experiments, could be a beneficial feature for industrial produced xanthan. For instance because less xanthan has to be used for a desired product viscosity. To explain the differential viscosity values, one has to consider that xanthan characteristics, like secondary structures, molecular weight or acetylation and pyruvylation patterns might influence the rheological properties. Furthermore, it was already shown that these features are not fixed and can alter xanthan characteristics (Casas et al. 2000; Gulrez et al. 2012). Mostly, xanthan is thought to build up a double helix formed by two xanthan strands, however, to some extent single stranded xanthan occurs in isolated samples (Gulrez et al. 2012). A shift away from the normally occurring structure could be one explanation for differential viscosity. Other than that it was reported that a decrease in motility can lead to an altered more structured biofilm architecture in *P. aeruginosa* (Guttenplan and Kearns 2013), which might be connected to an increase in viscosities. However, xanthan production under the applied test conditions did not occur on a solid phase with adherent cells and the downstream processing of xanthan samples followed industrial protocols, therefore, it is unclear if or to what extent an altered biofilm structure, like the one described in *Pseudomonas*, is a feasible explanation. The best hints on differences between the xanthan of the flagellar mutant strains and initial strain Xcc JBL007 could be obtained by a compositional analysis by NMR and AFM.

In depth analysis of different xanthan samples indicates an explanation for viscosity changes of flagellar mutant xanthan

In order to find explanations for the increased viscosity values of the xanthan produced by a flagellar mutant of Xcc JBL007, chemical characterization approaches were carried out. Initially ¹H-NMR was applied to elucidate whether the atomic composition is changed between the strains. The NMR clearly revealed that the chemical composition of the different xanthan species was identical, suggesting the same amount of pyruvilation and acetylation in each of the three strains.

Further, it has to be taken into account that xanthan is an ionic polysaccharide, where single molecules interact with other xanthan fibers, depending on the concentration of the polymer and the external salt amounts (Rinaudo et al. 1983; CPKelco 2008). Since the bacterial cultures from all three strains were treated equally, the xanthan was prepared identical and NMR showed no difference that indicated differences in the ionic pyruvate or acetate groups, it is unlikely that big differences in external salts were the reason for the differences in viscosity. Nevertheless, the molecular weight or differences in the degree of helical conformations in the isolated samples might have been responsible for viscosity changes in Xcc JBL007 *fliC*⁻ and Xcc JBL007 *fliM*⁻.

The obtained AFM results of xanthan by Xcc JBL007 *fliM*⁻ compared to Xcc JBL007 xanthan, gave hints towards the detected viscosity changes, because in contrast to the NMR measurements differences could be spotted. The overall length of the xanthan fibers appeared to be longer in the flagellar mutant strain *fliM*⁻, however, due to the standard deviation no significance could be observed. Although, a study performed by Galvan and colleagues reported an increase in viscosity that could indeed be explained by higher xanthan contour length of a xanthan produced by a mutant strain (Galvan et al 2013). Nevertheless, a significant increase the persistence length of 54 nm compared to 33 nm was found in Xcc JBL007 *fliM*⁻ and Xcc JBL007 xanthan, respectively. This could explain the increased viscosity, because the persistence length in xanthan polymers indicates its stiffness, which accounts for the rheological properties, as was found by Sho and colleagues (Sho et al. 1986) and since is an indicator for xanthan properties (CPKelco 2008; Gulrez et al. 2012).

Conclusions concerning flagellar gene mutations as a targeted mutation approach in Xcc driven by xanthan production

The analysis of two *Xanthomonas campestris* flagellar mutants in two Xcc strains revealed insights with a possible industrial impact. Mutants in the genes *fliC* and *fliM* resulted in good xanthan producer strains in Xcc B100 and the results could even be transferred from laboratory strain B100 to production strain Xcc JBL007. For the mutants Xcc JBL007 *fliM*⁻ and Xcc JBL007 *fliC*⁻ an increase in rheological properties of their respective xanthan in solution could be measured, as compared to Xcc JBL007. The best production strain was the mutant of the basal gene *fliM* in production strain Xcc JBL007. Its production exceeded both, the initial

JBL007 and the already enhanced JBL007 *fliC*⁻ production. In every tested approach, it showed a remarkable improvement coupled with an increase in xanthan viscosity. Obtained xanthan production values were putatively only in part due to more available resources or ATP. The regulatory system that leads to EPS production and is co-dependent on the flagellum, could be a suitable explanation to further elucidate the shown xanthan productions, particularly for the basal mutant in *fliM*. Similar considerations, of inversed regulation of biofilm production and the flagellum were already published, e. g. for *P. aeruginosa* (Caiazza et al. 2007; Belas 2013).

These results highlighted the biotechnological potential of interfering with the flagellar synthesis in order to obtain enhanced xanthan production. Therefore, the performed study might serve as an example, especially since it showed that even modern production strains are not yet at their respective limits. Furthermore, the results indicated that not only enhanced xanthan production can be a target. Xanthan properties, like the industrial important rheological characteristics (CPKelco 2008; Hublik 2012), might be altered in order to create a product with different characteristics, while the chemical composition could be unaffected. Overall, improved production strains, with enhanced xanthan yields and improved viscosity characteristics were presented, which could widen the door for rational strain design in Xcc.

5 The Influence of Mutations in Two Regulator Genes of *Xanthomonas campestris* pv. *campestris* B100 and Production Strain JBL007 on Xanthan Production

Regulation of xanthan production

Not much is described concerning the regulation of xanthan under industrial cultivation conditions. It is known that xanthan production is initiated after nitrogen starvation, therefore after biomass production (Kreyenschulte et al. 2014). Most regulation patterns in *Xanthomonas* are described in the context of virulence and quorum sensing (Slater et al. 2000; Vojnov et al. 2001; He and Zhang 2008). It was reported that the genes *rpfA-G* (regulation of pathogenicity factors) are involved in EPS production (Figure 5-1) (Slater et al. 2000; He and Zhang 2008) and that mutants in these genes are characterized through reduced virulence, production of extracellular proteins and through reduced EPS production (Barber et al. 1997). Other than that the quorum sensing signals DF (Diffusible Factor) and *rpf* dependent DSF (Diffusible Signal Factor), both seem to be important signal molecules that are exported by the bacteria (Poplawsky et al. 1998; He and Zhang 2008). DF was discovered when a mutant in the gene *pigB* that resulted in a non-pigmented strain with four fold less EPS production and reduced virulence, could be restored by addition of culture supernatant of the wild type (Poplawsky et al. 1998). Similarly, the DSF factor was described. Mutants in *rpfF*, which produce significantly less EPS and show reduced extracellular enzyme activity, were restored by wild type co-cultivation (Poplawsky et al. 1998; He and Zhang 2008). DSF could be purified and identified as *cis*-11-methyl-2-dodecenoic acid, while DF seems to show a butyrolactone structure. Studies on the DSF-dependent transcriptome showed that 165 genes are the core of what is influenced by DSF, while in other experiments even more genes could be identified (He and Zhang 2008). Around 80% of the regulated genes are activated, while ~20% are repressed. The targeted genes can be grouped in 12 classes, amongst them: LPS and EPS synthesis and secretion, flagellum biosynthesis, motility and chemotaxis or the TCA cycle (Figure 5-1) (He and Zhang 2008). The DSF signal itself is transduced by a two component system encoded by *rpfC* and *rpfG*, with a cyclic di-GMP phosphodiesterase domain at RpfG (Figure 5-1) (He and Zhang 2008). This implies that the second messenger cyclic di-GMP plays a crucial role in quorum sensing and EPS production in *Xanthomonas*. Following these results

it was shown that the global transcriptional regulator Clp (CAP-like-protein) is a key part of the regulatory network of DSF signaling. The *clp* mutant shows the same phenotype as DSF-deficient mutants, but Clp regulates not all of the DSF functions (He et al. 2007). Clp affects 299 genes directly or indirectly through interplay with other regulators. It shows a conserved helix turn helix domain and binds the DNA at a specific symmetrical DNA sequence located near or in the promoters (He et al. 2007; He and Zhang 2008).

Overall, it was shown that DSF and Clp regulate the transcription of genes that can be grouped in 12 functional categories involved in many cellular activities, with EPS production being only one example, and several hundred genes (He et al. 2007; He and Zhang 2008). Regulation can occur through a direct transcriptional regulation or through the regulation of downstream transcriptional regulators (He et al. 2007; He and Zhang 2008). Additionally, it seems as if the Xcc DSF signal is able to auto induce its biosynthesis over the DSF producing *rpf* genes (He and Zhang 2008).

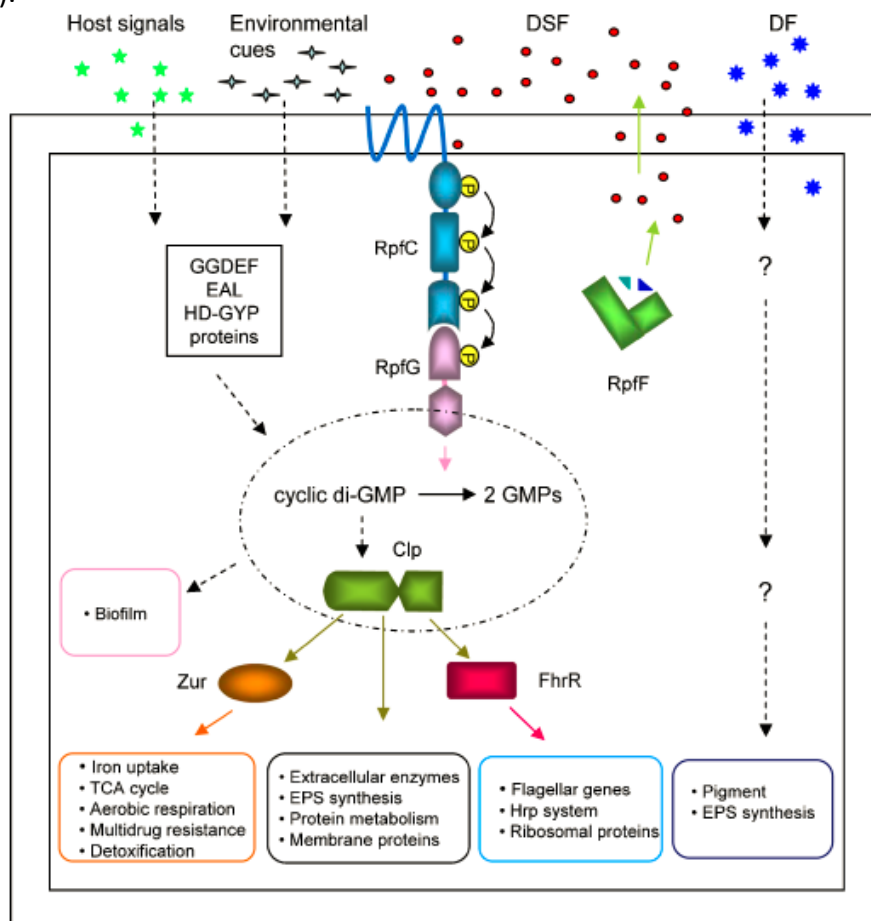


Figure 5-1: Schematic overview on the Xcc quorum sensing signaling network. Next to environmental and host signals, the DSF signaling, transduced by RpfC and RpfG, involving cyclic di-GMP, DF signaling and involvement of Clp at the transcriptional level are depicted. The boxes highlight the influenced metabolic pathways, including EPS biosynthesis. From He and Zhang 2008, License number: 4000421367724.

Aim

Two novel Xcc B100 carbohydrate related transcriptional regulators, *Crt1* and *Crt2*, were recently detected in a study characterizing sucrose related regulation. The hypothesis for this part of the thesis was that both regulators might not only be involved in sucrose related signaling, but could also be involved in xanthan production. To test this hypothesis, *crt1*⁻ and *crt2*⁻ mutant strains were analyzed towards their xanthan phenotypes.

Results

Two novel regulators are involved in the *Xanthomonas campestris* pv. *campestris* carbohydrate metabolism

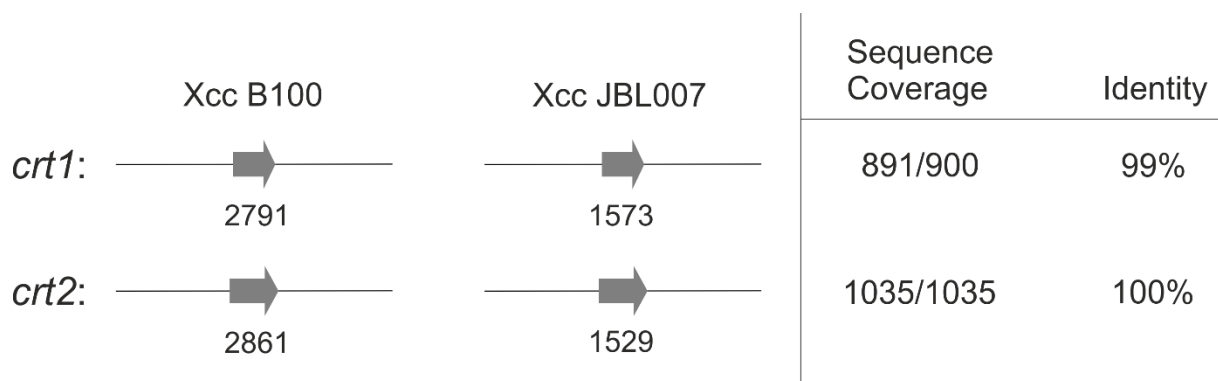


Figure 5-2: Comparison of the target regulator genes *crt1* and *crt2* in *Xanthomonas campestris* pv. *campestris* B100 and JBL007. Depicted underneath the strain names are the corresponding locos tags (GenDB, Meyer et al. 2003). Sequence coverage (identical bases) and Identity were obtained through BLAST (Altschul et al. 1990) analyses of the genes from Xcc B100 vs. JBL007.

Recently a study to specifically screen for sucrose related transcriptional regulators was performed in Xcc B100 (Leßmeier et al. 2016). Next to several known regulators, two novel regulators were detected. Since they were not yet named, they were called by their respective locus tag, *xcc-b100_2791* and *xcc-b100_2861*. However, because their impact on the Xcc carbohydrate metabolism became apparent, they are now addressed by the names: carbohydrate related transcriptional regulators (*crt*), *crt1* for *xcc-b100_2791* and *crt2* for *xcc-b100_2861*. Both regulators were found to belong to the LysR regulator family. For neither of the regulators a functional connection could be drawn to neighboring genes (Leßmeier et al. 2016). Still, while the regulator *crt1* has not yet been characterized, the homolog of regulator

crt2 in Xcc 8004 (XC_2801) was described in 2014 (An et al. 2014), in the background of cyclic di-GMP related signaling. Nevertheless, since both regulators have been shown to be active in carbohydrate related transcriptional regulation, mutants were constructed in order to test for phenotypes, especially in regard to an altered xanthan production. First knock-out mutants, resulting in kanamycin resistant strains Xcc B100 *crt1*⁻ and Xcc B100 *crt2*⁻, were constructed (Loka 2012) using a vector based integration. However, in order to work with the production strain Xcc JBL007, homologue genes had to be identified through sequence comparison. With the help of the draft genome of Xcc JBL007 in GenDB (Meyer et al. 2003) and BLAST analyses (NCBI, Altschul et al. 1990), a sequence showing an identity of 891 of 900 bases or 99%, could be assigned to the Xcc JBL007 gene with locus tag 1573 (*crt1*) and therefore was found to be the homologue of *xcc-b100_crt1*. The same was performed to find the Xcc JBL007 homologue of *xcc-b100_crt2* and the gene with locus tag 1529 (*crt2*) even showed a 100% identity (1035 of 1035 bases) (Figure 5-2). Following these results mutant strains Xcc JBL007 *crt1*⁻ and *crt2*⁻ could be constructed. Thus, kanamycin resistance gene carrying vector pk18mob (Schäfer et al. 1994) was used as backbone and central parts of the target genes were cloned into the multiple cloning site. The constructs were then transformed into *E. coli* DH5 α and cells were plated on kanamycin containing agar plates, followed by blue-white selection. Vectors were checked for integration of the specific gene insert and positive constructs were then electroporated into Xcc.

Xanthan production of Xcc B100 regulator mutants Xcc B100 *crt1*⁻ and Xcc B100 *crt2*⁻

The mutant strains were cultivated in parallel to the wild type in XMD minimal medium, supplemented with 0.6 g per l nitrate and 30 g per l glucose. Xanthan was harvested after 96 h of cultivation and depicted xanthan amounts originated from dried xanthan.

In Figure 5-3 the mean production amounts of two cultivations of each strain are shown. The Xcc B100 wild type produced a mean of 6.34 g xanthan per g biomass during these two cultivations. Simultaneously, the mutant Xcc B100 *crt1*⁻ produced around 8.11 g per g, indicating an enhanced production of more than 1.7 g xanthan per g biomass or a productivity increase of 28%. Quite similar to the strain deficient in the regulator *crt1*, the strain Xcc B100 *crt2*⁻ showed a mean production of 8.07 g g⁻¹. Again hinting towards an increased xanthan production as compared to the Xcc B100 wild type, since the productivity rose by 27%. These

results indicated the potential of both regulator mutant strains towards an enhanced xanthan production. Therefore, constructed mutants of the production strain Xcc JBL007 were taken for cultivation under industrial conditions.

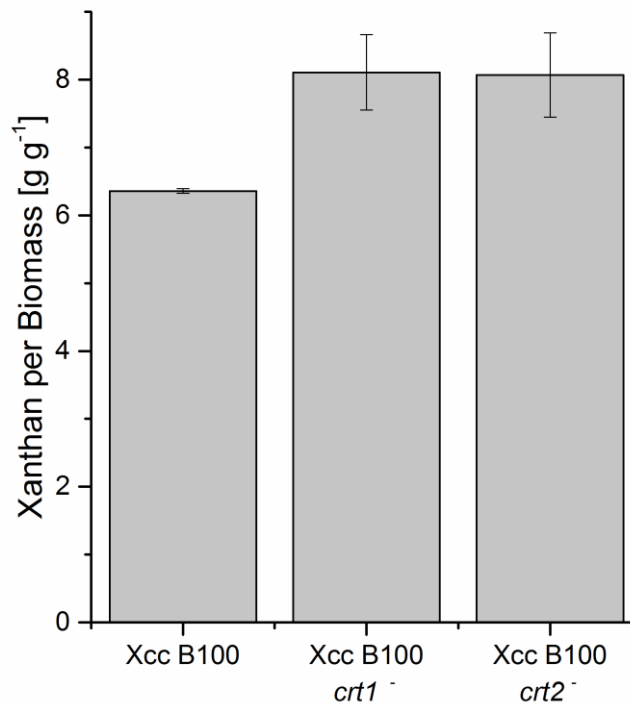


Figure 5-3: Xanthan production of *Xanthomonas campestris* pv. *campestris* B100 wild type and derived mutant *crt1*⁻ and *crt2*⁻. Production was measured as dry weight [g] xanthan per [g] biomass. Samples from 2 replicates each. Harvest was after 96 h in the late stationary phase. Bars give the normalized mean xanthan yields, with error bars indicating the standard deviations. Values are depicted in Supplementary table 7.

Xanthan production under industrial conditions by production strain Xcc JBL007 compared to the regulator mutant strains

Depicted results were obtained at Jungbunzlauer Austria AG in Pernhofen, Austria. The methods used by Jungbunzlauer were applied in order to mimic the industrial production. Fermentations were carried out in 10 l scale, applying fermenter systems filled with xanthan production medium at pH 7. Oxygen was monitored and stirring as well as gas flow were adjusted in order to generate a suitable culture environment. Nitrogen and glucose consumption only had to be checked in order to control the growth. 400 ml overnight culture

of Xcc were used to start the fermenter cultures. Compared results were always obtained during simultaneous cultivations. Depicted xanthan values originated from dried samples.

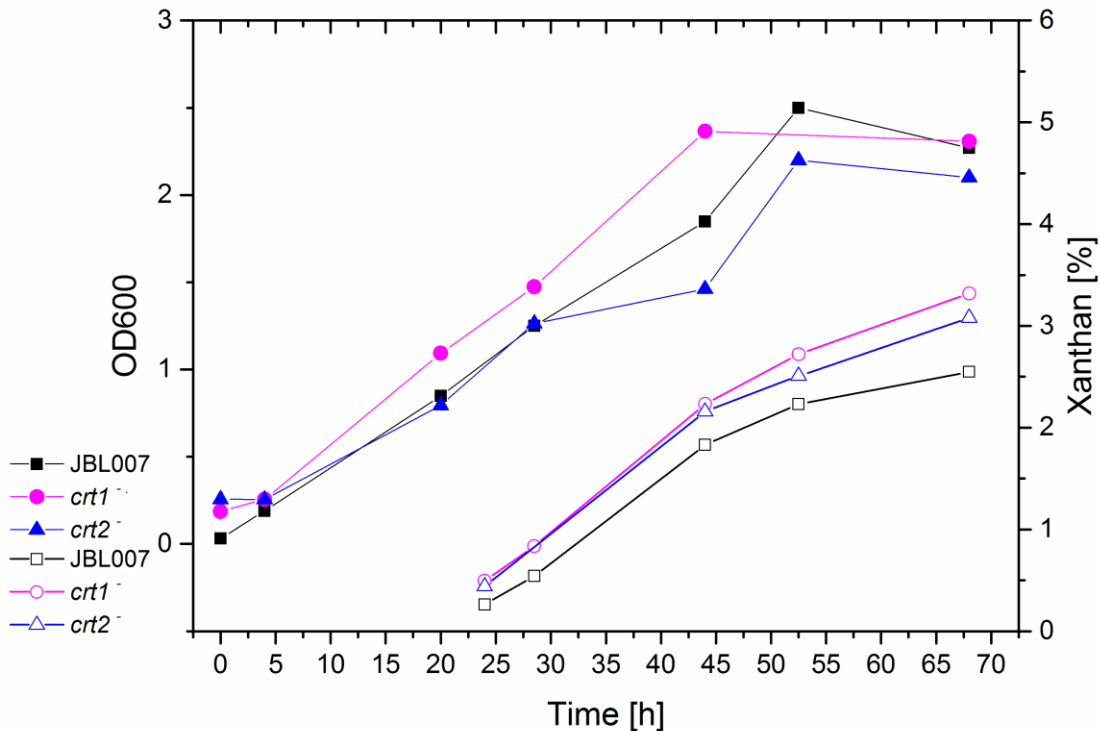


Figure 5-4: Fermentation of *Xanthomonas campestris* pv. *campestris* JBL007 and derived mutants JBL007 *crt1*⁻ and JBL007 *crt2*⁻. Depicted is the growth behavior (OD600) with filled symbols and xanthan production [% (w/v) of the culture] with open symbols. Fermentation was carried out in minimal medium with 0.2 g l⁻¹ corn-extract, 0.6 g l⁻¹ of a nitrogen source and 45 g l⁻¹ glucose from glucosesirup.

Table 5-1: Xanthan production of *Xanthomonas campestris* pv. *campestris* JBL007 and derived mutants JBL007 *crt1*⁻ and *crt2*⁻ after fermentation. Harvest occurred after 68 h.

	Xanthan Yield (g l ⁻¹)
Xcc JBL007	25.5
Xcc JBL007 <i>crt1</i> ⁻	32.2
Xcc JBL007 <i>crt2</i> ⁻	30.8

The fermentation process (Figure 5-4) went on for 68 h. The maximum OD600 for the initial strain Xcc JBL007 was 2.5 and was reached after around 52 h. Also after 52 h the mutant in *crt2* showed its highest OD value of 2.2. The mutant strain Xcc JBL007 *crt1*⁻ grew faster and the peak OD value of 2.4 was reached after 44 h. Following these values the strains entered

the stationary phase, with slight decreases in culture densities (Figure 5-4). First xanthan measurements occurred after 24 h of cultivation. The strain JBL007 had produced 2.64 g l⁻¹, while both mutant strains already showed a production of 4.9 g per l and 4.4 g l⁻¹, respectively, for Xcc JBL007 *crt1*⁻ and *crt2*⁻. From there the production went on until the end of the cultivation (Figure 5-4). The yield in the end was 25.5 g per l for the initial strain Xcc JBL007 and 30.8 g l⁻¹ for the strain deficient in the gene *crt2*. The best production was achieved by Xcc JBL *crt1*⁻ with a yield of 32.2 g xanthan per l (Table 5-1). In total these fermenter cultivations showed an increased production of 5 g l⁻¹ for Xcc JBL007 *crt2*⁻ and of 6.7 g l⁻¹ for Xcc JBL007 *crt1*⁻. These results even exceed the already promising flask cultivations (Table 5-2). Three cultivations applying production medium were performed at Jungbunzlauer Austria AG and the mutant strains showed an enhanced production. Again, Xcc JBL007 *crt1*⁻ produced the highest amounts of xanthan.

Table 5-2: Xanthan production of *Xanthomonas campestris* pv. *campestris* JBL007 and derived mutants JBL007 *crt1*⁻ and JBL007 *crt2*⁻ after shaking flask cultivations. Depicted are the individual values of three measurements and their respective mean with according standard deviation.

Cultivation	Xanthan Yield (g l ⁻¹)			Mean
	1	2	3	
JBL007	15.7	18.7	23.8	19.4 +/- 3.3
JBL007 <i>crt1</i> ⁻	18.9	23	25.5	22.5 +/- 2.7
JBL007 <i>crt2</i> ⁻	18.9	22.4	20.7	21 +/- 1.4

Then the best strain from the regulator mutant approach, which was Xcc JBL007 *crt1*⁻, was used for a fed batch fermentation and compared to the initial strain Xcc JBL007. The medium was almost identical to the previously used medium, however, for the fed batch 0.7 g l⁻¹ of a nitrogen source was used. After 29 h 700 ml of 34% glucosesirup were added to each fermentation in order to feed new carbon into the cultivations. The growth as well as xanthan production are depicted in Figure 5-5. The addition of glucose is shown by an arrow. Clearly, the growth of both cultures enhanced after feeding. Both cultures entered the stationary phase after 44 h and at optical densities of around 2.8. Nevertheless, the end point optical density of the strain Xcc JBL007 went up to 3.4, while the mutant Xcc JBL007 *crt1*⁻ showed an OD of 3.2. The total increase in optical densities could be explained with the increase of

nitrogen. Again production was measured starting at 24 h culture time. Xcc JBL007 had produced 5.5 g l⁻¹, while the mutant strain showed a production of 6.2 g l⁻¹, at the first sampling point. The production naturally went up in both strains and only clearly separated during the late time points of the fermentation (Figure 5-5). The total production yield was 31.45 g l⁻¹ for Xcc JBL007 versus 34.44 g l⁻¹ for Xcc JBL007 *crt1*⁻ (Table 5-3). These results equaled for a notable increased production of almost 3 g xanthan per l or roughly 10%.

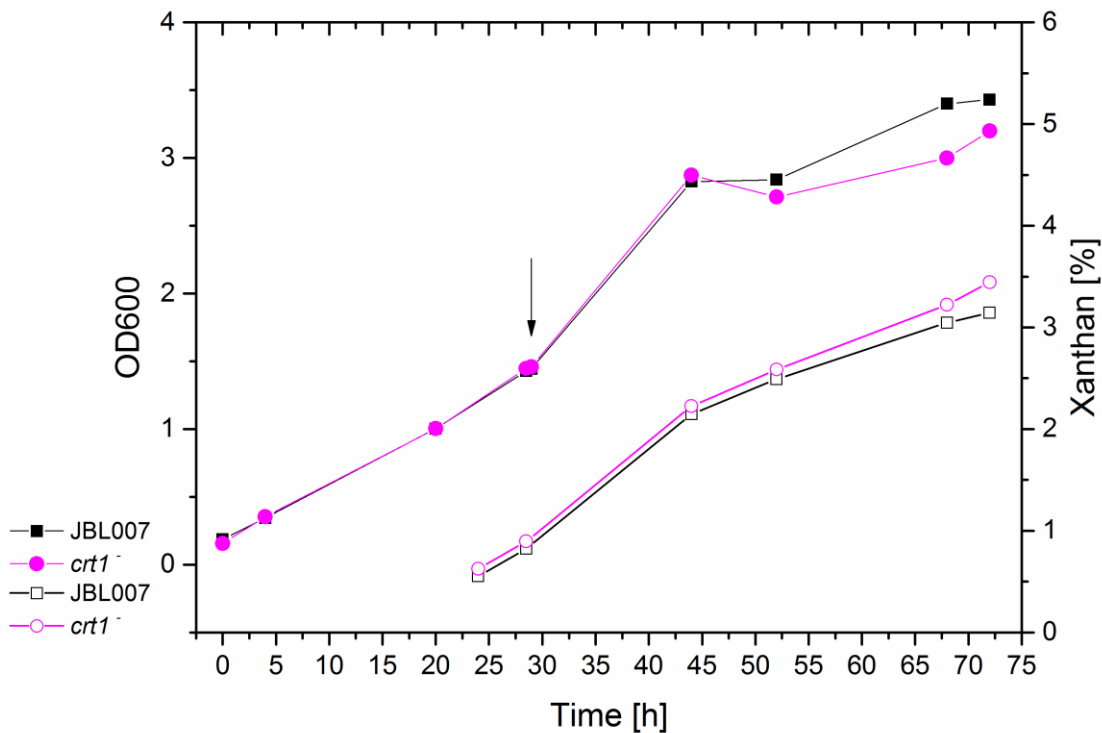


Figure 5-5: Fed batch Fermentation of *Xanthomonas campestris* pv. *campestris* JBL007 and derived mutant JBL007 *crt1*⁻. Depicted is the growth behavior (OD600) with filled symbols and xanthan production [% (w/v) of the culture] with open symbols. Fermentation was carried out in minimal medium with 0.2 g l⁻¹ corn-extract, 0.7 g l⁻¹ nitrogen source and 45 g l⁻¹ glucose from glucosesirup. The arrow indicates the addition of 700 ml 34% glucosesirup after 29 h.

Table 5-3: Xanthan production of *Xanthomonas campestris* pv. *campestris* JBL007 and derived mutants JBL007 *crt1*⁻ and *crt2*⁻ after fed batch fermentation. Harvest occurred after 72 h.

	Xanthan Yield (g l ⁻¹)
Xcc JBL007	31.45
Xcc JBL007 <i>crt1</i> ⁻	34.44

Rheological properties of xanthan produced by Xcc JBL007 compared to the rheological properties of xanthan produced by Xcc JBL007 *crt1*⁻

During the fermentation process the culture broth of the regulator mutant strains did not behave visibly different than the compared Xcc JBL007 culture. However, in order to ensure, the xanthan of the best production strain, strain Xcc JBL007 *crt1*⁻, was taken and its rheological potential was compared to the values of xanthan produced by initial strain Xcc JBL007. Results are depicted in Figure 5-6 with corresponding values in Table 5-4. No notable differences in viscosity values could be measured. Through the whole range of tested shear rates the values of both xanthan species were fairly similar and behaved typical for xanthan solutions. At low shear ranges the highest viscosities were measured, while they decreased over the course of measurements with increasing shear rates. This indicated that Xcc JBL007 *crt1*⁻ produced xanthan with the same rheological quality as compared xanthan of initial strain Xcc JBL007, while the production was enhanced.

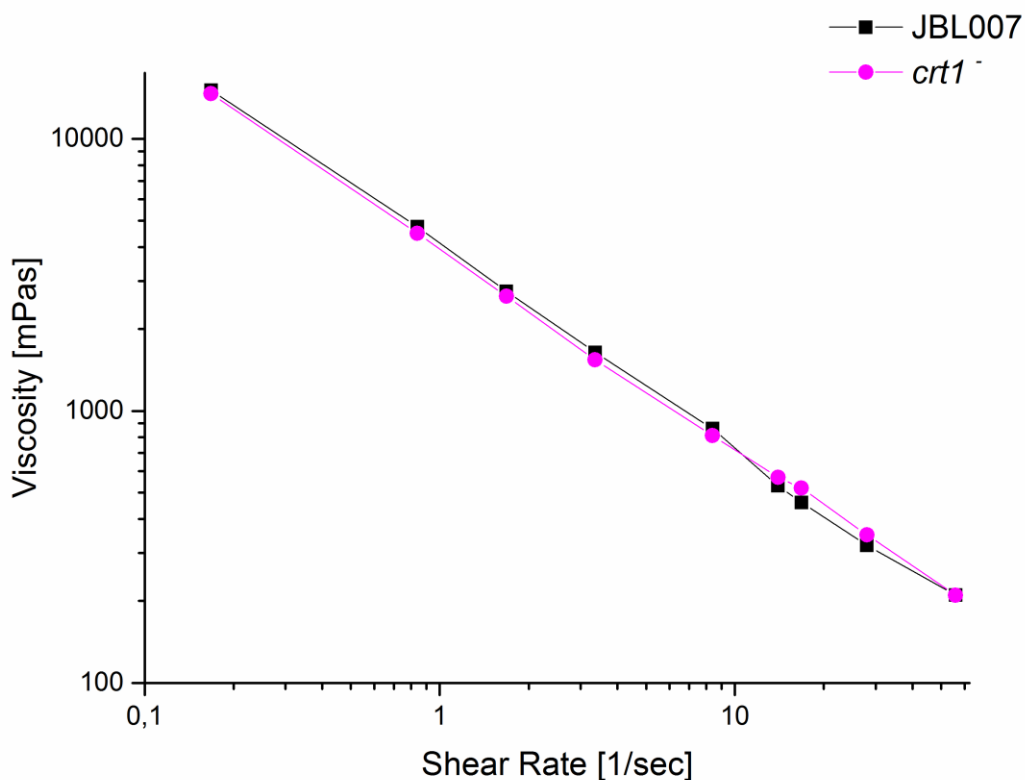


Figure 5-6: Viscosity of the *Xanthomonas campestris* pv. *campestris* strains JBL007 and derived mutant JBL007 *crt1*⁻ in a logarithmic scale. Xanthan was harvested from fermenter cultivations, dried and milled. Measurements were carried out with 1% (w/v) xanthan in water at room temperature.

Table 5-4: Measured viscosity values of *Xanthomonas campestris* pv. *campestris* strains JBL007 and derived mutant JBL007 *crt1*⁻. Measurements were carried out with 1% (w/v) of dried and milled xanthan in water at room temperature.

Shear rate (1*sec ⁻¹)	JBL007 (mPas)	JBL007 <i>crt1</i> ⁻ (mPas)
0,168	15090	14650
0,84	4750	4500
1,68	2750	2640
3,36	1640	1540
8,4	860	810
14	530	570
16,8	460	520
28	320	350
56	210	210

Discussion

Two genes encoding for regulators as mutational targets in Xcc

Prior to this work a study aiming to identify transcriptional regulators of the sucrose related regulation was performed in Xcc B100 (Leßmeier et al. 2016). Next to *suxR*, a known key protein during sucrose dependent regulation (Blanvillain et al. 2007) and the global regulator *clp*, two other, unexpected regulators were identified (Leßmeier et al. 2016). Both regulators were not yet named and therefore addressed by their locus tags *xcc-b100_2791* (*crt1*) and *xcc-b100_2861* (*crt2*), respectively. In Xcc 8004 the gene XC_2801, that resembles *crt2*, was described as a transcriptional regulator that builds a complex with XC_3701, a molecule with a high affinity towards cyclic di-GMP. It was shown that together, these molecules are involved in the regulation of virulence (An et al. 2014). In contrast, *crt1* was not described yet. However, through bioinformatical analyses both regulator molecules could be assigned to the LysR family (Leßmeier et al. 2016). LysR type transcriptional regulators are the most abundant regulators in bacteria. They are characterized by a N-terminal DNA-binding motif and a

C-terminal co-inducer binding motif (Maddocks and Oyston 2008). This regulator family was found to influence the regulation of many different genes, including genes responsible for virulence, quorum sensing or motility (Maddocks and Oyston 2008).

Although the distinct functions of both regulators could not yet been assigned, the fact that they were found to have an influence on the sucrose and therefore carbohydrate metabolism in Xcc B100, made their genes a target for mutations. The aim of the mutations was to screen for an effect in xanthan production, although cultivations were then performed with glucose instead of sucrose.

Furthermore, not only Xcc B100 mutants should be analyzed, but the mutations were also transferred into production strain Xcc JBL007. The genome of Xcc JBL007 is not published, nevertheless, a draft genome was available and through sequence analyses homologue genes to *crt1* and *crt2* were found in Xcc JBL007. The genes in question have the assigned locus tags, *xcc-jbl007_1573* for *crt1* and *xcc-jbl007_1529* for *crt2* and are close or completely identical, to the Xcc B100 gene sequences. This analysis showed the close relationship between laboratory strain Xcc B100 and production strain Xcc JBL007 and can further serve as proof of principle on the possibility to transfer mutants from one strain into the other.

Mutations in two regulator genes are characterized by an increased xanthan production in Xcc

First the mutants in Xcc B100 were analyzed towards xanthan production in glucose containing medium. Both, Xcc B100 *crt1*⁻ and *crt2*⁻ showed remarkable results in terms of productivity. Hence, both mutants were transferred into production strain Xcc JBL007. The derived mutants were cultivated at the Jungbunzlauer Austria AG in Pernhofen, Austria, under authentic industrial cultivation conditions. Due to the work with company standards the obtained results increased in value and impact. The fermentations of both regulator mutant strains, Xcc JBL007 *crt1*⁻ and *crt2*⁻, showed enhanced xanthan production of more than 5 g l⁻¹ as compared to the initial production strain Xcc JBL007. Unfortunately, it was not yet possible to repeat fermentations with the outlined culture conditions. However, three replicates of Erlenmeyer flask cultivations, also performed at the company laboratory applying industrial production medium, correspondingly indicated an increased xanthan production for both mutant strains. Furthermore, a fed batch fermentation could be performed for the strain Xcc

JBL007 *crt1*⁻ in comparison to the initial strain Xcc JBL007 and again the yield clearly pointed to an increased production.

Taken together it can be assumed that the achieved results are due to a better general xanthan production ability by the regulator mutant strains, since in every approach, regardless of applied conditions an increased production was measured. Although both regulator mutations showed to be beneficial for xanthan production, the mutation in *crt1* even exceeded *crt2*.

Since not much is known about either of the regulators, it is difficult to find explanations for their productivity. Both regulator genes were chosen as target, because it could be shown that they are involved in sucrose and therefore sugar related signaling (Leßmeier et al. 2016) and obtained results of this work indicated that both regulators are involved in an even broader range of carbohydrate regulation. A homologue for *crt2* in Xcc JBL007 or B100, was solely described in one study in Xcc 8004 (An et al. 2014). It showed to be an important co-regulator involved in cyclic di-GMP transcriptional regulation. Cyclic di-GMP in Xcc is an important co-factor in many regulated metabolic networks, including quorum sensing, motility and virulence, which all can be influential for biofilm and therefore EPS production (He and Zhang 2008; Guttenplan and Kearns 2013; An et al. 2014). However, these results are drawn from a study focusing on pathogenicity and the function of *crt2* in xanthan production remains obscure. The second regulator Xcc B100 *crt1* or JBL007 *crt1* was not yet functionally described, allowing no conclusion on its functions in xanthan production. Nevertheless, bioinformatical analyses revealed that both regulators belong to the LysR type transcriptional regulator family (Leßmeier et al. 2016). This family of regulators is highly conserved amongst bacteria and can be involved in many different metabolic networks, like virulence, quorum sensing or motility (Maddocks and Oyston 2008).

In order to resolve functions of both regulators and reveal their impact on the Xcc carbohydrate metabolism more research should be performed. The, for Xcc, recently established RNA sequencing (Alkhateeb et al. 2016) would be a good opportunity to gain more information, but also flux balance analyses with labeled glucose could be performed, like it was done for the Xcc B100 amino acid biosynthesis (Schatschneider et al. 2011). It would be highly interesting to find out about the regulators hierarchy and their respective networks. Moreover, focusing on xanthan, it would be important to know, if these regulators are directly involved in xanthan production or if the enhanced productivity is a side effect.

Next to the xanthan production, the rheological properties of xanthan by the regulator mutant *crt1*⁻ was tested. Yet, no altered viscosities could be measured. This showed that the product quality staid on an equal level, when comparing Xcc JBL007 to the mutant in *crt1*⁻.

Regulator gene mutations as target for an enhanced xanthan production in Xcc

The measured increase in productivity regarding xanthan production, in both mutated regulators, in two different bacterial strains, Xcc B100 and Xcc JBL007, and under every applied condition was remarkable. Although the reasons for the shown xanthan production increase are hardly explainable, this study serves as example on possible future targets in Xcc production strain design. The applied regulator fishing may become the method of choice to screen for mutational targets. The screen for regulators involved in sucrose dependent regulation (Leßmeier et al. 2016) led to the identification of two unforeseen mutational targets and the constructed mutant strains showed notable production values that account for a substantial industrial impact. Now different scenarios for applying regulator fishing might arise. For instance, it would be feasible to screen for regulators of the glucose metabolism, since glucose is the primary carbon source during industrial xanthan production (Hublik 2012). Another possibility would be a screening for regulators under xanthan preventing growth conditions, like in complex medium. The outcome could help to construct a constitutive xanthan producer strain. The same might be possible, if a screening under different nitrogen conditions would be executed, since nitrogen and the deviation of nitrogen compared to carbon are essential factors for xanthan production (Kreyenschulte et al. 2014). However, the results are dependent on the correct set of promotor sequences to fish for the DNA binding proteins. Transcriptional studies and start site analyses of Xcc, like recently reported (Alkhateeb et al. 2016), should provide promising sequences, especially in regard to xanthan. Results of such approaches might reveal known and unknown regulators, activators as well as inhibitors. Besides for production, novel results would be of great interest in order to comprehend regulatory networks in Xcc. If novel strains would then be constructed, gathered data could produce results that provide information with scientific and industrial value.

6 Concluding Remarks

The foundation of this work is built upon three major approaches, following different hypotheses. First, mutations in the O-antigen biosynthesis genes *wxcB*, *wxcK* and *wxcN*, were analyzed. The nucleotide sugar metabolism was in the center of attention and it was tested if nucleotide sugars might be redirected towards an enhanced production of xanthan.

Subsequently, the genes *fliM* and *fliC* served as mutational targets in order to inhibit the flagellar biosynthesis. The flagellum is a cost intensive cellular structure, characterized by the demand of copious amounts of building blocks and constant consumption of protons. Furthermore, the flagellum is involved in signaling processes. Therefore, the possibility of flagellar mutant strains being beneficial for xanthan production was analyzed.

The third part of this work was a range of follow up experiments addressing two transcriptional regulators (Crt1 and Crt2) that have been previously identified via a regulator fishing approach in Xcc B100. Their putative impact on xanthan production should be determined through mutant strains deficient in *crt1* and *crt2*, respectively.

The O-antigen biosynthesis as target: Enhanced xanthan productivity and new insights into the Xcc LPS biosynthesis

Three Xcc strains carrying mutations in different genes of the O-antigen gene cluster *wxc* were analyzed with regard to their LPS phenotypes and xanthan production capacities. The strain Xcc H21012 carrying a mutation in *wxcB* was characterized through an altered LPS biosynthesis, since no O-antigen could be identified as part of its LPS structure. Furthermore, the strain showed an enhanced xanthan productivity, as compared the Xcc B100 wild type. The mutant strains Xcc H28110 and H20110, deficient in *wxcK* and *wxcN*, respectively, did not show alterations in their xanthan production, as compared to the Xcc B100 wild type. However, in those mutant strains, a novel LPS phenotype could be determined. Both, Xcc H28110 (*wxcK*) and H20110 (*wxcN*) possessed an O-antigen molecule that lacks the FucNAc side branches. Still, an increase in rhamnose could be measured, indicating an elongation of the rhamnan main chain.

All together these results revealed new insights in the Xcc B100 carbohydrate metabolism. The inhibition of the O-antigen biosynthesis was initially thought to widen the bottleneck

towards xanthan production, however, issues related to cellular stability always had to be taken into account. Based on that, the biosynthesis of the O-antigen branches seemed to be a suitable target for mutations. The side branch biosynthesis depends on *wxcK* and *wxcN* (Vorhölter et al. 2001). It was expected that not as many building blocks, as compared to a complete inhibition of the O-antigen, would be available to enhance the xanthan production. Nevertheless, a better availability of Undp lipid carrier that serve as crucial molecules during xanthan biosynthesis, were assumed to be beneficial for xanthan production. Xanthan repeating units are built at the inner phase of the inner membrane. During the glycosylation reactions, the growing oligo saccharide is bound to a lipid carrier molecule inside the inner membrane and later on the lipid carrier bound repeating unit is translocated into the periplasmic space (Vorhölter et al. 2008). Likewise, Undp lipid carrier are essential for the O-antigen side branch synthesis (Guan and Verma 1999; Vorhölter et al. 2001). Despite this fact, no increase in xanthan production was observed in either of the O-antigen side branch mutant strains. Yet, a putative redirection of resources was detected, since an elongation in the O-antigen rhamnose main chain was determined. This represented a novel LPS phenotype and could help to explain the inconspicuous xanthan phenotypes of Xcc H28110 (*wxcK*) and H20110 (*wxcN*), as compared to the Xcc B100 wild type. Naturally, redirection of resources might not only resolve in favorable outcomes, which in this case was towards xanthan biosynthesis, but also other metabolic pathways with similar precursors might benefit. The O-antigen main chain was still synthesized and the required resources of nucleotide sugars and lipid carrier are identical for the synthesis of both, xanthan and the O-antigen (Vorhölter et al. 2001; Vorhölter et al. 2008). Thus, it might be possible that the inhibition of the O-antigen side branch biosynthesis led to an increased demand of nucleotide sugar precursors for the O-antigen main chain. Furthermore, it cannot be excluded that the O-antigen side branch biosynthesis is involved in main chain length regulation and is therefore important towards precursor consumption. Generally, the LPS chain length determination is still not fully understood. However, in the year 2014 a new model was published by King and colleagues. This model describes a chain length regulation depending on a variable stoichiometry of a complex by the *E. coli* O-antigen biosynthesis proteins WbdA and WbdD, which they named “variable geometry model” (King et al. 2014). Although the O-antigen biosynthesis of both, *E. coli* and Xcc, depends on the same conserved ABC-transporter dependent pathway (Vorhölter et al. 2001; King et al. 2014), there are considerable differences. King and

colleagues worked with *E. coli* O9a, a strain exhibiting a linear O-antigen, and their model seems to fit well on the nature of that O-antigen. Xcc on the other hand, possesses an O-antigen including side branches (Molinaro et al. 2003). In 1999 a model for the addition of side chain residues onto an O-antigen main chain independently of main chain polymerization was developed (Guan and Verma 1999), which is not a part of the model by King and colleagues. Furthermore, in *X. campestris* pv. vitians, a close relative to Xcc, it was already reported that the side branches are linked to the main chain independent of the main chain polymerization (Molinaro et al. 2002). Therefore, the O-antigen chain length model by King and colleagues might not be suitable for Xcc or might have to be extended. Additionally, more research will be necessary to reveal the complex regulation of the O-antigen and to explain the redirection of precursor molecules towards the elongation of the O-antigen main chain. While the O-antigen phenotypes of Xcc H28110 (*wxcK*) and Xcc H20110 (*wxcN*) indicated a higher demand of nucleotide sugar precursors for the O-antigen biosynthesis, different results were determined for the Xcc H21012 (*wxcB*) mutant. No O-antigen residues were identified as part of the expressed LPS molecules, however, an increase in xanthan production could be measured. The gene *wxcB* was reported to be essential for the Xcc B100 O-antigen (Vorhölter et al. 2001), which is in accordance with the detected phenotype in this work. Yet, the precise functions of WxcB were still obscure. In 2014, Park and colleagues published a study on the functional characterization of WxcB in *Xanthomonas campestris* pv. vesicatoria (*X. euvesicatoria*). They reported that the protein WxcB is involved in virulence, detergent tolerance, motility and biofilm formation (Park et al. 2014). It is known that different reagents interact with LPS and decrease the cellular stability (Alexander and Rietschel 2001). Furthermore, a decrease in motility and an increase in biofilm component xanthan could be measured in Xcc H21012 (*wxcB*). However, in contrast to Xcc H21012 (*wxcB*) where no O-antigen could be detected, an altered LPS phenotype could not be measured in the study by Park and colleagues. During an analysis regarding the sequences of genes involved in nucleotide sugar and xanthan biosynthesis, notable differences between Xcc B100 and a strain of *X. campestris* pv. vesicatoria were detected (Vorhölter et al. 2008). Hence, an explanation for the different LPS phenotypes might involve a different genetic subset. Furthermore, Park and colleagues used a gel based analysis to describe the LPS phenotype, which does not allow a detailed structural characterization compared to other methods such as GC-MS or MALDI-TOF-MS. Additionally, polar effects in Xcc H21012 (*wxcB*) cannot be excluded. Nevertheless,

in the *wxcB* mutant strain of *X. campestris* pv. *vesicatoria* an increase in biofilm was reported, which is in accordance with the measured increase in xanthan in Xcc H21012 (*wxcB*), taking into consideration that xanthan is in fact essential for biofilm formation in *Xanthomonas* (Torres et al. 2007). The accumulated lines of evidence provided the basics to assume that an increase in xanthan production can be achieved by interfering with competing metabolic pathways. The increase in xanthan production through the *wxcB* mutant strain was significant, still, limitations in productivity might arise. In Xcc it is thought that LPS account for about 3% of the total biomass (Schatschneider et al. 2013) and some parts of the LPS are essential to the Gram negative bacterial cell as they help to maintain their cellular structure (Alexander and Rietschel 2001). On such basis, and despite its success, the applied approach that aimed to inhibit LPS biosynthesis to favor xanthan biosynthesis, might already reach limitations. On the other hand, other bacterial saccharides might come into play as useful targets. In 1988, the glucose flow in *X. campestris* was measured and during the course of that study it was determined that up to 16% of the cells biomass can consist of the storage saccharide glycogen, as long as glucose does not become a limiting factor (Pielken et al. 1988). Thus, it could be sensible to mutate genes involved in glycogen biosynthesis with the aim of enhancing xanthan production. Besides, inhibition of potential bottlenecks might not only lead to enhanced xanthan production, but also new insights towards a better understanding of the entire bacterial system, especially in regard to the carbohydrate metabolism, might be revealed. However, evaluating the glucose flow in Xcc O-antigen mutant strains could as well lead to valuable information concerning the glucose related metabolism. Similar approaches have already been performed in *Xanthomonas campestris* (Pielken et al. 1988; Schatschneider et al. 2011).

The flagellar biosynthesis as target: Enhanced xanthan quantity and quality

During this particular part of the thesis, mutant strains deficient in the flagellar biosynthesis genes *fliM* and *fliC* were constructed in the Xcc B100 background. The gene *fliM* is transcribed early during flagellar biosynthesis and essential for basal flagellar structures. On the other hand, the gene *fliC* encodes for the structural protein flagellin that is responsible for building up the flagellar filament during later phases of the flagellar biosynthesis process (Macnab 2003). Both mutant strains were shown to be good xanthan producers, therefore the

corresponding genes were systematically mutated in the production strain Xcc JBL007, provided by Jungbunzlauer Austria AG. During fermentations under industrial conditions, both, Xcc JBL007 *fliM*⁻ and *fliC*⁻ produced xanthan in an amount exceeding the production of initial strain Xcc JBL007, with Xcc JBL007 *fliM*⁻ showing the best production values. Furthermore, it could be shown that the xanthan produced by the flagellar mutant strains exhibited enhanced rheological properties, which might be explained through an increase in persistence length, as compared to the xanthan produced by Xcc JBL007, while the chemical properties did not change.

Substantial amounts of building blocks and energy are required for the biosynthesis as well as for the operation of the flagellum (Berg 2003; Macnab 2003). Therefore, in contrast to the O-antigen inhibiting approach, it was thought that not only building blocks could be saved, but also inhibiting the flagellar rotation and thus inhibition of the proton flux, might be beneficial for xanthan production. Additionally, the flagellum is involved in the regulation leading to biofilm and therefore EPS production (Belas 2013; Guttenplan and Kearns 2013). In *P. aeruginosa* even inversed regulation of biofilm production and motility was reported (Caiazza et al. 2007). It was shown that both, xanthan production and flagellar biosynthesis are influenced by quorum sensing and their regulation might be connected through a common signaling pathway involving the action of the so called diffusible signal factor (DSF) (He and Zhang 2008). Nevertheless, most studies focusing on the connection of biofilm production and the flagellum were performed in the context of virulence (Li and Wang 2011; Guttenplan and Kearns 2013). Yet, in order to construct better xanthan production strains, reported findings were taken into account. The protein Flagellin, a product of the *fliC* gene is one of the most abundant proteins in a cell and suggested to play an important role during biofilm formation (Berg 2003; Macnab 2003; Guttenplan and Kearns 2013). However, it cannot be excluded that the mutation of *fliC* solely inhibited the filament biosynthesis and therefore the basal flagellar body is still expressed. The flagellar biosynthesis in general follows a hierarchical order and also in *X. campestris* it was demonstrated that *fliC* is expressed late, after expression of the genes encoding for the basal body has already taken place (Yang et al. 2009). Thus, it is possible that the basal body is built and therefore the proton influx is not inhibited. This led to the construction of a *fliM* mutant strain. FliM is part of the flagellar switch that controls the flagellar rotation (Toker et al. 1996; Macnab 2003). In the hierarchical flagellar gene expression, the gene *fliM* is expressed earlier than *fliC* and it was reported that a *fliM* mutation

can lead to non-flagellated cells (Toker et al. 1996; Yang et al. 2009). However, during a study using *Xanthomonas axonopodis* pv. citri, both *fliM* and *fliC* were identified as important genes in regard to biofilm formation (Li and Wang 2011). Even though the bacterial biofilm does not only consist of EPS, xanthan builds up the essential matrix of the Xcc biofilm (Crossman and Dow 2004). Taken together, both mutant strains showed an enhanced xanthan production that could even be transferred to a modern industrial production strain. The reason why the production strain deficient in *fliM* produced more xanthan than the *fliC*⁻ mutant strain is not yet apparent. Presumably, the inhibition that takes place early during the flagellar biosynthesis is favorable for an enhanced xanthan production, nevertheless, further experimental validation is needed to verify such an assumption. Also, to what extent regulation or redirection of building blocks and protons contributed to the enhanced production remains unknown and is hardly predictable. Moreover, further influences might play an unpredictable role in xanthan production. For instance, a recent study reported that flagella can be glycosylated, which would draw a direct connection to the saccharide metabolism (Merino and Tomas 2014). Although until now no glycosylation pattern for *Xanthomonas* is known, it was shown that e. g. *P. aeruginosa* possesses flagellar glycosylations and that flagellar glycostructures on polar flagellins appear to be the norm (Merino and Tomas 2014). Additionally, the inhibition of the flagellar structure could lead to more available membrane space. This might be favorable for other proteins like carbohydrate importer, xanthan or energy production proteins, which could relieve the competition of ATP production and carbohydrate uptake systems and might be beneficial for xanthan production (Zhuang et al. 2011). Although the enhanced xanthan production cannot be illustrated through one simple explanation, the approach showed that the inhibition of flagellar genes provides great potential for the construction of enhanced xanthan producer strains.

Remarkably, besides the increase in xanthan quantity, also enhanced rheological properties of the xanthan by both flagellar mutant strains were achieved, compared to xanthan from the initial strain Xcc JBL007. In contrast to the production rates, rheological values of xanthan by Xcc JBL007 *fliM*⁻ and Xcc JBL007 *fliC*⁻ were found to be similar. The rheological or viscosifying properties are important features that determine the xanthan quality (CPKelco 2008; Hublik 2012). Structural analyses of xanthan were performed in order to elucidate the chemical composition and to visualize its conformation (Rinaudo et al. 1983; Galván et al. 2013; Moffat et al. 2016). It is reported that an increase in polymer or xanthan chain length and persistence

length or stiffness are important factors for the determination of viscosity properties (Sho et al. 1986; Zhang et al. 2013). A study presenting biological data explaining the enhanced xanthan viscosity properties was published in 2013. Within that study, it was described that the upregulation of *gumB* in combination with *gumC* led to an increase in xanthan chain length that correlated to an increased viscosity in solution (Galván et al. 2013). Nevertheless, the detected enhancement of rheological properties in xanthan by Xcc JBL007 *fliM*⁻ and Xcc JBL007 *fliC*⁻ could not be explained with an increase in chain length, but with an increase in persistence length. However, persistence length determining factors in Xcc are currently unknown. The bacterial cultures and the xanthan samples of the flagellar mutant strains and of the initial strain Xcc JBL007 were treated equally at all times. Thus, a change in external conditions, such as the amounts of salts in solution can be excluded. Furthermore, the chemical composition of all xanthan samples was identical. In conclusion, the reason for an increase in xanthan persistence length remains obscure, but the gathered evidences point out that such a difference could not be attributed to technical variations and that an underlying biological reason might be involved.

In order to further verify the impact of flagellar mutations on xanthan production, different genes of flagellar gene clusters could be mutated. Also interacting genes that should be important, e. g. for signaling involving biofilm and EPS production, might be promising targets. The clutch protein CheY would be a suitable example. This protein interacts with FlIM and together they coordinate the clockwise or counterclockwise flagellar rotation (Macnab 2003). The outcome of a *cheY* mutation would be of interest, because in contrast to the *fliM* mutant, it will possibly not have an inhibitory effect on the flagellar biosynthesis itself. Thus, this mutation could help to determine the importance of signaling biased by the flagellar rotational direction when no structural inhibition of the flagellum occurs. Moreover, the rheological properties of xanthan produced by a *cheY*⁻ mutant would be of interest. Furthermore, Toker and colleagues described that it is possible to construct mutants deficient in small fractions of *fliM*, which show a flagellar counterclockwise rotation bias (Toker et al. 1996). Due to lack of biological data modulating persistence length of xanthan, samples of such mutations could help to elucidate if the flagellar rotation has an influence on the persistence length or if the flagellar structure, e. g. through sensory signaling, has an influence on the xanthan stiffness. Based on the outcome of such a study, additional approaches involving the flagellum or flagellar signaling in regard to EPS or xanthan production might be designed.

Overall, the flagellum is a complex structure, involved in many cellular processes. Thus, it should not only be seen as competing structure for building blocks and potentially ATP, but its putative involvement in signaling events and functions as mechanosensory system (Belas 2014), might be considered and implemented for further applications targeting rational strain design for biotechnological use.

Regulator genes as targets: A novel approach towards enhanced xanthan production

The foundation of this approach was built upon the detection of two interesting regulators in Xcc B100 (Leßmeier et al. 2016). The regulators were termed Crt1 and Crt2 and they were shown to be involved in sucrose related regulation. Crt1 and Crt2 mutant strains in the Xcc B100 background were analyzed towards their xanthan productivities. Interestingly an enhanced xanthan production could be detected, therefore, both mutations were transferred into the production strain Xcc JBL007. Similarly, both mutant strains were characterized through an increased xanthan production. Additionally, no differences could be measured when the rheological properties of xanthan produced by Xcc JBL007 *crt1*⁻ and Xcc JBL007 were compared.

The precise functions of both, Crt1 and Crt2 are still unknown. However, it was revealed that both regulators play a crucial role in sucrose regulated transcriptional signaling (Leßmeier et al. 2016). During the course of this thesis, cultivation was performed with glucose as exclusive carbon source, yet both mutants, *crt1*⁻ and *crt2*⁻, showed an enhanced xanthan production in either of the tested bacterial systems, Xcc B100 and JBL007. This strongly indicated a function for both regulators that is not limited to sucrose related regulation, but to carbohydrate related transcriptional regulation (*crt*) in general. However, in order to elucidate precise functions of both regulators and determine their role during xanthan biosynthesis, more data need to be gathered. At the moment, only one transcriptional regulator with similarities to Xcc B100 *crt2* was briefly characterized in the context of virulence (An et al. 2014). In Xcc 8004, a transcriptional regulator termed XC_2801 was described to bind to a protein with high affinity to cyclic di-GMP, termed XC_3703. Under high concentrations of cyclic di-GMP, the transcriptional activation by XC_2801 seemed to be prevented as indicated by analyses with several detected target promoters and genes (An et al. 2014). Interestingly, some of the detected target genes were shown to be responsible for the flagellar biosynthesis,

indicating an interplay of the flagellum and regulation that could influence xanthan production. Previously it was reported that cyclic di-GMP is important in many signaling networks, including the flagellum and EPS production (He and Zhang 2008; Guttenplan and Kearns 2013). In contrast to Crt2, Crt1 has not been described before. Yet, sequential annotation analyses indicated that both Crt1 and Crt2 belong to the LysR transcriptional regulator family (Leßmeier et al. 2016). LysR type transcriptional regulators are highly abundant in bacteria and they show a conserved structure, with a DNA-binding site and a co-inducer binding site (Maddocks and Oyston 2008). They are known to influence diverse types of genes, including genes of the metabolism, quorum sensing, virulence and motility (Maddocks and Oyston 2008). Although the general regulator family of Crt1 and Crt2 is known and the study by An and colleagues reported a regulator similar to Crt2, precise functions relevant to xanthan production cannot be predicted. However, the detection and mutation of *crt1* and *crt2* in both Xcc B100 as well as Xcc JBL007, with an equal outcome of enhanced xanthan production, indicated an influence in *Xanthomonas campestris* pv. *campestris* EPS production.

As a quality measurement the viscosifying ability of xanthan produced by Xcc JBL007 *crt1*⁻ was compared to xanthan produced by Xcc JBL007. Both xanthan solutions showed the same viscosities, implying identical xanthan properties. Xanthan chain length and persistence length are important factors for the rheological characteristics (Sho et al. 1986; Zhang et al. 2013) and it is not completely understood how these features are regulated. Results of these measurements showed that an increase in xanthan production does not necessarily lead to an increase in viscosifying characteristics.

Still, due to the obtained results concerning xanthan production, mutations of regulator genes should be promoted in order to construct novel producer strains. It was shown that a regulator fishing approach, performed by Leßmeier and colleagues (2016), led to the identification of novel transcriptional regulators that were suitable mutation targets for the construction of strains with enhanced xanthan production capability. Both, Crt1 and Crt2 were detected during a study focusing on sucrose related transcriptional regulation (Leßmeier et al. 2016). Therefore, taken xanthan production into account, this approach could be further applied using different experimental settings. Moreover, recently RNA sequencing, including transcriptional start site analysis, was established for Xcc B100 (Alkhateeb et al. 2016). Regarding xanthan production, obtained data could be further used to identify binding motifs

for transcriptional regulators, whose genes could become mutational targets. Furthermore, since research addressing regulation in Xcc was mostly based on approaches focusing on virulence (Vojnov et al. 2001; He and Zhang 2008; An et al. 2014), further research on xanthan related regulation might lead to substantial insights towards the understanding of Xcc EPS production and regulation.

Towards an enhanced xanthan production

In conclusion, the data gathered throughout the course of this thesis showed that different approaches were successfully applied in order to target enhanced xanthan production (Figure 6-1). Through the transfer of mutations during this work, the close connection of the laboratory strain Xcc B100 and production strain Xcc JBL007 was shown. This indicated that the laboratory strain B100 provides a feasible system gathering valid results towards an enhanced xanthan production in general. Furthermore, the results obtained with Xcc JBL007 showed that even a modern industrial xanthan production strain is not yet limited in its capacity and that therefore genetic engineering approaches might still be feasible. Next to the mutation of novel identified target genes, also the construction of stains with multiple mutations might present a promising future objective. For instance, it could be possible that a strain carrying mutations in the flagellar as well as in the LPS biosynthesis shows to be an even better xanthan production strain than either of the strains carrying only one mutation. However, this approach is strongly dependent on the cells general productivity potential. Overall, results obtained during the course of this thesis are of high industrial value and therefore showed the biotechnological potential of genetic engineering towards xanthan production.

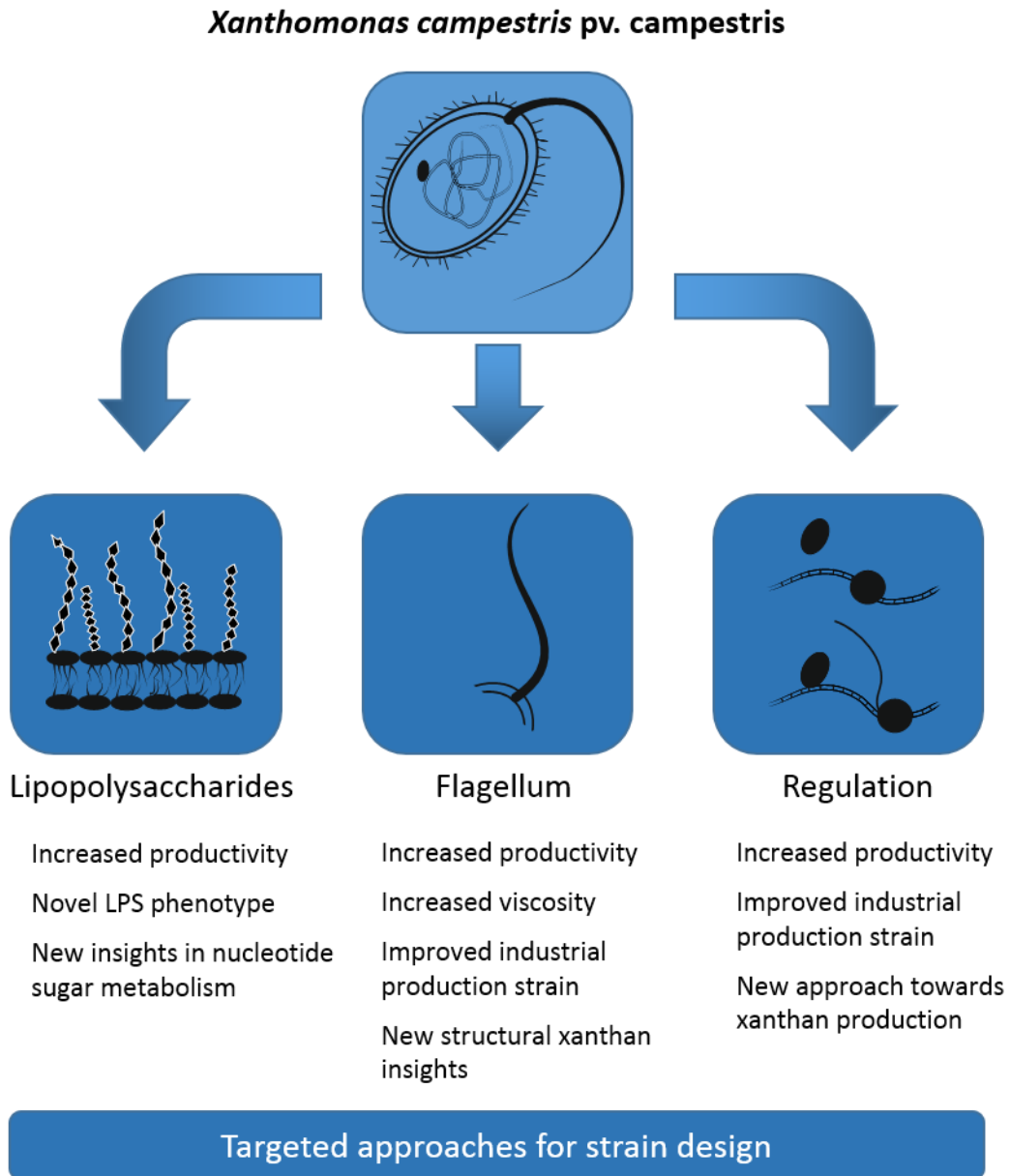


Figure 6-1: Schematic overview of the presented thesis. Three distinct approaches were chosen to obtain improved xanthan production strains and to reveal new insights into the Xcc metabolism. Mutations in genes of the Xcc LPS biosynthesis, the flagellar biosynthesis or in different regulators, build up the fundamental design of this work. Listed underneath each approach are the most important results.

7 Material and Methods

The Influence of the O-antigen as Target for an Enhanced Xanthan Production in *Xanthomonas campestris* pv. *campestris* B100

Strains and cultivation

All strains used in this study are listed in Table 7-1. Cultures were grown at 30°C and 180 rpm (New Brunswick Scientific, Innova 44) in shaking flasks. Pre-cultures of Xcc and cultures destined for LPS isolation were grown in TY rich media (Beringer 1974) (5 g tryptone, 3 g yeast extract, 0.7 g CaCl₂, per l), intermediate and main cultures were grown in XMD minimal media (Schatschneider et al. 2013), supplemented with 30 g l⁻¹ glucose and 0.6 g l⁻¹ KNO₃ as nitrogen source. The pH was adjusted to 7.

When necessary, antibiotics were used in the following concentrations: Streptomycin (Sm): 800 µg ml⁻¹, kanamycin (Km): 80 µg ml⁻¹.

Growth rate (RGR) was determined using the following equation, OD: optical density, t: timepoint:

$$RGR = \frac{\ln(OD2) - \ln(OD1)}{t2 - t1}$$

Table 7-1: Applied bacterial strains for the study of the Xcc O-antigen.

Strain	Relevant Features	Reference
<i>X. campestris</i> pv. <i>campestris</i> B100	Wild type, Sm ^r	Hötte et al. 1990; Vorhölter et al. 2008
Xcc H21012 (<i>wxcB</i>)	<i>wxcB</i> ::Tn5-B20, Km ^r (Simon et al. 1989), Sm ^r	Hötte et al. 1990; Vorhölter et al. 2001
Xcc H28110 (<i>wxcK</i>)	<i>wxcK</i> ::Tn5-B20, Km ^r (Simon et al. 1989), Sm ^r	Hötte et al. 1990; Vorhölter et al. 2001
Xcc H20110 (<i>wxcN</i>)	<i>wxcN</i> ::Tn5-B20, Km ^r (Simon et al. 1989), Sm ^r	Hötte et al. 1990; Vorhölter et al. 2001

Glucose determination

Glucose amounts were determined using the SuperGI ambulance device from Dr. Müller Gerätebau (Freital, Germany). Measurements were carried out in accordance to their given description. 20 µl of 1/5 (v/v) sample in water was taken and given into a pre-packed haemolysis system solution (Hitado, Möhnesee, Germany). Triplicates were measured for each time point.

Nitrate determination

Nitrate determination was performed with 1/5 (v/v) sample in water. Samples were treated according to the instructions of the Merck Spectroquant nitrate kit (Merck Chemicals GmbH, Darmstadt, Germany). Briefly, sample was added to a pre-packed reaction solution 1/16 (v/v), then reagent NO₃⁻ 1K was added 1/8 (v/v). After mixing the samples were incubated for 10 min. Photometric measurements were carried out at 340 nm and for each time point duplicates were measured.

Xanthan and biomass determination

Xanthan and biomass determination was adapted from Palaniraj and colleagues (Palaniraj et al. 2011). Briefly, 5 ml of culture were taken after 96 h of cultivation and diluted with water 1/8 (v/v), followed by centrifugation for 1 h at 12,500 rpm. The xanthan containing supernatant was separated from the bacterial pellet. The pellet was then dried at 60°C for biomass determination. Isopropanol was poured to the supernatant [3/1 (v/v)], followed by 30 min chilling on ice and centrifugation for 1:30 h at 9,000 rpm. Xanthan settled as pellet and the supernatant was discarded. The xanthan pellet was dried at 60°C for 48 h.

LPS isolation

LPS isolation was performed with stationary cultures grown in TY rich media. The LPS was isolated using the hot phenol / water method, described by Westphal and Jann (Westphal, O. and Jann 1965). Briefly, bacteria were centrifuged and the culture supernatant was discarded. Water was added to the sediment, followed by heating to 95°C. Then 95°C hot phenol was

added 1/1 (v/v). The mixture was incubated for 45 min. During incubation the LPS mixture was gently shaken every few minutes to prevent phase separation. Then, samples were incubated on ice for 20 min, to allow phase separation. Phases were harvested individually and put into dialysis tubes (6,000 – 8,000 Da cutoff). Dialysis was performed against distilled water (renewed 3 times a day) and until the phenolic scent had vanished. After Dialysis 5 μ l RNase (3 mg ml⁻¹) and 150 μ l DNase (3 mg ml⁻¹) were given per 50 ml of sample. This was incubated overnight at 37°C and then 150 μ l Proteinase K (2.5 mg ml⁻¹) was given to the samples and again incubated over night at 37°C. The resulting solution was once more dialyzed for two days against distilled water, then transferred out of the dialysis tubes, frozen and freeze dried. The yields were strongly dependent on the phase separation of water and phenol.

Methanolysis and peracetylation of LPS

100 μ g of LPS were methanolized using 0.5 M HCl / methanol for 45 min at 85°C. Methanolysis solution was prepared by addition of acetyl chloride into methanol. After incubation samples were dried under a stream of nitrogen and then washed with methanol and again dried. Samples were peracetylated using pyridine and acetic anhydride 2/1 (v/v) for 30 min at 85°C. Samples were then washed with chloroform and solved in chloroform for GC measurements.

Hydrolysis, reduction and peracetylation of LPS

500 μ g of LPS were hydrolyzed using 0.1 M HCl for 48 h at 100°C. Then 15 μ g xylose was added as an internal standard and samples were dried under a stream of nitrogen, followed by three times washing with 10% ether / hexane and then drying. This was necessary to remove the fatty acids. Then the samples could be reduced. Therefore they were dissolved in 0.5 ml water and the pH was adjusted to 8. Three times 100 μ l of a 10 mg ml⁻¹ NaBH₄ solution were added. Samples were incubated overnight at room temperature and in the dark. Afterwards some drops of 2 M HCl were added. Samples were dried and washed three times with 5% (v/v) acetic acid / methanol, then washed again three times with methanol alone and dried. Peracetylation was performed with pyridine and acetic anhydride 1/1 (v/v) for 10 min at 85°C. Samples could then be washed with chloroform, dried and dissolved in chloroform and used for GC measurements.

In order to determine the exact quantities of rhamnose inside the LPS samples, with the help of xylose as internal standard, a response factor had to be determined. Therefore, 20 µg of rhamnose and 20 µg of xylose were mixed and treated like the other samples prior to GC. Through integration of the peak areas a response factor could be calculated and for rhamnose this factor was 1.17. Total amounts of rhamnose were then calculated as follows: A_C : Corrected peak area; A_{rha} : Measured area of the rhamnose peak; R : Ratio of the corrected rhamnose peak towards the xylose peak; A_{xyl} : Measured area of the xylose peak; $C_{\mu g}$: Amount of peracetylated rhamnose in µg; 1.17: correction reference for rhamnose; 15: Amount of xylose in each sample, in µg.

$$A_C = A_{rha} \times 1.17$$

$$R = \frac{A_C}{A_{xyl}}$$

$$C_{\mu g} = R \times 15$$

Gas Chromatography (GC) (Mass Spectrometry)

Measurements were performed on a PolarisQ GC-MS system (ThermoFisher Scientific). The GC program started with an initial temperature of 150°C for 3 min, then went up to 250°C, with a rate of 3°C per minute. Lastly a rate of 25°C per minute until 320°C was applied and held for 10 min. The Restek Rxi 5Sil MS column in 30 m was used. OA constituent rhamnose, as well as core moieties were identified through reference measurements and FucNAc was detected with the help of the Mass Spectra analyzed by the Xcalibur software from Bruker (Bremen, Germany).

Sample preparation for MALDI-TOF-MS analysis

For the MALDI-TOF-MS experiments 1,5-diamminonaphthalene (DAN) was applied as matrix. DAN solution (7 g l⁻¹) was prepared in acetonitrile. The LPS was also mixed with acetonitrile in a concentration of 5 mg ml⁻¹. 1 µL of LPS analyte and 1 µl of matrix were mixed and then 1 µl of the analyte-matrix solution was spotted directly on the target plate (MTP Anchor Chip 384, Bruker, Bremen, Germany). Samples could then be analyzed by MALDI-TOF-MS.

MALDI-TOF-MS measurements

MALDI-TOF mass spectrometry analyses were performed applying the linear negative mode accelerating potential on a time-of-flight mass spectrometer (Bruker Ultraflex extreme III TOF-TOF; Bruker Daltonik, Bremen, Germany. Ion source 1 voltage -20,0 kV, ion source 2 voltage -18,8 kV, reflector 1 voltage 0 kV, reflector 2 voltage 0 kV and lens voltage -6 kV) which was equipped with a Smartbeam laser (Nd:YAG 355 nm) capable of a repetition rate of 1000 Hz with optimized delayed extraction time. The laser beam size was set to large and the number of shots was 500. Laser energy was optimized for signal-to-noise in each preparation. For every sample 20-50 spectra were accumulated and summarized. MALDI-TOF-MS analyses were performed in cooperation with Marco Giampa.

The Inhibition of Flagellar Structures and the Effects on Xanthan Production and Quality in *Xanthomonas campestris* pv. *campestris* B100 and Production Strain JBL007

Bacterial strains and mutation strategy

The initial strains used for mutation and as control were production strain *Xanthomonas campestris* pv. *campestris* JBL007 from Jungbunzlauer Austria AG and laboratory strain *Xanthomonas campestris* pv. *campestris* B100. Mutations were achieved by single crossover plasmid integration. The chosen plasmid was kanamycin resistance carrying pk18mob (Schäfer et al. 1994). A homologue fragment of the target genes was amplified by PCR. A single colony of Xcc was incubated in sterile water (Milli-Q) at 94°C for 15 min. 5 µl were used as DNA template. PCR was performed using 1 µl of each primer in solution (water, Milli-Q) and 0.25 µl of GoTaq Polymerase (Promega) with according buffers (Promega). PCR: 30 cycles, annealing 60°C, elongation at 72°C, time was template dependent. PCR products were purified, applying the Macherey Nagel NucleoSpin Gel and PCR Clean-Up kit, according to the description. The PCR product was then cloned into the multiple cloning site of pk18mob, which lays inside of a *lacZ* gene, using the HindIII restriction enzyme (ThermoScientific) with according buffer, followed by ligation with T4 DNA Ligase (Fermentas), also using the according buffer. All reaction followed the suppliers' recommended protocols. The ligated

plasmid was then transferred into chemical competent *E. coli* DH5 α . Briefly, 10 μ l Plasmid solution was given to 100 μ l cells and put for 30 min on ice followed by 2 min at 42°C, then incubation for 1 h at 37°C in 1 ml Antibiotic Medium No. 3 Assay Broth (Oxoid). The bacteria were then plated on agar plates containing pre-packed Antibiotic Medium No. 3 Assay Broth (Oxoid) supplemented with X-Gal and IPTG and stored at 37°C. Plasmids from white single colonies were isolated (Plasmid Miniprep Kit, Qiagen) and integration was checked. Then the constructed plasmids were electroporated into competent *Xcc* (2.5 kV cm⁻¹) and the bacteria were incubated in 1 ml SOB medium (5 g l⁻¹ yeast extract, 2 g l⁻¹ tryptone, 10 mM NaCl, 2.5 mM KCl, pH 7) for 2 h and then plated on kanamycin containing TY media agar plates (5 g tryptone, 3 g yeast extract, 0.7 g CaCl₂, 15 g agar, per l) and stored at 30°C. Single colonies were picked and plasmid integration into the target genes was checked. The bacterial strains and used plasmid are depicted in Table 7-2 and the PCR primers used to generate the integration fragments are shown in Table 7-3.

Table 7-2: Bacterial strains and vector used in the approach regarding the flagellum.

Strain or plasmid	Relevant features	Source or reference
<i>X. campestris</i> pv. <i>campestris</i>		
Xcc B100	Wild type, Sm ^r	Hötte et al. 1990; Vorhölter et al. 2008
Xcc JBL007	Derived from <i>Xanthomonas campestris</i> NRRL B-1459	Jungbunzlauer Austria AG
Xcc B100 <i>fliC</i> ⁻	pk18mob inserted in <i>fliC</i> , Km ^r	This work
Xcc B100 <i>fliM</i> ⁻	pk18mob inserted in <i>fliM</i> , Km ^r	This work
Xcc JBL007 <i>fliC</i> ⁻	pk18mob inserted in <i>fliC</i> , Km ^r	This work
Xcc JBL007 <i>fliM</i> ⁻	pk18mob inserted in <i>fliM</i> , Km ^r	This work
<i>E. coli</i>		
DH5α		Strain collection CeBiTec, Bielefeld University
Plasmid		
pk18mob		(Schäfer et al. 1994)

Table 7-3: Primers, including restriction sites, used for mutant constructions.

Target	Forward Primer	Reverse Primer	Restriction Enzyme
<i>fliM</i>	AAAAAAGCTTCCAATCTTCAGGCCGGTGAG	AAAAAAGCTTCGACCCTGGAGATGGTCAAC	HindIII
<i>fliC</i>	AAAAAAGCTTGGAGTTGACCGATGTCAATG	AAAAAAGCTTCCAACGACGGTATCTCACTG	HindIII

Preparation of chemical competent *E. coli* cells

50 ml culture were grown to OD₆₀₀ 0.8 followed by incubation on ice (15 min). Then cells were centrifuged for 10 min at 4,000 g and the pellet was dissolved in 2 ml cold buffer 1 (0.1 M CaCl₂, 2 mM Tris-HCl, pH 7.4). Followed again by centrifugation for 10 min at 4,000 g and resuspension of the cells in cold buffer 2 (0.1 M CaCl₂, 2 mM Tris-HCl, 10% (v/v) glycerin, pH 7.4). 100 µl were used per reaction. Cells could be stored at -80°C.

Preparation of electro competent Xcc cells

10 ml of Xcc overnight culture were incubated on ice for 10 min, followed by centrifugation (all centrifugation steps were performed at 8,000 rpm and 4°C). Cells were washed with water (Milli-Q) and centrifuged, 3 times. The resulting pellet was dissolved in 10 ml 15% (v/v) glycerin and centrifuged for 5 min. Then the pellet was dissolved in 1 ml 15% (v/v) glycerin and again centrifuged (5 min). Supernatant was discarded and cells were dissolved in 50 µl sterile water (Milli-Q) and used for electroporation.

Gene comparison between Xcc B100 and Xcc JBL007

The published genome of Xcc B100 (Vorhölter et al. 2008) and a draft genome of Xcc JBL007 were sequenced at the CeBiTec (Center for Biotechnology), Bielefeld University and are available through the software GenDB (Meyer et al. 2003). Known genome information of Xcc B100 (genomic neighborhood, gene length) were compared to the genome of Xcc JBL007 and putatively homologue genes were run through BLAST (Basic local alignment search tool) against each other (Altschul et al. 1990).

Cultivation conditions

Cultures grown at the CeBiTec, Bielefeld University, were shaken at 30°C and 180 rpm (New Brunswick Scientific, Innova 44) in Erlenmeyer flasks. Pre-cultures of Xcc were grown in TY rich media (Beringer 1974) (5 g tryptone, 3 g yeast extract, 0.7 g CaCl₂, per l), intermediate and main cultures were grown in XMD minimal media (Schatschneider et al. 2013), supplemented with 30 g l⁻¹ glucose and 0.6 g l⁻¹ KNO₃ as nitrogen source. The pH was adjusted to 7.

Erlenmeyer flask cultures grown at Jungbunzlauer Austria AG in Pernhofen, Austria, were grown applying the company protocols. Cultivation occurred at 30°C and 240 rpm (Infors HT, RO-TK), with medium containing 0.6 g l⁻¹ of a nitrogen source, 0.2 g l⁻¹ corn extract and 45 g l⁻¹ glucose from glucosesirup as carbon source at pH 7.

Fermenter cultures were grown at Jungbunzlauer Austria AG in Pernhofen, Austria, in 15 l fermenter system (Braun, Biostat) equipped with rotary stirrer systems, according to industrial standards. Fermenter contained Jungbunzlauer minimal medium with 0.6 g l⁻¹ or 0.7 g l⁻¹ of a nitrogen source, 0.2 g l⁻¹ corn extract and 45 g l⁻¹ glucose from glucosesirup as carbon source. Feeding of fed batch fermentations was performed by the addition of 700 ml of glucosesirup. pH was adjusted to 7 and stirring as well as air supply were adjusted to prevent limitations. All values were chosen equally for every culture. Each fermentation was started with 400 ml overnight culture in Jungbunzlauer complex medium from Erlenmeyer flasks. If necessary the medium for the mutants was supplemented with 80 mg l⁻¹ kanamycin.

Fermentation repeats were performed by Jungbunzlauer Austria AG, under supervision of Dr. Gerd Hublik.

Swarming assay

90 mm petri dishes were prepared with TY medium (5 g tryptone, 3 g yeast extract, 0.7 g CaCl₂ per l) containing 0.3% (w/v) agar. Bacteria were applied into the medium at one spot in the middle of the plate and incubated at 30°C. After 48 h the plates were analyzed.

Xanthan determination

Xanthan determinations performed at the CeBiTec, Bielefeld University were adapted from Palaniraj and colleagues (Palaniraj et al. 2011). 5 ml of culture was taken after 96 h of cultivation and diluted with water 1/8 (v/v), followed by centrifugation for 1 h at 12,500 rpm. The xanthan containing supernatant was separated from the bacterial pellet. The pellet was then dried at 60°C for biomass determination. Isopropanol was poured to the supernatant (3/1 (v/v)), followed by 30 min chilling on ice and centrifugation for 1:30 h at 9,000 rpm. Xanthan settled as pellet and the supernatant was discarded. The xanthan pellet was dried at 60°C for 48 h.

Xanthan determinations performed at Jungbunzlauer Austria AG in Pernhofen, Austria, were executed applying industrial standard methods. Due to different glucose syrup qualities, parallel cultivations were compared. Culture was harvested and two times precipitated with isopropanol [3/1 (v/v)]. To achieve precipitation rigorous mixing was necessary. Resulting xanthan was collected, dried and weight.

Rheometrical measurements

Dried xanthan was milled and the resulting powder was used to produce 1% (w/v) xanthan in distilled water (at least 60 min stirring was applied in order to dissolve the xanthan). A viscosimeter (Rheotec Rotational Viscosimeter) was equipped with a spindle for small sample volumes (Rheotec) and used according to the suppliers' instruction. Different viscosities over a variety of rounds per minute were measured. According to the used viscosimeter spindle shear rates could be calculated.

Transmission electron microscopy

The examination of flagella was performed by transmission electron microscopy (TEM), bacteria from mid-growth-phase broth cultures were washed by gentle centrifugation and re-suspended in buffer. The cells were adsorbed onto Formvar-coated copper grids and fixed on a drop of 2% glutaraldehyde in 0.1 M cacodylate buffer, pH 7.2, for 2 min. The grids were then washed three times in the same buffer, for 20 s each time. Then the grids were negatively stained with 1% (w/v) uranyl acetate and lead citrate for time intervals varying between 10 and 30 s. Excess of the staining solution was removed and the grids were allowed to dry without further washing. The grids were stored in a dessicator over silica gel.

Transmission electron microscopy (TEM) was carried out on a Zeiss EM 109 (Zeiss, Oberkochen, Germany) at 50 kV. Photos were recorded on Rollei ORTHO 25 film (Maco-Photo, Hamburg, Germany) and scanned after development with further electronic image processing. TEM was performed in cooperation with Prof. Dr. Karsten Niehaus and Dr. Hanna Bednarz.

Atomic Force Microscopy

Atomic Force Microscopy was performed at the Biophysics and Nanoscience group at Bielefeld University in cooperation with Julia Teckentrup. Samples were stored at a concentration of 1 mg ml^{-1} , prior to AFM analysis they were further diluted to a working concentration of $2 - 10 \text{ } \mu\text{g ml}^{-1}$. $5 \text{ } \mu\text{l}$ were pipetted onto a cleaved mica sheet and incubated for 30 seconds. Samples were dried under a flow of nitrogen. Topographic imaging was performed, applying a commercial AFM (Multimode 5 and Multimode 8, Bruker, USA), using Tap300 Al-G monolithic silicon cantilevers (BudgetSensors, Bulgaria) with aluminum reflex coating. To provide a disturbance-free environment a vibration isolation table TS150 (TableStable LTD, Switzerland) and an acoustic enclosure (Park Systems, Korea) were used during measurements. Scanning and imaging processes were performed by the controller software Nanoscope (versions 5.30 and 8.15). Imaging resolution was 1280×1280 pixels for overview images and smaller regions were scanned with a resolution of 512×512 pixels. The scan rate was 1 Hz .

Raw data were then processed and analyzed using the Gyddion software package and structural analysis (contour length and persistence length) was performed with the Easyworm software package (Joerg Gsponer Lab, University of British Columbia, Vancouver, Canada).

NMR measurements

Xanthan was slowly dissolved (gentle shaking) in deuterium oxide (99.9%) and freeze dried. This was repeated two times. Then xanthan was again dissolved in deuterium oxide (99.9%) and approximately 10 mg xanthan in solution were used for NMR analysis. Analyses were performed at the Inorganic and Structural Chemistry group at Bielefeld University on a Bruker MRX 550 MHz at 90°C and 128 spectra were accumulated.

The Influence of Mutations in Two Regulator Genes of *Xanthomonas campestris* pv. *campestris* B100 and Production Strain JBL007 on Xanthan Production

Bacterial strains and mutation strategy

The initial strains used for mutation and as control were production strain *Xanthomonas campestris* pv. *campestris* JBL007 from Jungbunzlauer Austria AG and laboratory strain *Xanthomonas campestris* pv. *campestris* B100. Mutations in Xcc B100 were achieved by single crossover plasmid integration, performed by Tobias Loka, the identical mutation strategy was used for Xcc JBL007. The chosen plasmid was kanamycin resistance carrying pk18mob (Schäfer et al. 1994). A homologue fragment of the target genes was amplified by PCR. A single colony of Xcc was incubated in sterile water (Milli-Q) at 94°C for 15 min. 5 µl were used as DNA template. PCR was performed using 1 µl of each primer in solution (water, Milli-Q) and 0.25 µl of GoTaq Polymerase (Promega) with according buffers (Promega). PCR: 30 cycles, annealing 60°C, elongation at 72°C, time was template dependent. PCR products were purified, applying the Macherey Nagel NucleoSpin Gel and PCR Clean-Up kit, according to the description. The PCR product was then cloned into the multiple cloning site of pk18mob, which lay inside of a *lacZ* gene, using the BamHI restriction enzyme (ThermoScientific) with according buffer, followed by ligation with T4 DNA Ligase (Fermentas), also using the according buffer. All reaction followed the suppliers' recommended protocols. The ligated plasmid was then transferred into chemical competent *E. coli* DH5α. Briefly, 10 µl Plasmid solution was given to 100 µl cells and put for 30 min on ice followed by 2 min 42°C, then incubation for 1 h at 37°C in 1 ml Antibiotic Medium No. 3 Assay Broth (Oxoid). The bacteria were then plated on agar plates containing pre-packed Antibiotic Medium No. 3 Assay Broth (Oxoid) supplemented with X-Gal and IPTG and stored at 37°C. Plasmids from white single colonies were isolated (Plasmid Miniprep Kit, Qiagen) and integration was checked. Then, the constructed plasmids were electroporated into competent Xcc (2.5 kV cm⁻¹) and the bacteria were incubated in 1 ml SOB medium (5 g l⁻¹ yeast extract, 2 g l⁻¹ tryptone, 10 mM NaCl, 2.5 mM KCl, pH 7) for 2 h and then plated on kanamycin containing TY media agar plates (5 g tryptone, 3 g yeast extract, 0.7 g CaCl₂, 15 g agar, per l) and stored at 30°C. Single colonies were picked and plasmid integration into the target genes was checked. The bacterial strains and used plasmid are depicted in Table 7-4 and the PCR primers used to generate the integration fragments are shown in Table 7-5.

Table 7-4: Bacterial strains and vector used in the approach regarding *crt1* and *crt2*.

Strain or plasmid	Relevant features	Source or reference
<i>X. campestris</i> pv. <i>campestris</i>		
Xcc B100	Wild type, Sm ^r	Hötte et al. 1990; Vorhölter et al. 2008
Xcc JBL007	Derived from <i>Xanthomonas campestris</i> NRRL B-1459	Jungbunzlauer Austria AG
Xcc B100 <i>crt1</i> ⁻	pk18mob inserted in <i>crt1</i> , Km ^r	Loka 2012
Xcc B100 <i>crt2</i> ⁻	pk18mob inserted in <i>crt2</i> , Km ^r	Loka 2012
Xcc JBL007 <i>crt1</i> ⁻	pk18mob inserted in <i>crt1</i> , Km ^r	This work
Xcc JBL007 <i>crt2</i> ⁻	pk18mob inserted in <i>crt2</i> , Km ^r	This work
<i>E. coli</i>		
DH5α		Strain collection CeBiTec, Bielefeld University
Plasmid		
pk18mob		(Schäfer et al. 1994)

Table 7-5: Primers, including restriction sites, used for mutant constructions.

Target	Forward Primer	Reverse Primer	Restriction Enzyme
<i>crt1</i>	TAGGGATCCACCATCCGCCAACTCAGTTAT	ATAGGATCCAGCAATTCGGCGATAAGCCC	BamHI
<i>crt2</i>	TAGGGATCCCACCTGATCTTCGTCAAGG	ATAGGATCCCTCCAAAATGCGCTTACCCTC	BamHI

Preparation of chemical competent *E. coli* cells

50 ml culture were grown to OD₆₀₀ 0.8 followed by incubation on ice (15 min). Then cells were centrifuged for 10 min at 4,000 g and the pellet was dissolved in 2 ml cold buffer 1 (0.1 M CaCl₂, 2 mM Tris-HCl, pH 7.4). Followed again by centrifugation for 10 min at 4,000 g and resuspension of the cells in cold buffer 2 (0.1 M CaCl₂, 2 mM Tris-HCl, 10% [v/v] glycerin, pH 7.4). 100 µl were used per reaction. Cells could be stored at -80°C.

Preparation of electro competent Xcc cells

10 ml of Xcc overnight culture was incubated on ice for 10 min, followed by centrifugation (all centrifugation steps were performed at 8,000 rpm and 4°C). Cells were washed with water (Milli-Q) and centrifuged, 3 times. The resulting pellet was dissolved in 10 ml 15% (v/v) glycerin and centrifuged for 5 min. Then the pellet was dissolved in 1 ml 15% (v/v) glycerin and again centrifuged (5 min). Supernatant was discarded and cells were dissolved in 50 µl sterile water (Milli-Q) and used for electroporation.

Gene comparison between Xcc B100 and Xcc JBL007

The published genome of Xcc B100 (Vorhölter et al. 2008) and a draft genome of Xcc JBL007 were sequenced at the CeBiTec (Center for Biotechnology), Bielefeld University and are available through the software GenDB (Meyer et al. 2003). Known genome information of Xcc B100 (genomic neighborhood, gene length) were compared to the genome of Xcc JBL007 and putatively homologue genes were run through BLAST (Basic local alignment search tool) against each other (Altschul et al. 1990).

Cultivation conditions

Cultures grown at the CeBiTec, Bielefeld University, were grown at 30°C and 180 rpm (New Brunswick Scientific, Innova 44) in shaking flasks. Pre-cultures of Xcc were grown in TY rich media (Beringer 1974) (5 g tryptone, 3 g yeast extract, 0.7 g CaCl₂, per l), intermediate and main cultures were grown in XMD minimal media (Schatschneider et al. 2013), supplemented with 30 g l⁻¹ glucose and 0.6 g l⁻¹ KNO₃ as nitrogen source. The pH was adjusted to 7.

Erlenmeyer flask cultures grown at Jungbunzlauer Austria AG in Pernhofen, Austria, were grown applying the company protocols. Cultivation occurred at 30°C and 240 rpm (Infors HT, RO-TK), with medium containing 0.6 g l⁻¹ of a nitrogen source, 0.2 g l⁻¹ corn extract and 45 g l⁻¹ glucose from glucose syrup as carbon source at pH 7.

Fermenter cultures were grown at Jungbunzlauer Austria AG in Pernhofen, Austria, in 15 l fermenter system (Braun Biostat) equipped with rotary stirrer systems, according to industrial standards. Fermenter contained Jungbunzlauer minimal medium with 0.6 g l⁻¹ or 0.7 g l⁻¹ of a nitrogen source, 0.2 g l⁻¹ corn extract and 45 g l⁻¹ glucose from glucose syrup as carbon source. Feeding of fed batch fermentations was performed by the addition of 700 ml of glucose syrup. pH was adjusted to 7 and stirring as well as air supply were adjusted to prevent limitations. All values were chosen equally for every culture. Each fermentation was started with 400 ml overnight culture in Jungbunzlauer complex medium from Erlenmeyer flasks. If necessary the medium for the mutants was supplemented with 80 mg l⁻¹ kanamycin.

Swarming assay

90 mm petri dishes were prepared with TY medium (5 g tryptone, 3 g yeast extract, 0.7 g CaCl₂ per l) containing 0.3% (w/v) agar. Bacteria were applied into the medium at one spot in the middle of the plate and incubated at 30°C. After 48 h the plates were analyzed.

Xanthan determination

Xanthan determinations performed at the CeBiTec, Bielefeld University were adapted from Palaniraj and colleagues (Palaniraj et al. 2011). 5 ml of culture was taken after 96 h of cultivation and diluted with water 1/8 (v/v), followed by centrifugation for 1 h at 12,500 rpm. The xanthan containing supernatant was separated from the bacterial pellet. The pellet was then dried at 60°C for biomass determination. Isopropanol was poured to the supernatant [3/1 (v/v)], followed by 30 min chilling on ice and centrifugation for 1:30 h at 9,000 rpm. Xanthan settled as pellet and the supernatant was discarded. The xanthan pellet was dried at 60°C for 48 h.

Xanthan determinations performed at Jungbunzlauer Austria AG in Pernhofen, Austria, were executed applying industrial standard methods. Due to different glucose syrup qualities,

parallel cultivations were compared. Briefly, culture was harvested and two times precipitated with isopropanol [3/1 (v/v)]. To achieve that rigorous mixing was necessary. Resulting xanthan was collected, dried and weight.

Rheometrical measurements

Dried xanthan was milled and the resulting powder was used to produce 1% (w/v) xanthan in distilled water (at least 60 min stirring was applied in order to dissolve the xanthan). A viscosimeter (Rheotec Rotational Viscosimeter) was equipped with a spindle for small sample volumes (Rheotec) and used according to the suppliers' instruction. Different viscosities over a variety of rounds per minute were measured. According to the used viscosimeter spindle shear rates could be calculated.

8 List of Figures and Tables

Figure 1-1: The bacterium *Xanthomonas campestris* pv. *campestris*. a: *X. campestris* pv. *campestris* caused black rot on a cabbage field. b: lesion on a cabbage leaf. c: Two infested savoy cabbage plants next to a healthy control. d: Electron microscopy image of a *X. campestris* pv. *campestris* cell, with one polar flagellum. e: *X. campestris* pv. *campestris* growing on Kings medium. f: *X. campestris* pv. *campestris* growing on yeast dextrose calcium carbonate medium. From Vicente and Holub, 2013, License number: 3983650320184..... 12

Figure 1-2: Circular genome plot of the *X. campestris* pv. *campestris* B100 genome. Grey arrows highlight gene clusters that were important for this work. Displayed within the plot are the conventional gene names of the specific regions (for the flagellum only the *fli* genes). Xanthan biosynthesis: *gum* cluster; Xanthan and LPS precursors and LPS O-antigen biosynthesis: *wxc/rml* cluster and *xanAB*; flagellar biosynthesis: flagellum cluster. Additionally, regulator genes *crt1* and *crt2* are highlighted. The scale accounts for the genomic positions. Image provided by Dr. Vera Ortseifen..... 13

Figure 1-3: Comprehensive sequence analysis of xanthan precursor genes (A) and xanthan biosynthesis *gum* genes (B). Grey arrows show directions and authentic size comparison of the genes. *X. campestris* pv. *campestris* B100 (Xcc B100) is used as basis and compared to *X. campestris* pv. *campestris* ATCC33913 (Xcc ATCC33913), *X. campestris* pv. *campestris* 8004 (Xcc 8004), *X. campestris* pv. *vesicatoria* 85-10 (Xcv 85-10), *X. axonopodis* pv. *citri* 306 (Xac 306), *X. oryzae* pv. *oryzae* KACC 10331 (Xoo KACC10331) and to *X. oryzae* pv. *oryzae* MAFF311018 (Xoo MAFF311018). Conventional gene names are given above the arrows. Numbers within the arrows indicate the deviation of nucleotides. From Vorhölter et al. 2008, License number: 3998990345087..... 15

Figure 1-4: Reconstruction of the nucleotide sugar metabolism in *X. campestris* pv. *campestris* B100. Symbols for genes, proteins, metabolites, catalysis and transition are depicted in the legend. Metabolic reconstruction followed the information of the *X. campestris* pv. *campestris* B100 genome annotation. Xanthan, as well as its precursors UDP-glucose, UDP-glucuronic acid and GDP-mannose are highlighted in red. Further, precursor synthesis for LPS and murein are included in the reconstructed network. From Vorhölter et al. 2008, License number: 3983651418225. 17

- Figure 1-5: Repeating unit of xanthan.** Provided with a glucose backbone to which mannose, glucuronic acid and a second mannose are bound. Here the first mannose is shown with an acetate and the second with a pyruvate group. M: Cation binding site. From Hublik 2012. 18
- Figure 1-6: Model of the *X. campestris* xanthan biosynthesis.** Proteins encoded by the *gum* genes are depicted in green. Initially UDP-glucose (UDPglc) is added onto an UndP lipid carrier by GumD at the inner phase of the inner membrane. Subsequently GumMHKI add a second glucose, as backbone, two mannoses, as well as a glucuronic acid. The mannose originates from GDP-mannose (GDPman) and the glucuronic acid from UDP-glucuronic acid (UDPglcA). The outer mannose can be pyruvylated by GumL or both mannoses can be acetylated by GumFG. The repeating units are translocated into the periplasm by GumJ, polymerized, putatively by GumE and exported by GumBC. From Vorhölter et al. 2008, License number: 3983651418225..... 20
- Figure 1-7: Culture broth of *X. campestris* pv. *campestris* JBL007.** Sample was cultivated in production medium and harvested in the stationary phase. Depicted is the culture directly after harvest from a fermenter..... 22
- Figure 2-1: Schematic overview of the presented thesis.** Three distinct approaches were chosen to obtain improved xanthan production strains and to reveal new insights into the Xcc metabolism. Mutations in genes of the Xcc LPS biosynthesis, the flagellar biosynthesis or in different regulator genes, build up the fundamental design of this work..... 26
- Figure 3-1: General overview of LPS structure and biosynthesis.** a: Depicted are the different forms and states of LPS molecules, next to that a SDS-PAGE of LPS is shown. The lowest, heavily stained band represents lipid A-core LPS, then each band represents LPS with growing repeating units in the O-antigen (from *E. coli*). b: Overview of the principal steps for LPS transport. Abbreviations: R-LPS: rough LPS, LOS: lipooligosaccharide, S-LPS: smooth LPS, OS: oligosaccharide, PS: polysaccharide. From Whitfield and Trent, 2014..... 29
- Figure 3-2: ABC-transporter dependent O-antigen synthesis and transport.** Glycosyltransferases (green) use nucleotide sugars for the chain polymerization, while the ABC-transporter formed by Wzt (purple) and Wzm (yellow) hydrolyses ATP and translocates the lipid carrier-bound O-Antigen through the membrane. Adapted from Raetz and Whitfield 2002. 32

- Figure 3-3: Structure of the Xcc 8004 O-antigen.** The O-antigen main chain consists of a rhamnose polymer and attached to every second rhamnose is a N-acetyl fucosamine side branch. From Molinaro et al. 2003. 34
- Figure 3-4: The LPS export machinery.** Lpt proteins span the periplasm and the outer membrane. ATP hydrolysis is the driving force behind the transport. The LPS is extracted from the inner membrane and transported through a pore onto the outer membrane. Adapted from Whitfield and Trent, 2014. 35
- Figure 3-5: Genetic background of the LPS O-antigen biosynthesis in *Xanthomonas campestris* pv. *campestris* B100.** A: Mutant names Xcc H21012 (*wxcB*), Xcc H28110 (*wxcK*) and Xcc H20110 (*wxcN*) and positions of Tn5 insertions in the Xcc B100 genome (Hötte et al. 1990; Vorhölter et al. 2001). The flag shows the orientation of the *lacZ* reading frame. B: Map of the *wxc* gene cluster including the conventional gene names. Mutated genes are shown in black. C: Functional organization of the gene cluster following the analyses of Vorhölter and colleagues (Vorhölter et al. 2001): Region 1 is putatively involved in the biosynthesis of the poly-rhamnan backbone, region 2 is crucial for the nucleotide sugars biosynthesis leading to GDP-rhamnose. Region 3 is putatively responsible for the N-acetyl-fucosamine branches of the Xcc O-antigen. Adapted from Steffens et al. 2016. 36
- Figure 3-6: Relevant details of the *Xanthomonas campestris* pv. *campestris* nucleotide sugar metabolism producing precursors for the LPS O-antigen and the exopolysaccharide xanthan.** Enzymatic reactions are indicated by arrows and names of the involved genes. Mutated genes of the strains Xcc H21012 (*wxcB*), Xcc H20110 (*wxcN*) and Xcc H28110 (*wxcK*) are shown in bold red letters at their respective position within the metabolic pathway. Molecules are numbered as follows: 1: D-glucose; 2: D-glucose 6-phosphate; 3: D-glucose 1-phosphate; 4: D-mannose 1-phosphate; 5: GDP-D-mannose; 6: GDP-D-rhamnose; 7: dTDP-4-keto-6-deoxy-D-glucose; 8: dTDP-3-keto-6-deoxy-D-galactose; 9: dTDP-3-amino-3,6-dideoxy-D-galactose (dTDP-D-fucosamine); 10: dTDP-N-acetyl-fucosamine; 11: dTDP-4-keto-6-deoxy-L-mannose; 12: dTDP-L-rhamnose; 13: UDP-D-glucose; 14: UDP-D-glucuronic acid; 15: UDP-D-galacturonic acid; 16: OA repetitive subunit, dashed lines indicate uncertainties regarding the OA biosynthesis from rhamnose precursors. Xanthan precursors (5, 13, 14) are marked in green. From Steffens et al. 2016. 38
- Figure 3-7: Analysis of the LPS O-antigen constituents of *Xanthomonas campestris* pv. *campestris* B100 wild type and derived mutant strains by gas chromatography following**

methanolysis. Wild type data are compared to H21012 (*wxcB*), H28110 (*wxcK*) and H20110 (*wxcN*). A: Complete chromatogram with the O-antigen main constituent rhamnose (Rha) followed by a box indicating signals related to the second O-antigen constituent N-acetyl fucosamine (FucNAc) and LPS core moieties. B: Zoom-in of the boxed area of the chromatogram with peaks identified as O-antigen constituent FucNAc and the LPS core constituent galacturonic acid (GalA). Both are represented by two peaks. Measurements were carried out after LPS isolation applying the hot phenol/water method followed by methanolysis with 0.5 M HCl in methanol and the respective peracetylation of 100 µg LPS. From Steffens et al. 2016.39

Figure 3-8: MALDI-TOF-MS analysis of the LPS O-antigen of *Xanthomonas campestris* pv. *campestris* B100 wild type, the O-antigen branch mutants Xcc H28110 (*wxcK*) and Xcc H20110 (*wxcN*) and O-antigen deficient mutant Xcc H21012 (*wxcB*). Spectra related to the mutants Xcc H28110 (*wxcK*), Xcc H20110 (*wxcN*) and to the wild type O-antigen were compared in order to verify the inhibition of the OA side branches and the increase in rhamnose moieties. Displayed are ranges of the spectra with a focus on the O-antigen constituents, rhamnose (rha) and N-acetyl fucosamine (FucNAc). Examples of repeating peaks are highlighted. No OA residues were detected in the LPS of H21012 (*wxcB*), but different lipid A moieties and a peak representing the rough-type LPS could be measured. Measurements were carried out with 5 µg LPS of each strain. From Steffens et al. 2016..... 41

Figure 3-9: GC chromatograms of a rhamnose:xylose 1:1 (20 µg) standard, Xcc B100 wild type and OA mutant strains. Due to the standard peaks a response factor for rhamnose towards xylose could be calculated. B100 Wild type data were compared to the *wxcB* mutant H21012, *wxcK* mutant H28110 and *wxcN* mutant H20110 towards their rhamnose amounts, after hydrolysis and reduction of 500 µg LPS. Standard chromatogram is depicted as zoom to optimize the view. From Steffens et al. 2016..... 42

Figure 3-10: Model of putative LPS structures of the *Xanthomonas campestris* pv. *campestris* B100 wild type and the mutants Xcc H21012 (*wxcB*), Xcc H28110 (*wxcK*) and (*wxcN*) following obtained results. Data indicated an elongation of the O-antigen rhamnose main chain in both of the branchless mutants, implying that the FucNAc branches play a role in O-antigen chain length determination. The linkage type between the rough-type LPS to the O-antigen is unknown and thus shown as a dashed line. The legend indicates the monosaccharide moieties. From Steffens et al. 2016. 44

Figure 3-11: Cultivation of the *Xanthomonas campestris* pv. *campestris* B100 wild type (A), mutants Xcc H21012 (*wxcB*) (B), Xcc H28110 (*wxcK*) (C) and Xcc H20110 (*wxcN*) (D). All strains were grown in XMD minimal media with 0.6 g l⁻¹ KNO₃ as nitrogen source and supplemented with 30 g l⁻¹ glucose as carbon source, at 30°C and 180 rpm. The cultivation occurred simultaneously under the same conditions for 96 h. Displayed are the culture titer (OD), glucose and nitrogen concentration over time. From Steffens et al. 2016. 45

Figure 3-12: Xanthan production of *Xanthomonas campestris* pv. *campestris* B100 wild type and derived mutants H21012 (*wxcB*), H28110 (*wxcK*) and H20110 (*wxcN*). Production was measured as dry weight [g] xanthan per [g] biomass. Samples from 10 replicates each (Supplementary tables 2 and 3). Harvest was after 96 h in the late stationary phase. Bars give the normalized mean xanthan yields, with error bars indicating the standard deviations. Xanthan production was compared in regard to Xcc B100 production. * indicates a p-value of < 0.05. From Steffens et al. 2016. 47

Figure 4-1: General schematic arrangement of bacterial flagella. A: Monotrichous; B: Lophotrichous; C: Amphitrichous; D: Peritrichous. <https://commons.wikimedia.org/wiki/File:Flagella.png>; CC BY 3.0. 57

Figure 4-2: Schematic overview of the conserved flagellar assembly and genes involved in this process. Depicted is the pathway from *Salmonella*. The name of the respective substructures is given under the images. Names of the genes involved in the biosynthesis of given substructures are depicted at the arrows. Brackets indicate substructures that are assembled prior to the flagellar type III system. Biosynthesis starts with a basal body, followed by the export apparatus. Only then structural parts, including hook and filament can be assembled. From Macnab, 2003. 60

Figure 4-3: Genomic region of the flagellar target genes *fliC* and *fliM* (black) in *Xanthomonas campestris* pv. *campestris*. Depicted are the neighboring regions of the target genes. Integration of a kanamycin (Km) resistance carrying plasmid is shown. The figure was constructed in accordance to the genome in the GenDB database (Meyer et al. 2003). 62

Figure 4-4: Xanthan production of *Xanthomonas campestris* pv. *campestris* B100 wild type and derived mutant *fliC* Δ. Production was measured as dry weight [g] xanthan per [g] biomass. Samples from five replicates each. Harvest was after 96 h in the late stationary phase. Bars give

the normalized mean xanthan yields, with error bars indicating the standard deviations. Values are depicted in Supplementary table 5. 64

Figure 4-5: Xanthan production of *Xanthomonas campestris* pv. *campestris* B100 wild type and derived mutant *fliM*⁻. Production was measured as dry weight [g] xanthan per [g] biomass. Samples from two replicates each. Harvest was after 96 h in the late stationary phase. Bars give the normalized mean xanthan yields, with error bars indicating the standard deviations. Values are depicted in Supplementary table 5. 64

Figure 4-6: Transmission electron microscopy and swarm assay of the strain Xcc JBL007 and derived mutants *fliM*⁻ and *fliC*⁻. Cells for microscopy were harvested at mid-growth-phase. Swarming was tested on 90 mm 0.3% agar plates. Plates were incubated for 48 h. Bacteria are motile when a halo appears on the plates (JBL007), otherwise they are non-motile (mutant strains).....66

Figure 4-7: Fermentation of *Xanthomonas campestris* pv. *campestris* JBL007 and derived mutants JBL007 *fliC*⁻ and JBL007 *fliM*⁻. Depicted is the growth behavior (OD600) with filled symbols and xanthan production [% (w/v) of the culture] with open symbols. Fermentation was carried out in minimal medium with 0.2 g l⁻¹ corn-extract, 0.6 g l⁻¹ of a nitrogen source and 45 g l⁻¹ glucose from glucosesirup..... 67

Table 4-1: Xanthan production of *Xanthomonas campestris* pv. *campestris* JBL007 and derived mutants JBL007 *fliC*⁻ and JBL007 *fliM*⁻ after fermentation. Depicted are the individual values of three measurements and their respective mean with according standard deviation. Harvest occurred after 68 h..... 67

Figure 4-8: Xanthan production of *Xanthomonas campestris* pv. *campestris* JBL007 wild type and derived mutants *fliC*⁻ and *fliM*⁻. Production was measured as dry weight [g] xanthan per [l] culture. Samples from 3 fermenter replicates each. Bars give the mean xanthan yields, with error bars indicating the standard deviations..... 68

Table 4-2: Xanthan production of *Xanthomonas campestris* pv. *campestris* JBL007 and derived mutants JBL007 *fliC*⁻ and JBL007 *fliM*⁻ after shaking flask cultivations. Depicted are the individual values of three measurements and their respective mean with according standard deviation..... 69

Figure 4-9: Fed batch Fermentation of *Xanthomonas campestris* pv. *campestris* JBL007 and derived mutant JBL007 *fliM*⁻. Depicted is the growth behavior (OD600) with filled symbols and xanthan production [% (w/v) of the culture] with open symbols. Fermentation was carried out in minimal medium with 0.2 g l⁻¹ corn-extract, 0.7 g l⁻¹ nitrogen source and 45 g l⁻¹ glucose from glucosesirup. The arrow indicates the addition of 700 ml 34% glucosesirup after 29 h. 71

Table 4-3: Xanthan production of *Xanthomonas campestris* pv. *campestris* JBL007 and derived mutant JBL007 *fliM*⁻ after fed batch fermentations. Depicted are the individual values of two measurements. Harvest occurred after 72 h. 71

Figure 4-10: Viscosity of the *Xanthomonas campestris* pv. *campestris* strains JBL007 and derived mutants JBL007 *fliC*⁻ and JBL007 *fliM*⁻ in a logarithmic scale. Xanthan was harvested from fermenter cultivations, dried and milled. Measurements were carried out with 1% (w/v) xanthan in water at room temperature. 73

Table 4-4: Measured viscosity values of *Xanthomonas campestris* pv. *campestris* strains JBL007 and derived mutants JBL007 *fliC*⁻ and JBL007 *fliM*⁻. Measurements were carried out with 1% (w/v) of dried and milled xanthan in water at room temperature. 73

Figure 4-11: ¹H-NMR of Xanthan isolated from Xcc JBL007 and derived mutants JBL007 *fliM*⁻ and JBL007 *fliC*⁻. Samples were solved in D₂O. The differences in scaling of the y-axis are due to slightly different amounts of xanthan used for the measurements. Highlighted are the methyl groups of the xanthan acetate and pyruvate groups. Sugar ring proton signals occur at around 4 – 6 ppm. 75

Figure 4-12: Atomic force microscopy analysis of xanthan by Xcc JBL007 and derived mutant Xcc JBL007 *fliM*⁻. A: Topography of single xanthan fibers in example AFM images of equally prepared xanthan samples. Samples were harvested after 68 h of fermentation. B: Measured xanthan characteristics (contour length and persistence length) shown as bar diagrams of the mean values with standard deviation. Measured were 16 strands for Xcc JBL007 and 21 strands for Xcc JBL007 *fliM*⁻. 76

Table 4-5: Comparison of xanthan fibers from Xcc JBL007 and Xcc JBL007 *fliM*⁻ xanthan. Data were derived by atomic force microscopy. Shown are the mean values with standard deviation of 16 samples for Xcc JBL007 and 21 for Xcc JBL007 *fliM*⁻. 76

Figure 5-1: Schematic overview on the Xcc quorum sensing signaling network. Next to environmental and host signals, the DSF signaling, transduced by RpfC and RpfG, involving cyclic di-GMP, DF signaling and involvement of Clp at the transcriptional level are depicted. The boxes highlight the influenced metabolic pathways, including EPS biosynthesis. From He and Zhang 2008, License number: 4000421367724. 85

Figure 5-2: Comparison of the target regulator genes *crt1* and *crt2* in *Xanthomonas campestris* pv. *campestris* B100 and JBL007. Depicted underneath the strain names are the corresponding locos tags (GenDB, Meyer et al. 2003). Sequence coverage (identical bases) and Identity were obtained through BLAST (Altschul et al. 1990) analyses of the genes from Xcc B100 vs. JBL007. 86

Figure 5-3: Xanthan production of *Xanthomonas campestris* pv. *campestris* B100 wild type and derived mutant *crt1*⁻ and *crt2*⁻. Production was measured as dry weight [g] xanthan per [g] biomass. Samples from 2 replicates each. Harvest was after 96 h in the late stationary phase. Bars give the normalized mean xanthan yields, with error bars indicating the standard deviations. Values are depicted in Supplementary table 7. 88

Figure 5-4: Fermentation of *Xanthomonas campestris* pv. *campestris* JBL007 and derived mutants JBL007 *crt1*⁻ and JBL007 *crt2*⁻. Depicted is the growth behavior (OD600) with filled symbols and xanthan production [% (w/v) of the culture] with open symbols. Fermentation was carried out in minimal medium with 0.2 g l⁻¹ corn-extract, 0.6 g l⁻¹ of a nitrogen source and 45 g l⁻¹ glucose from glucosesirup. 89

Table 5-1: Xanthan production of *Xanthomonas campestris* pv. *campestris* JBL007 and derived mutants JBL007 *crt1*⁻ and *crt2*⁻ after fermentation. Harvest occurred after 68 h. 89

Table 5-2: Xanthan production of *Xanthomonas campestris* pv. *campestris* JBL007 and derived mutants JBL007 *crt1*⁻ and JBL007 *crt2*⁻ after shaking flask cultivations. Depicted are the individual values of three measurements and their respective mean with according standard deviation. 90

Figure 5-5: Fed batch Fermentation of *Xanthomonas campestris* pv. *campestris* JBL007 and derived mutant JBL007 *crt1*⁻. Depicted is the growth behavior (OD600) with filled symbols and xanthan production [% (w/v) of the culture] with open symbols. Fermentation was carried out in minimal medium with 0.2 g l⁻¹ corn-extract, 0.7 g l⁻¹ nitrogen source and 45 g l⁻¹ glucose from glucosesirup. The arrow indicates the addition of 700 ml 34% glucosesirup after 29 h. 91

Table 5-3: Xanthan production of <i>Xanthomonas campestris</i> pv. <i>campestris</i> JBL007 and derived mutants JBL007 <i>crt1</i>⁻ and <i>crt2</i>⁻ after fed batch fermentation. Harvest occurred after 72 h.....	91
Figure 5-6: Viscosity of the <i>Xanthomonas campestris</i> pv. <i>campestris</i> strains JBL007 and derived mutant JBL007 <i>crt1</i>⁻ in a logarithmic scale. Xanthan was harvested from fermenter cultivations, dried and milled. Measurements were carried out with 1% (w/v) xanthan in water at room temperature.	92
Table 5-4: Measured viscosity values of <i>Xanthomonas campestris</i> pv. <i>campestris</i> strains JBL007 and derived mutant JBL007 <i>crt1</i>⁻. Measurements were carried out with 1% (w/v) of dried and milled xanthan in water at room temperature.	93
Figure 6-1: Schematic overview of the presented thesis. Three distinct approaches were chosen to obtain improved xanthan production strains and to reveal new insights into the Xcc metabolism. Mutations in genes of the Xcc LPS biosynthesis, the flagellar biosynthesis or in different regulators, build up the fundamental design of this work. Listed underneath each approach are the most important results.....	107
Table 7-1: Applied bacterial strains for the study of the Xcc O-antigen.....	108
Table 7-2: Bacterial strains and vector used in the approach regarding the flagellum.	114
Table 7-3: Primers, including restriction sites, used for mutant constructions.	114
Table 7-4: Bacterial strains and vector used in the approach regarding <i>crt1</i> and <i>crt2</i>.	120
Table 7-5: Primers, including restriction sites, used for mutant constructions.	120

9 References

- Alexander C, Rietschel ET. 2001. Bacterial lipopolysaccharides and innate immunity. *J. Endotoxin Res.* 7:167–202.
- Alkhateeb RS, Vorholter F-J, Ruckert C, Mentz A, Wibberg D, Hublik G, Niehaus K, Puhler A. 2016. Genome wide transcription start sites analysis of *Xanthomonas campestris* pv. *campestris* B100 with insights into the gum gene cluster directing the biosynthesis of the exopolysaccharide xanthan. *J. Biotechnol.* 225:18–28.
- Altschul SF, Gish W, Miller W, Myers EW, Lipman DJ. 1990. Basic local alignment search tool. *J. Mol. Biol.* 215:403–10.
- An S qi, Caly DL, McCarthy Y, Murdoch SL, Ward J, Febrer M, Dow JM, Ryan RP. 2014. Novel Cyclic di-GMP Effectors of the YajQ Protein Family Control Bacterial Virulence. *PLoS Pathog.* 10.
- Barber CE, Tang JL, Feng JX, Pan MQ, Wilson TJ, Slater H, Dow JM, Williams P, Daniels MJ. 1997. A novel regulatory system required for pathogenicity of *Xanthomonas campestris* is mediated by a small diffusible signal molecule. *Mol. Microbiol.* 24:555–566.
- Becker A, Katzen F, Pühler A, Ielpi L. 1998. Xanthan gum biosynthesis and application: A biochemical/genetic perspective. *Appl. Microbiol. Biotechnol.* 50:145–152.
- Belas R. 2013. When the swimming gets tough, the tough form a biofilm. *Mol. Microbiol.* 90:1–5.
- Belas R. 2014. Biofilms, flagella, and mechanosensing of surfaces by bacteria. *Trends Microbiol.* 22:517–527.
- Berg HC. 2003. The rotary motor of bacterial flagella. *Annu. Rev. Biochem.* 72:19–54.
- Beringer JE. 1974. R factor transfer in *Rhizobium leguminosarum*. *J. Gen. Microbiol.* 84:188–198.

- Blanvillain S, Meyer D, Boulanger A, Lautier M, Guynet C, Denancé N, Vasse J, Lauber E, Arlat M. 2007. Plant carbohydrate scavenging through TonB-dependent receptors: A feature shared by phytopathogenic and aquatic bacteria. *PLoS One* 2.
- Caiazza NC, Merritt JH, Brothers KM, O'Toole GA. 2007. Inverse regulation of biofilm formation and swarming motility by *Pseudomonas aeruginosa* PA14. *J. Bacteriol.* 189:3603–3612.
- Casas J a., Santos VE, García-Ochoa F. 2000. Xanthan gum production under several operational conditions: Molecular structure and rheological properties. *Enzyme Microb. Technol.* 26:282–291.
- Collins RF, Beis K, Dong C, Botting CH, McDonnell C, Ford RC, Clarke BR, Whitfield C, Naismith JH. 2007. The 3D structure of a periplasm-spanning platform required for assembly of group 1 capsular polysaccharides in *Escherichia coli*. *Proc. Natl. Acad. Sci. USA* 104:2390–2395.
- CPKelco. 2008. KELTROL® / KELZAN® xanthan gum.
- Crossman L, Dow JM. 2004. Biofilm formation and dispersal in *Xanthomonas campestris*. *Microbes Infect.* 6:623–629.
- Doige EM. 1921. A TOMATO CANKER. *Ann. Appl. Biol.* 7:1744–7348.
- Dow JM, Osbourn a E, Wilson TJ, Daniels MJ. 1995. A locus determining pathogenicity of *Xanthomonas campestris* is involved in lipopolysaccharide biosynthesis. *Mol. Plant. Microbe. Interact.* 8:768–777.
- Dowson WJ. 1939. On the systematic position and generic names of the Gram negative bacterial plant pathogens. :177–193.
- Frese M, Schatschneider S, Voss J, Vorhölter FJ, Niehaus K. 2014. Characterization of the pyrophosphate-dependent 6-phosphofructokinase from *Xanthomonas campestris* pv. *campestris*. *Arch. Biochem. Biophys.* 546:53–63.
- Galván EM, Ielmini M V., Patel YN, Bianco MI, Franceschini EA, Schneider JC, Ielpi L. 2013. Xanthan chain length is modulated by increasing the availability of the polysaccharide copolymerase protein GumC and the outer membrane polysaccharide export protein GumB. *Glycobiology* 23:259–272.

- Gram HC. 1884. Über die isolierte Färbung der Schizomyceten in Schnitt- und Trockenpräparaten. *Fortschr. Med.*:185–189.
- Guan S, Verma NK. 1999. Functional analysis of the O antigen glycosylation gene cluster of *Shigella flexneri*. 1263–1273.
- Gulrez SKH, Al-Assaf S, Fang Y, Phillips GO, Gunning AP. 2012. Revisiting the conformation of xanthan and the effect of industrially relevant treatments. *Carbohydr. Polym.* 90:1235–1243.
- Guttenplan SB, Kearns DB. 2013. Regulation of flagellar motility during biofilm formation. *FEMS Microbiol. Rev.* 37:849–871.
- Hagelueken G, Huang H, Clarke BR, Lebl T, Whitfield C, Naismith JH. 2012. Structure of WbdD: a bifunctional kinase and methyltransferase that regulates the chain length of the O antigen in *Escherichia coli* O9a. *Mol. Microbiol.* 86:730–742.
- He YW, Ng AYJ, Xu M, Lin K, Wang LH, Dong YH, Zhang LH. 2007. *Xanthomonas campestris* cell-cell communication involves a putative nucleotide receptor protein Clp and a hierarchical signalling network. *Mol. Microbiol.* 64:281–292.
- He YW, Zhang LH. 2008. Quorum sensing and virulence regulation in *Xanthomonas campestris*. *FEMS Microbiol. Rev.* 32:842–857.
- Hötte B, Rath-Arnold I, Puhler A, Simon R. 1990. Cloning and Analysis of a 35 . 3-Kilobase DNA Region Involved in Exopolysaccharide Production by *Xanthomonas campestris* pv . *campestris* In. *J. Bacteriol.* 172:2804–2807.
- Hublik G. 2012. Xanthan. In: *Polymer Science: A Comprehensive Reference*. Vol. 10. p. 221–229.
- Jansson P-E, Kenne L, Lindberg B. 1975. Structure of the Extracellular Polysaccharide from *Xanthomonas campestris*. *Carbohydr. Res.* 45:275–282.
- Jeanes A, Pittsley JE, Senti FR. 1961. Polysaccharide B-1459: A new hydrocolloid polyelectrolyte produced from glucose by bacterial fermentation. *J. Appl. Polym. Sci.* 5:519–526.

- Jones JB, Lacy GH, Bouzar H, Stall RE, Schaad NW. 2004. Reclassification of the xanthomonads associated with bacterial spot disease of tomato and pepper. *Syst. Appl. Microbiol.* 27:755–762.
- Kalinowski J, Bathe B, Bartels D, Bischoff N, Bott M, Burkovski A, Dusch N, Eggeling L, Eikmanns BJ, Gaigalat L, et al. 2003. The complete *Corynebacterium glutamicum* ATCC 13032 genome sequence and its impact on the production of L-aspartate-derived amino acids and vitamins. *J. Biotechnol.* 104:5–25.
- Katzen F, Ferreiro DU, Oddo CG, Ielmini MV, Becker A, Pühler A, Ielpi L. 1998. *Xanthomonas campestris* pv. *campestris* gum mutants: Effects on xanthan biosynthesis and plant virulence. *J. Bacteriol.* 180:1607–1617.
- Keck M, Gisch N, Moll H, Vorhölter FJ, Gerth K, Kahmann U, Lissel M, Lindner B, Niehaus K, Holst O. 2011. Unusual outer membrane lipid composition of the gram-negative, lipopolysaccharide-lacking myxobacterium *sorangium cellulosum* so ce56. *J. Biol. Chem.* 286:12850–12859.
- King JD, Berry S, Clarke BR, Morris RJ, Whitfield C. 2014. Lipopolysaccharide O antigen size distribution is determined by a chain extension complex of variable stoichiometry in *Escherichia coli* O9a. *Proc. Natl. Acad. Sci. U. S. A.* 111:6407–12.
- Kocks CG, Zadoks JC. 1996. Cabbage Refuse Piles as Sources of Inoculum for Black Rot Epidemics. :789–792.
- Koplin R, Arnold W, Hotte B, Simon R, Wang G, Puhler a. 1992. Genetics of xanthan production in *Xanthomonas campestris*: The *xanA* and *xanB* genes are involved in UDP-glucose and GDP-mannose biosynthesis. *J. Bacteriol.* 174:191–199.
- Koplin R, Wang G, Hotte B, Priefer UB, Puhler A. 1993. A 3.9-kb DNA region of *Xanthomonas campestris* pv. *campestris* that is necessary for lipopolysaccharide production encodes a set of enzymes involved in the synthesis of dTDP-rhamnose. *J. Bacteriol.* 175:7786–7792.
- Kreyenschulte D, Krull R, Margaritis A. 2014. Recent advances in microbial biopolymer production and purification. *Crit. Rev. Biotechnol.* 34:1–15.

- Kunst F, Ogasawara N, Moszer I, Albertini a M, Alloni G, Azevedo V, Bertero MG, Bessières P, Bolotin A, Borchert S, et al. 1997. The complete genome sequence of the Gram-positive bacterium *Bacillus subtilis*. *Nature* 390:249–256.
- Lavery G, Gorman S, Gilmore B. 2014. Biomolecular Mechanisms of *Pseudomonas aeruginosa* and *Escherichia coli* Biofilm Formation. *Pathogens* 3:596–632.
- Lee BM, Park YJ, Park DS, Kang HW, Kim JG, Song ES, Park IC, Yoon UH, Hahn JH, Koo BS, et al. 2005. The genome sequence of *Xanthomonas oryzae* pathovar *oryzae* KACC10331, the bacterial blight pathogen of rice. *Nucleic Acids Res.* 33:577–586.
- Leßmeier L, Alkhateeb RS, Schulte F, Steffens T, Loka TP, Pühler A, Niehaus K, Vorhölter FJ. 2016. Applying DNA affinity chromatography to specifically screen for sucrose-related DNA-binding transcriptional regulators of *Xanthomonas campestris*. *J. Biotechnol.*
- Letisse F, Chevallereau P, Simon JL, Lindley N. 2002. The influence of metabolic network structures and energy requirements on xanthan gum yields. *J. Biotechnol.* 99:307–317.
- Li J, Wang N. 2011. Genome-wide mutagenesis of *xanthomonas axonopodis* pv. *citri* reveals novel genetic determinants and regulation mechanisms of biofilm formation. *PLoS One* 6.
- Loka T. 2012. Bachelorarbeit Globale Analyse der Rolle zweier neuer transkriptionaler Regulatoren aus *Xanthomonas*.
- Macnab RM. 2003. How bacteria assemble flagella. *Annu. Rev. Microbiol.* 57:77–100.
- Maddocks SE, Oyston PCF. 2008. Structure and function of the LysR-type transcriptional regulator (LTTR) family proteins. *Microbiology* 154:3609–3623.
- Mansfield J, Genin S, Magori S, Citovsky V, Sriariyanum M, Ronald P, Dow M, Verdier V, Beer S V., Machado M a., et al. 2012. Top 10 plant pathogenic bacteria in molecular plant pathology. *Mol. Plant Pathol.* 13:614–629.
- Medzhitov R, Janeway C. 2000. Innate immune recognition: mechanisms and pathways. *Immunol. Rev.* 173:89–97.

- Merino S, Tomas JM. 2014. Gram-negative flagella glycosylation. *Int. J. Mol. Sci.* 15:2840–2857.
- Meyer F, Goesmann A, McHardy AC, Bartels D, Bekel T, Clausen J, Kalinowski J, Linke B, Rupp O, Giegerich R, et al. 2003. GenDB - An open source genome annotation system for prokaryote genomes. *Nucleic Acids Res.* 31:2187–2195.
- Moffat J, Morris VJ, Al-Assaf S, Gunning AP. 2016. Visualisation of xanthan conformation by atomic force microscopy. *Carbohydr. Polym.* 148:380–389.
- Molinaro A, De Castro C, Lanzetta R, Parrilli M, Petersen BO, Broberg A, Duus JØ. 2002. NMR and MS evidences for a random assembled O-specific chain structure in the LPS of the bacterium *Xanthomonas campestris* pv. *vitians*: A case of unsystematic biosynthetic polymerization. *Eur. J. Biochem.* 269:4185–4193.
- Molinaro A, Lanzetta R, Evidente A, Parrilli M, Holst O. 1999. Isolation and characterisation of the lipopolysaccharide from *Xanthomonas hortorum* pv. *vitians*. *FEMS Microbiol. Lett.* 181:49–53.
- Molinaro A, Silipo A, Lanzetta R, Newman MA, Dow JM, Parrilli M. 2003. Structural elucidation of the O-chain of the lipopolysaccharide from *Xanthomonas campestris* strain 8004. *Carbohydr. Res.* 338:277–281.
- Newman M-A, Dow JM, Molinaro A, Parrilli M. 2007. Priming, induction and modulation of plant defence responses by bacterial lipopolysaccharides. *J. Endotoxin Res.* 13:69–84.
- Neyen C, Lemaitre B. 2016. Sensing Gram-negative bacteria: A phylogenetic perspective. *Curr. Opin. Immunol.* 38:8–17.
- Norton IT, Goodall DM, Frangou SA, Morris ER, Rees DA. 1984. Mechanism and dynamics of conformational ordering in xanthan polysaccharide. *J. Mol. Biol.* 175:371–394.
- Oster G, Wang H. 2003. Rotary protein motors. *Trends Cell Biol.* 13:114–121.
- Palaniraj A, Jayaraman V, Hariram SB. 2011. Influence of Nitrogen Sources and Agitation in Xanthan Gum Production By *Xanthomonas Campestris*. *Int. J. Adv. Biotechnol. Res.* 2:305–309.

- Park H-J, Jung HW, Han S-W. 2014. Functional and proteomic analyses reveal that wxcB is involved in virulence, motility, detergent tolerance, and biofilm formation in *Xanthomonas campestris* pv. *vesicatoria*. *Biochem. Biophys. Res. Commun.* 452:389–394.
- Pielken P, Schmitz KL, Eggeling L, Sahm H. 1988. Glucose metabolism in *Xanthomonas campestris* and influence of methionine on the carbon flow. *Can. J. Microbiol.* 34:1333–1337.
- Poplawsky AR, Chun W, Slater H, Daniels MJ, Dow JM. 1998. Synthesis of Extracellular Polysaccharide , Extracellular Enzymes , and Xanthomonadin in *Xanthomonas campestris* : Evidence for the Involvement of Two Intercellular Regulatory Signals. *Mol. Plant. Interact.* 11:68–70.
- Raetz CR. 1990. Biochemistry of endotoxins. *Annu. Rev. Biochem.* 59:129–170.
- Raetz CRH, Reynolds M, Trent MS, Bishop RE. 2007. Lipid A Modification Systems in Gram-negative Bacteria. *Annu. Rev. Biochem.*:295–329.
- Raetz CRH, Whitfield C. 2002. Lipopolysaccharide endotoxins. *Annu. Rev. Biochem.* 71:635–700.
- Ranf S, Gisch N, Schäffer M, Illig T, Westphal L, Knirel Y a, Sánchez-Carballo PM, Zähringer U, Hückelhoven R, Lee J, et al. 2015. A lectin S-domain receptor kinase mediates lipopolysaccharide sensing in *Arabidopsis thaliana*. *Nat. Immunol.*
- Rietschel ET, Cavaillon JM. 2003. Richard Pfeiffer and Alexandre Besredka: Creators of the concept of endotoxin and anti-endotoxin. *Microbes Infect.* 5:1407–1414.
- Rietschel ET, Kirikae T, Schade FU, Mamat U, Schmidt G, Loppnow H, Ulmer AJ, Zähringer U, Seydel U, Di Padova F, et al. 1994. Bacterial endotoxin: molecular relationships of structure to activity and function. *FASEB J.* 8:217–225.
- Rinaudo M, Milas M, Lambert F, Vincendon M. 1983. H-1 and C-13 Nmr Investigation of Xanthan Gum. *Macromolecules* 16:816–819.
- Rodriguez-R LM, Grajales A, Arrieta-Ortiz M, Salazar C, Restrepo S, Bernal A. 2012. Genomes-based phylogeny of the genus *Xanthomonas*. *BMC Microbiol.* 12:43.

- Schäfer A, Tauch A, Jäger W, Kalinowski J, Thierbach G, Pühler A. 1994. Small mobilizable multi-purpose cloning vectors derived from the *Escherichia coli* plasmids pK18 and pK19: selection of defined deletions in the chromosome of *Corynebacterium glutamicum*. *Gene* 145:69–73.
- Schatschneider S, Persicke M, Watt SA, Hublik G, Pühler A, Niehaus K, Vorhölter FJ. 2013. Establishment, in silico analysis, and experimental verification of a large-scale metabolic network of the xanthan producing *Xanthomonas campestris* pv. *campestris* strain B100. *J. Biotechnol.* 167:123–134.
- Schatschneider S, Vorhölter FJ, Rückert C, Becker A, Eisenreich W, Pühler A, Niehaus K. 2011. Genome-enabled determination of amino acid biosynthesis in *Xanthomonas campestris* pv. *campestris* and identification of biosynthetic pathways for alanine, glycine, and isoleucine by ¹³C-isotopologue profiling. *Mol. Genet. Genomics* 286:247–259.
- Schuhmacher JS, Thormann KM, Bange G. 2015. How bacteria maintain location and number of flagella? *FEMS Microbiol. Rev.* 39:812–822.
- Sho T, Sato T, Norisuye T. 1986. Viscosity behaviour and persistence length of sodium xanthan in aqueous sodium chloride. *J. Polym. Sci. Polym. Chem. Ed.* 25:307–313.
- Silipo A, Molinaro A, Sturiale L, Dow JM, Erbs G, Lanzetta R, Newman MA, Parrilli M. 2005. The elicitation of plant innate immunity by lipooligosaccharide of *Xanthomonas campestris*. *J. Biol. Chem.* 280:33660–33668.
- Silipo A, Sturiale L, Garozzo D, Erbs G, Jensen TT, Lanzetta R, Dow JM, Parrilli M, Newman MA, Molinaro A. 2008. The acylation and phosphorylation pattern of lipid A from *Xanthomonas campestris* strongly influence its ability to trigger the innate immune response in *Arabidopsis*. *ChemBioChem* 9:896–904.
- da Silva AC, Ferro JA, Reinach FC, Farah CS, Furlan LR, Quaggio RB, Monteiro-Vitorello CB, Van Sluys MA, Almeida NF, Alves LM, et al. 2002. Comparison of the genomes of two *Xanthomonas* pathogens with differing host specificities. *Nature* 417:459–463.
- Simon R, Quandt J, Klipp W. 1989. New derivatives of transposon Tn5 suitable for mobilization of replicons, generation of operon fusions and induction of genes in gram-negative bacteria. *Gene* 80:161–169.

- Slater H, Alvarez-Morales A, Barber CE, Daniels MJ, Maxwell Dow J. 2000. A two-component system involving an HD-GYP domain protein links cell-cell signalling to pathogenicity gene expression in *Xanthomonas campestris*. *Mol. Microbiol.* 38:986–1003.
- Steffens T, Duda K, Lindner B, Vorhölter F-J, Bednarz H, Niehaus K, Holst O. 2016. The lipopolysaccharide of the crop pathogen *Xanthomonas translucens* pv. *translucens*: chemical characterization and determination of signaling events in plant cells. *Glycobiology*:1–11.
- Steffens T, Vorhölter F-J, Giampà M, Hublik G, Pühler A, Niehaus K. 2016. The influence of a modified lipopolysaccharide O-antigen on the biosynthesis of xanthan in *Xanthomonas campestris* pv. *campestris* B100. *BMC Microbiol.* 16:93.
- Steigmiller S, Turina P, Gräber P. 2008. The thermodynamic H⁺/ATP ratios of the H⁺-ATPsynthases from chloroplasts and *Escherichia coli*. *Proc. Natl. Acad. Sci. U. S. A.* 105:3745–3750.
- Teckentrup J, Al-Hammood O, Steffens T, Bednarz H, Walhorn V, Niehaus K, Anselmetti D. 2016. Comparative analysis of different xanthan samples by atomic force microscopy. *J. Biotechnol.*
- Thieme F, Koebnik R, Bekel T, Berger C, Boch J, Büttner D, Caldana C, Gaigalat L, Goesmann A, Kay S. 2005. Insights into genome plasticity and pathogenicity of the plant pathogenic bacterium *Xanthomonas campestris* pv. *vesicatoria* revealed by the complete genome. *J. Bacteriol.* 187:7254–7266.
- Toker A, Kihara M, Macnab RM. 1996. Deletion analysis of the FlIM flagellar switch protein of *Salmonella typhimurium*. *J. Bacteriol.* 178:7069–7079.
- Torres PS, Malamud F, Rigano L a., Russo DM, Marano MR, Castagnaro AP, Zorreguieta A, Bouarab K, Dow JM, Vojnov A a. 2007. Controlled synthesis of the DSF cell-cell signal is required for biofilm formation and virulence in *Xanthomonas campestris*. *Environ. Microbiol.* 9:2101–2109.
- Vauterin L, Hoste B, Kersters K, Swings J. 1995. Reclassification of *Xanthomonas*. *Int. J. Syst. Bacteriol.* 45:472–489.

- Vicente JG, Holub EB. 2013. *Xanthomonas campestris* pv. *campestris* (cause of black rot of crucifers) in the genomic era is still a worldwide threat to brassica crops. *Mol. Plant Pathol.* 14:2–18.
- Vojnov AA, Slater H, Daniels MJ, Dow JM, Centre JI, Lane C, Nr N. 2001. Expression of the gum Operon Directing Xanthan Biosynthesis in *Xanthomonas campestris* and Its Regulation In Planta. 14:768–774.
- Vorhölter FJ, Niehaus K, Pühler a. 2001. Lipopolysaccharide biosynthesis in *Xanthomonas campestris* pv. *campestris*: A cluster of 15 genes is involved in the biosynthesis of the LPS O-antigen and the LPS core. *Mol. Genet. Genomics* 266:79–95.
- Vorhölter FJ, Schneiker S, Goesmann A, Krause L, Bekel T, Kaiser O, Linke B, Patschkowski T, Rückert C, Schmid J, et al. 2008. The genome of *Xanthomonas campestris* pv. *campestris* B100 and its use for the reconstruction of metabolic pathways involved in xanthan biosynthesis. *J. Biotechnol.* 134:33–45.
- Westphal, O. and Jann K. 1965. Bacterial Lipopolysaccharides. Extraction with Phenol-Water and Further Applications of the Procedure. *Methods Carbohydr. Chem.* 5, 83-91. 5:83 – 91.
- Whitfield C. 2006. Biosynthesis and Assembly of Capsular Polysaccharides in *Escherichia coli*. *Annu. Rev. Biochem.*:39–68.
- Whitfield C, Sutherland IW, Cripps RE. 1982. Glucose Metabolism in *Xanthomonas campestris*. *J. Gen. Microbiol.*:981–985.
- Whitfield C, Trent MS. 2014. Biosynthesis and Export of Bacterial Lipopolysaccharides. *Annu. Rev. Biochem.* 83:99–128.
- Williams PH. 1980. Black rot: A continuing. *Plant Dis.* 64:736–742.
- Yang TC, Leu YW, Chang-Chien HC, Hu RM. 2009. Flagellar Biogenesis of *Xanthomonas campestris* Requires the Alternative Sigma Factors RpoN2 and FliA and Is Temporally Regulated by FlhA, FlhB, and FlgM. *J. Bacteriol.* 191:2266–2275.
- Zhang B, Kroeger A, Schlüter AD, Wegner G. 2013. The viscosity law of dendronized linear polymers. *Macromol. Rapid Commun.* 34:1537–1541.

Zhao K, Liu M, Burgess RR. 2007. Adaptation in bacterial flagellar and motility systems: From regulon members to “foraging”-like behavior in *E. coli*. *Nucleic Acids Res.* 35:4441–4452.

Zhao X, Norris SJ, Liu J. 2014. Molecular Architecture of Bacterial Flagellar Motor in Cells. *Biochemistry* 53:4323–4333.

Zhuang K, Vemuri GN, Mahadevan R. 2011. Economics of membrane occupancy and respiration. *Mol. Syst. Biol.* 7:500.

10 Supplement

Frequently used abbreviations

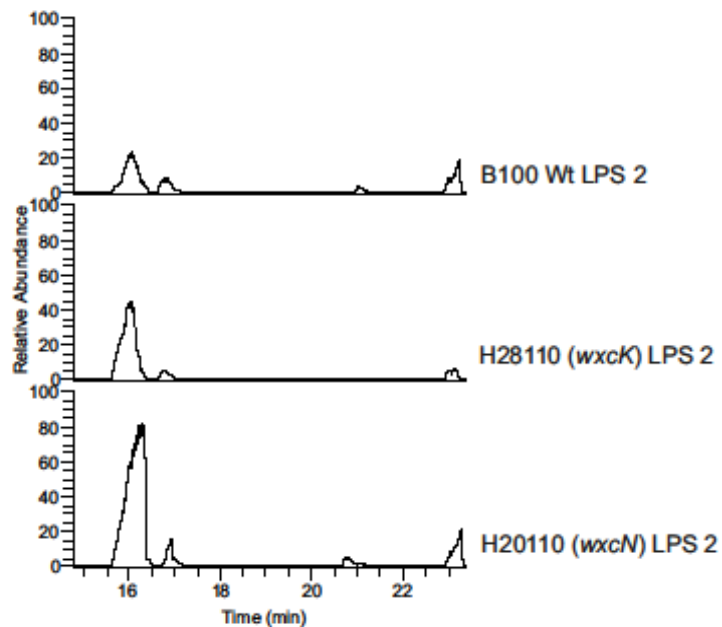
ABC:	ATP-binding cassette
AFM:	Atomic force microscopy
ATP:	Adenosine triphosphate
BLAST:	Basic Local Alignment Search Tool
bp:	Base pairs
CeBiTec:	Center for Biotechnology
CCW:	Counterclockwise
Clp:	CAP-like protein
Crt:	Carbohydrate related transcriptional regulation
CW:	Clockwise
DF:	Diffusible factor
DSF:	Diffusible signal factor
dTDP:	Deoxythymidine diphosphate
F-T3SS:	Flagellar type III secretion system
FucNAc:	N-acetyl fucosamine
galA:	galacturonic acid
GC-MS:	Gas chromatography – mass spectrometry
GDP:	Guanosine diphosphate
glcA:	glucuronic acid
GMP:	Guanosine monophosphate
Kdo:	3-Deoxy-D-manno-oct-2-ulosonic acid
Km:	Kanamycin
Lps:	Lipopolysaccharide
MALDI-TOF-MS:	Matrix assisted laser desorption ionization – time of flight – mass spectrometry
NMR:	Nuclear magnetic resonance
OA:	O-antigen
OD:	Optical density
PAMP:	Pathogen associated molecular pattern

PCR:	Polymerase chain reaction
Rpm:	Rounds per minute
Sm:	Streptomycin
TEM:	Transmission electron microscopy
TLR-4:	Toll-like receptor 4
TxSS:	Type x secretion system
UDP:	Uridine diphosphate
Undp:	Undecaprenylphosphate
Undpp:	Undecaprenylpyrophosphate
Wt:	Wild type
Xcc:	<i>Xanthomonas campestris</i> pv. <i>campestris</i>

Supplementary data

The Influence of the O-antigen as Target for an Enhanced Xanthan Production in *Xanthomonas campestris* pv. *campestris* B100

Chemical analysis of the O-antigen in three Xcc B100 mutant strains: Xcc H21012 (*wxcB*), Xcc H20110 (*wxcN*) and Xcc H28110 (*wxcK*)

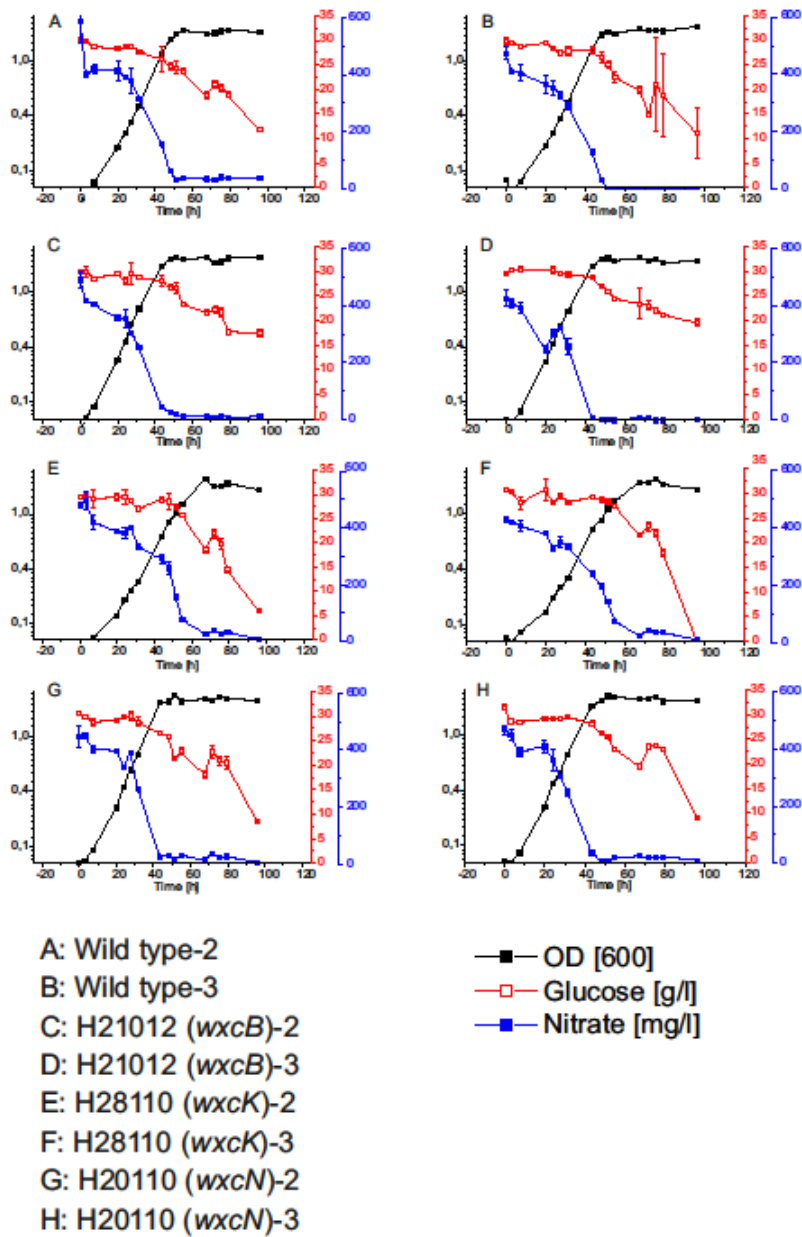


Supplementary figure 1: GC chromatogram replicates of Xcc B100 wild type and OA mutant strains. B100 Wild type data were compared to *wxcK* mutant H28110 and *wxcN* mutant H20110 towards their rhamnose amounts, after hydrolysis and reduction of 500 µg LPS.

Supplementary table 1: Calculation from measured peak areas during GC measurements of LPS constituent rhamnose in comparison to an internal standard xylose. Rhamnose peak area was corrected with obtained reference factor: 1.17.

Strain	Peak area rhamnose	Peak area xylose	Peak area rhamnose (corrected)	Rhamnose/Xylose	Rhamnose (μg)	Mean (μg)	Standard Deviation
Xcc B100	273594232	53018062	321746817	6.07	91.03		
Xcc B100	196494833	49461487	231077924	4.7	70.08	80.55	10.48
Xcc H21012	172663887	66884825	203052731	3.03	45.54		
Xcc H28110	1129754477	77245670	1328591265	17.12	258		
Xcc H28110	389225667	27083048	457729384	16.9	253.51	255.75	2.24
Xcc H20110	673143146	28818036	791616340	27.5	412.04		
Xcc H20110	1449345286	107858346	1704430056	26.34	395.06	403.55	8.49

Xanthan production of the analyzed Xcc B100 O-antigen mutant strains



Supplementary figure 2: Cultivation replicates of the *Xanthomonas campestris* pv. *campestris* B100 wild type (A, B) the three mutants Xcc H21012 (*wxcB*) (C,D), Xcc H28110 (*wxcK*) (E,F) and Xcc H20110 (*wxcN*) (G,H). All strains were grown in XMD minimal media with 0.6 g/l KNO₃ as nitrogen source and supplemented with 30 g/l glucose as carbon source, at 30 °C and 180 rpm. The cultivation occurred simultaneously under the same conditions for 96 h. Displayed are the culture titer (OD), glucose and nitrogen consumption over time.

Supplementary table 2: Xanthan production and t-test of the *Xanthomonas campestris* pv. *campestris* B100 wild type and mutants H21012 (*wxcB*), H28110 (*wxcK*) and H20110 (*wxcN*). Data are shown with extracted extreme values and as g xanthan per g biomass.

B100	H21012 (<i>wxcB</i>)	H28110 (<i>wxcK</i>)	H20110(<i>wxcN</i>)
5.94		5.66	5.81
5.87	7.36	4.74	5.35
5.21	5.86	6.26	4.2
5.47	5.98	5.93	5
7.05	6.59	6.91	7.76
5.15	7.25		6.06
	5.62	4.184	4.92
3.98	6.45	2.596	5.43
3.14	6.31	3.24	
3.1	4.88		4.6
(two sided)t-test:	0.029034112	0.943806847	0.418261067

Supplementary table 3: Xanthan production and t-test of the *Xanthomonas campestris* pv. *campestris* B100 wild type and mutants H21012 (*wxcB*), H28110 (*wxcK*) and H20110 (*wxcN*). Data are shown including the extreme values and as g xanthan per g biomass.

B100	H21012 (<i>wxcB</i>)	H28110 (<i>wxcK</i>)	H20110 (<i>wxcN</i>)
5.94	9.1	5.66	5.81
5.87	7.36	4.74	5.35
5.21	5.86	6.26	4.2
5.47	5.98	5.93	5
7.05	6.59	6.91	7.76
5.15	7.25	8.15	6.06
1.57	5.62	4.184	4.92
3.98	6.45	2.596	5.43
3.14	6.31	3.24	2.7
3.1	4.88	1.21	4.6
(two sided)t-test:	0.009286433	0.781156127	0.434592817

The Inhibition of Flagellar Structures and the Effects on Xanthan Production and Quality in *Xanthomonas campestris* pv. *campestris* B100 and Production Strain JBL007

Characterization of the Xcc B100 xanthan production after mutagenesis of two flagellar genes

Supplementary table 5: Xanthan production of the *Xanthomonas campestris* pv. *campestris* B100 wild type and mutants *fliC*⁻ and *fliM*⁻. Data are shown as g xanthan per g biomass.

	Xanthan [g g ⁻¹]					MW	SD
Xcc B100	7.17	7.12	4.62	5.05	6.76	6.14	1.08
Xcc <i>fliC</i>⁻	8.98	11.77	7.76	4.77	6.73	8	2.34
Xcc B100	6.34	4.67				5.505	0.835
Xcc <i>fliM</i>⁻	6.67	6.5				6.585	0.085

Characterization of product quality of xanthan isolated from Xcc JBL007 and flagellar mutant strains

Supplementary table 6: Measured viscosity values of *Xanthomonas campestris* pv. *campestris* strains JBL007 and derived mutants JBL007 *fliC*⁻ and JBL007 *fliM*⁻. Measurements were carried out with 1% (w/v) of dried and milled xanthan in water at room temperature.

Shear rate (1*sec ⁻¹)	JBL007 (mPas)	<i>fliM</i> ⁻ (mPas)	<i>fliC</i> ⁻ (mPas)
0,168	25590	35580	40680
0,84	9660	12380	10880
1,68	5400	7000	5960
3,36	2870	3640	3370
8,4	1910	2350	2100
14	950	1120	970
16,8	800	960	840
28	550	--	550

The Influence of Mutations in Two Regulator Genes of *Xanthomonas campestris* pv. *campestris* B100 and Production Strain JBL007 on Xanthan Production

Xanthan production of Xcc B100 regulator mutants Xcc B100 *crt1*⁻ and Xcc B100 *crt2*⁻

Supplementary table 7: Xanthan production of the *Xanthomonas campestris* pv. *campestris* B100 wild type and mutants *crt1*⁻ and *crt2*⁻. Data are shown as g xanthan per g biomass.

	Xanthan [g g ⁻¹]		Mean	SD
Xcc B100	6.32	6.4	6.36	0.035
Xcc B100 <i>crt1</i>⁻	7.55	8.66	8.11	0.55
Xcc B100 <i>crt2</i>⁻	7.45	8.69	8.07	0.62

Danksagung

Ich möchte mich bei allen bedanken, die mich in den letzten Jahren begleitet und damit entscheidend zu meiner Arbeit beigetragen haben. Doch natürlich hatten die letzten Jahre nicht nur Auswirkungen auf diese Dissertation, sondern haben auch mich geprägt und geformt (und ich hoffe das Ergebnis ist erträglich).

Entscheidenden Anteil daran hatten natürlich meine Freunde und Familie, die Phytos, die Corynes, die Jungbunzlauer Crew um Dr. Gerd Hublik, Dr. Frank-Jörg Vorhölter, Prof. Dr. Alf Pühler und Prof. Dr. Karsten Niehaus.

Ferner möchte ich mich bei der Jungbunzlauer Austria AG und dem CLIB-GC für die Unterstützung bedanken, ohne die diese Arbeit nicht zustande gekommen wäre.

Vielen Dank euch allen,

Tim

11 Erklärung

Mit der vorliegenden Dissertation beantrage ich die Eröffnung des Promotionsverfahrens an der Fakultät für Biologie, Universität Bielefeld, nach der Promotionsordnung von 2012.

Hiermit erkläre ich, dass ich die vorliegende Dissertation selbst angefertigt und nur die angegebenen Quellen und Hilfsmittel verwendet habe. Sämtliche aus der Literatur entnommenen Zitate, sind durch Angaben der Herkunft kenntlich gemacht.

Im Zusammenhang mit dieser Arbeit wurden keinerlei geldwerte Leistungen an Dritte gegeben.

Weiterhin erkläre ich, dass die vorliegende Dissertation weder vollständig noch in Auszügen einer anderen Fakultät mit dem Ziel vorgelegt worden ist, um einen akademischen Titel zu erwerben. Ich bewerbe mich hiermit erstmalig um den Doktorgrad der Naturwissenschaften der Universität Bielefeld.

Bielefeld, den 06.12.2016

Tim Steffens

Ende gut, alles gut